# Molecular Recognition for Rapid Bioanalysis: Applications Using Antibody and Aptamer Systems

**By**

**Giridharan Gokulrangan**



Submitted to the Department of Chemistry and the Faculty of the Graduate School of the University of Kansas in partial fulfillment of the requirements for the degree of Doctor of Philosophy.



Signature redacted

**George Wilson**

Signat

Signature redacted

**Cynthia Larive**

Signature redacted

**Robert Dunn**

Signature redacted

**David Benson**

Signature redacted

**Christian Schoneich**

**Submitted:**

## Abstract

Giridharan Gokulrangan

Department of Chemistry, University of Kansas.

The main focus of this dissertation is to apply biomolecular recognition to carry out rapid, sensitive protein detection using a polyclonal antibody and a DNA aptamer.

Rapid immunosorption kinetics using reduced diffusion distances in microreactors were demonstrated at reduced diffusion distances using a model microchannel (40 x 100 μm dimension) architecture, based on a photoablated poly ethylene terephthalate (PET) surface. The detection of a potential warfare agent staphylococcal enterotoxin B (SEB) was implemented. Characterization of the Rb α SEB antibody adsorption on the photoablated channel surface revealed a maximum antibody coverage of 19.4 $pmol.cm^{-2}$ on the channel surfaces and 5.5 $pmol.cm^{-2}$ on the sealing laminate surfaces. Characterization of the photoablated surface using scanning electron microscopy (SEM) and attenuated total reflection - Fourier Transform infrared spectroscopy (ATR-FTIR) reveals the presence of charged functional groups on the surface along with an overall increase in the surface hydrophobicity. The bioactivity of the adsorbed antibody was found to be close to 30%. The kinetics of the immunosorption reaction was found to be rapid and the reaction was completed within a minute inside the microchannel. The modeling of such reactions using Fick's law predicts a diffusion rather then kinetically-controlled process.

Biorecognition by a DNA aptamer was implemented in a homogeneous approach

based on the fluorescence polarization (FP) detection of immunoglobulin E (IgE). The method is based on the anisotropy changes that occur during the binding event. End-labeled IgE aptamer using fluorescein and Texas Red as the fluorophores has been used for the successful detection of IgE. A LOD of 350 pM has been observed, under unoptimized conditions, for the IgE detection. The optimization of the sensitivity of the FP signal was a key objective of the current work. Factors found to be important in this regard include the choice of fluorophore, dye tether length, temperature and ionic composition of the binding buffer. A detailed understanding of the anisotropy results has been obtained using the time correlated single photon counting (TCSPC) spectroscopy. The importance of understanding the dye-DNA interactions and rotational dynamics of the labeled aptamer has proved to be crucial for the FP approach.

## Acknowledgements

As I pause to reflect on the experience that I have gained during my graduate school career, I am amazed about the impact it has had on my thinking and personality. I am absolutely convinced that this stay at Kansas for my doctoral program has molded me for greater things in life, academically and personally. I am thankful to my research mentor Dr. George Wilson for having given me the opportunity to pursue my degree under his tutelage. I feel deeply indebted to the unconditional support of my parents and all of my immediate family. It is not trivial to receive support like what I have had, especially considering that this program was a big commitment. I feel blessed to have had the opportunity to pursue what I like. The most important priority for my parents has always been quality education for all their children. I am ever thankful for all the sacrifices and extra efforts they have made to help all four of us realize our educational dreams. The fact that all my siblings and their families have been around here in US during my graduate school studies has also helped me a lot. It is great to have had continuous encouragement from all of them throughout my stay at Lawrence. My special thanks to my sister-in-law who took the pains of proof-reading my chapters and managed to return them with lavish compliments even in some cases when they were not very well written. Such things helped me cross this last part of the program called "writing up". I feel fortunate to be graduating from Dr. Wilson's research group. Surely I have had my bad phases and disappointing times when I have found it real hard to get where I wanted to be research-wise. But I shall never forget, for the rest of my life, the "focus" mantra that I heard from him. I have used it incessantly to get myself out of some trying, stressful situations. The image of

Dr. Wilson telling me "focus harder when things get tougher" is strongly etched in my mind. I am not sure if that is the answer all the time but it has definitely worked a lot of times for me since he started this on me. I have been amazed by the number of different things that he gets done everyday. I also like his open-minded approach to new ideas, new research areas and new problems. It is the breadth in the analytical projects that gets done in this group that I am especially proud to be a part of. I cannot help but agree that his way of dealing with students makes all his products self-reliant, self-motivated and full of leadership qualities. This method, I should confess, is not easy to deal with when one is trying to progress in graduate school but plays out well, I believe, for life-long results. I am also fortunate to be able to work in the midst of a nice, friendly group of labmates during the time that I have been here. Many thanks to Stan, Doug, Raeann, Johanna and others who were there to talk to and share thoughts with. My special thanks to Doug for helping me with so many things other than school related work. My heartfelt gratitude to Jan Akers as well for being so helpful at all times for so many different things. I had a good time in my apartment life also, during my program here. I would also like to acknowledge the support of all the divisional and departmental faculty members who are great people to work with and learn from. I would like to specially thank Dr. Carey Johnson and Jay Unruh, for their productive collaboration in the fluorescence work. It was a learning experience for me in the microchannel project with the Girault group at Lausanne, Switzerland. I cannot afford to forget my Swiss connection Dr. Joel Rossier who embodied the spirits of a fearless researcher who also had an infectious enthusiasm. I hope I will encounter such positive work experiences all my life.

## Table of Contents

## List of Figures

Page #

## List of Tables Page #

## 1.1 Introduction, Significance and Overall objectives

Molecular recognition has proven to be an effective tool to perform sensitive bioanalysis. Recognition elements like antibodies, enzymes, nucleic acid probes, ion-specific chelation ligands, molecularly imprinted polymers and other supramolecular recognition elements constitute a host of specific binders that can be used to design useful bioanalytical applications. A plethora of targets including small molecules, therapeutic drugs, peptides, proteins and even cell surfaces can be targeted using this approach. The overall objective of the current work has been to employ two classes of high affinity biomolecular recognition elements – antibody and nucleic acid based "aptamer" to carry out rapid, sensitive protein detection.

The initial part of this dissertation (Chapter 2) is focused on the objective of reducing the assay time in heterogeneous immunoassays. The conventional assay techniques like the Enzyme linked immunosorbent assay (ELISA) extend into few hours. As such assays are extensively employed, it is very useful to explore the possibilities for reducing the total assay time. Conventional approaches, including the elevated temperature condition method, do not offer significant improvements in achieving this objective. It has been hypothesized that reduction of diffusion distances for the immunoreactants can be the most promising approach in addressing this issue. As a result of improvements in the microfabrication technologies, it is conceivable that suitably fabricated immunoreactors with micrometer range dimensions can be adapted to explore this hypothesis. In collaboration with the Girault research group at Ecole Polytechnique Federal de Lausanne, this problem has been investigated and discussed in this chapter. The detection of a toxic protein Staphylococcal enterotoxin

B (SEB) has been approached using photoablated polyethylene terephthalate (PET) microchannels. These immunoreactors have micrometer range dimensions and are thus suitable to tackle the above-mentioned hypothesis. A main issue of concern in this method is the high sensitivity requirement for the detection system as the amount of biomaterials in contact with the channel surface is always very low, in the order of picomoles. Radiometry has been chosen in our case, as it is a mass dependent detection method that can quantify exceedingly small protein amounts. Other issues of concern that are discussed in this chapter include reactor microfabrication details, characterization of the polymer microchannel, amount of adsorbed anti-SEB antibody, rapidity of immunosorption kinetics and bioactivity of the immobilized antibody. These issues are crucial in order to clearly characterize the immunoassay approach. Adequate attention has been paid to compare the forward rate of the immunochemical reaction on the surface to the mass transport-limited rate of the diffusing reactant towards the immobilized primary immunoreactant. This is required as the approach of reducing the diffusion distances of the reactor can be futile if the inherent forward immunochemical reaction rate is the rate determining step. The significance of this section of the current work is thus related to the fundamental issue of improving immunoassay kinetics.

Chapter 3 of this dissertation is related to using a DNA aptamer for sensitive, rapid bioanalysis of Immunoglobulin E (IgE). Aptamers are novel recognition elements that are selected *in vitro* for analytes of interest. This is performed using combinatorial selection techniques that combine the advantages of nucleic acid amplification techniques with the technique of isolating tight binding nucleic acid ligands. The merit

of using such a novel ligand includes quicker isolation of a specific recognition element, in contrast to the long times associated with antibody isolation approach. Fluorescence Polarization (FP) approach has been used to monitor the binding of the aptamer to IgE. This approach can thus be a rapid, homogeneous method to carry out the bioanalysis of IgE. Considering the demands of high throughput for modern bioanalysis, this homogenous format for carrying out the bioanalysis is an attractive option. This chapter also involves discussion of the factors that have proven to be significant – choice of fluorophore, labeling strategy, temperature, ionic conditions and possible interferences, in optimizing the FP response.

Although the FP approach stands out for its user-friendly approach, the interpretation of data in relation to different probes may not be straightforward. A careful understanding of the photophysical and fluorescence characteristics of the probes is necessary to gauge their efficiency in being sensitive FP probes. In this context, detailed characterization of the FP probes has been performed. Chapter 4 deals with the details of this biophysical study performed using the principles of time correlated single photon counting (TCSPC) spectroscopy. This work has been done in collaboration with the Johnson research group here at the University of Kansas. The observations made from this study are useful to comprehend many of the steady state observations and are also useful to optimize the FP approach for the current application of IgE detection. Thus, the main emphasis of this dissertation is in utilizing biomolecular recognition elements to perform sensitive bioanalyses.

Finally, Chapter 5 is related to the overall discussion involving the results and observations made in course of this work. It also briefly discusses the future works in relation to the new areas of research that have been initiated, based on some results discussed in the current dissertation. These include surface plasmon resonance (SPR) spectroscopy for monitoring DNA-protein interactions and application of TCSPC spectroscopy for the characterization of novel dedrimeric DNA probes.

## Chapter 2

## Characterization of Protein adsorption and Immunosorption Kinetics in Photoablated Polymer Microchannels

Page #

## 2.1 Introduction and Objectives

### 2.1.1 Immunoassays – An overview

Molecular recognition, spectroscopy and separation science constitute the three main approaches to sensitive bioanalysis. The unique characteristic of molecular recognition is that it extends the application of bioanalysis into the realm of common consumers in the form of healthcare related diagnostic products, like kits for home-based testing and biosensing (1). This approach has yielded simple readout systems, especially by using the advances in microelectronics, for these practical applications (2). Such healthcare products are important to ensure the self-maintenance of critical health parameters like blood glucose, cholesterol and lipid levels (3).

Two established bioanalytical technologies meeting the requirements of molecular diagnostics are immunoassays and DNA/RNA based methods (3). The field of immunodiagnostics has advanced significantly since the initial discovery of immunoassays by Yalow and Berson (4). The development of a procedure for monoclonal antibody production by Kohler and Milstein (5) has helped in the evolution of many commercial products. Pertinent applications of such immunoassays include the analysis of disease markers, biotoxins, drugs of abuse, food pathogens and environmental analytes. General requirements for the development of a successful immunoassay product include simplicity, rapidity, sensitivity and specificity of analyte detection. Heterogeneous assay based solid phase immunoassays (SPI) are most commonly employed for commercial diagnostic products.

The basic component of heterogeneous immunoassays is the rapid immunochemical reaction between an immobilized antibody and the analyte of interest, aided by a convenient detection scheme that helps in qualitatively or quantitatively identifying the analyte. The readout is either qualitative or quantitative depending on the application. Some products, like the instrumentation-free test kits for human chorionic gonadotropin (HCG) detection in pregnancy testing and cholesterol analysis need only a qualitative response (6) whereas near-patient clinical analyzers require quantitative responses based on calibrated standards (7,8).

Different conjugation chemistries are used for SPI to immobilize the bioactive antibody to materials like polystyrene, polycarbonate, dextran, nylon and cellulose (9). Common reactors that are used for the development of immunoassays include polymeric microwell plates, derivatized microparticle surfaces, polymer coated magnetic particles and modified membranes (10). The antibody immobilization strategies include adsorption, covalent conjugation and affinity interactions (11). The different detection techniques commonly employed for SPI include spectrophotometry, fluorescence, turbidimetry and chemiluminescence. The Enzyme linked immunosorbent assay (ELISA) is a very successful example of SPI that uses the reactivity of an enzyme to assess the extent of binding reactions involved in immunoassays (12). A common issue with ELISA is that the total assay time, with few exceptions, extends into the range of hours. Hence, shortening the assay time is an important consideration. Although features like high sensitivity and

simplicity have made ELISAs commercially very successful, the inability to execute this assay more rapidly, without sacrificing sensitivity is an important disadvantage.

### 2.1.2 Microfabricated reactors – Scope for rapid assays: Current objectives

ELISAs often require long incubation times, in the range of 1 hour, even at elevated temperatures. Such incubation steps are necessary to allow the immunochemical reaction to go to completion and maximize the readout signal. A key contribution to the long incubation times is the lack of rapid mass transport of immunoreagents from the solution phase to the reactor surface in conventional assay reactors like microwell plates and microparticles (13). The high surface area/volume ratio of microparticles is a definite improvement over the microwell format (14) but the inherently fast kinetics of immunochemical reactions still cannot be exploited to achieve assay rapidity. It is hence desirable to investigate some possible assay methodology changes that will address this mass transport issue.

The development of microanalytical reactor systems, in the form of micro total analysis system (μ-TAS) devices, (15) has raised the possibility of performing very rapid assays. These are reactors that offer very high surface area/volume ratios due to their micrometer size dimensions. The typical surfaces that have been employed to make these reactors include glass, polydimethyl siloxane (PDMS) and other polymeric materials like polyethylene terephthalate (PET) and polycarbonate. The most progress has been made in bioanalysis using the μ-TAS devices is for electroosmotically driven separations. Such analyses (16) utilize the small reactor dimensions of the μ-TAS devices to carry out rapid assays, based on the principles of microchip capillary electrophoresis (CE). The small dimensions of these reactors

require only nanoliter sample volumes and are hence considered advantageous over the conventional CE instrumentation. These reactors, additionally, provide reduced diffusion distances, which is not possible in the conventional immunoassay reactors. Such small diffusion distances provide the possibility for improved mass transfer and, hence, can be potentially used to carry out rapid, heterogeneous immunoassays. However, the progress in the area of microanalytical chemistry (17) in relation to achieving fast assays, using such μ-TAS devices, has been very limited (18). It is a main objective of this study to examine the utility of polymeric microchannel surfaces (19) in carrying out fast immunoassays. The current work mainly deals in depth with the microfabricated, planar PET devices for examining the feasibility of detecting a protein target, Staphylococcal enterotoxin B (SEB).

In this report, SEB and a polyclonal rabbit anti-SEB (Rb α SEB) antibody have been used as the immunoreactants. Laser treatment of the PET surfaces, using photoablation, has been used to fabricate the microchannels. The rapid detection of SEB is of keen interest due to its potential as a biological warfare agent. This 29 kDa toxic protein is also a food toxin that can be lethal, upon ingestion. Conventional ELISA and other heterogeneous assays have been used to perform very sensitive SEB detection (20,21) in the time range of few hours. It is hypothesized in the current work that the strategy of working with reactors that have reduced diffusion distances for immunoreactants, as in the photoablated PET planar microchannels, will reduce significantly the reaction time for the completion of immunoassays. Such an approach, if successful, can be one solution to solving the problem of long reaction times when using the conventional SPI reactors. Although this approach may not be

valid for all immunoreactants, the current system can be considered a proof of principle work for selective future applications.

## 2.2 Principles, Prior art and Current approach

### 2.2.1 Antibody affinity and Avidity

The biospecific interactions between an antigen and antibody are reversible and are governed by the law of mass action under equilibrium conditions as follows (22):

$$Ag+Ab \Leftrightarrow Ag\text{-}Ab \qquad \textbf{Equation 2.1}$$

where Ag-Ab is the resulting immunocomplex. $K_a$ represents the association constant for this reaction, defined by the following expression:

$$K_a = k_f / k_r \qquad \textbf{Equation 2.2}$$

where $k_f$ is the kinetic forward reaction rate constant and $k_r$ is the reverse reaction rate constant. Typical values of $K_a$ for immunochemical reactions range from $10^6$ to $10^9$ $M^{-1}$ (23). The association constant, $K_a$, is an index of the affinity of the antibody towards the antigen and is most accurately determined when equilibrium binding conditions are assured. It is to be pointed out that the implicit assumption in arriving at Equation 2.1 is that the complex formation is from a monovalent stoichiometric reaction between the immunoreagents involved. Since this assumption has turned out not to be accurate, especially for macromolecular analytes like peptides and proteins, the binding affinity of an antibody represented by $K_a$ is often referred to as

the cumulative affinity or "avidity" (3), because the population of antibodies is best described as a distribution of antibodies having different affinities as described by Equation 2.1.

### 2.2.2 Immunoassay kinetics on solid surfaces - Reagent depletion issue

Immunochemical reactions are considered to be fast, bimolecular reactions that are predicted to be limited by diffusion in solution (24). This is based on the simplest rate theory model that considers the immunoreactants to be hydrated spheres. The diffusional rates, however, can become comparable to the forward reaction rate $k_f$ when steric effects are considered. This fact is confirmed when the additional factor of sizes of the reactive regions on the immunoreactants, that ultimately determine the reaction rate, are considered instead of hydrated molecules on the whole. A typical value for the $k_f$ is $10^6$ $M^{-1}sec^{-1}$ for a protein antigen and a nominal value for $k_r$ is in the range of $10^{-3}$ $sec^{-1}$ (25). The high binding affinity of immunoaffinity interactions, thus, arises from high forward reaction rates as well as from very slow complex dissociation rates. The rate constant values, especially the $k_r$, may vary depending on the nature of the analyte, although the values mentioned above are nominal for numerous immunoreactant systems. The above-mentioned experimental rate constant values have been determined from homogeneous experiments. These values typically determine the characteristics of the immunoassay being developed. The above-mentioned $k_f$ values also clearly indicate the possibility of carrying out rapid immunoassays. However there are differences between the solution-phase and surface reaction kinetics. The issue of the diffusing reagent depletion (23) at the solid-liquid interfacial layer of SPI reactors, as illustrated in Figure 2.0, possibly makes the reaction at surfaces diffusion-limited. This issue arises due to differences

in the concentration of the diffusing immunoreactant between the bulk solution and the surface layer close to the immobilized primary immunoreactant. The immunocomplexation process can thus be slowed on surfaces because the rate-determining step is mass transfer- controlled and is not governed by the kinetics of the immunocomplexation.

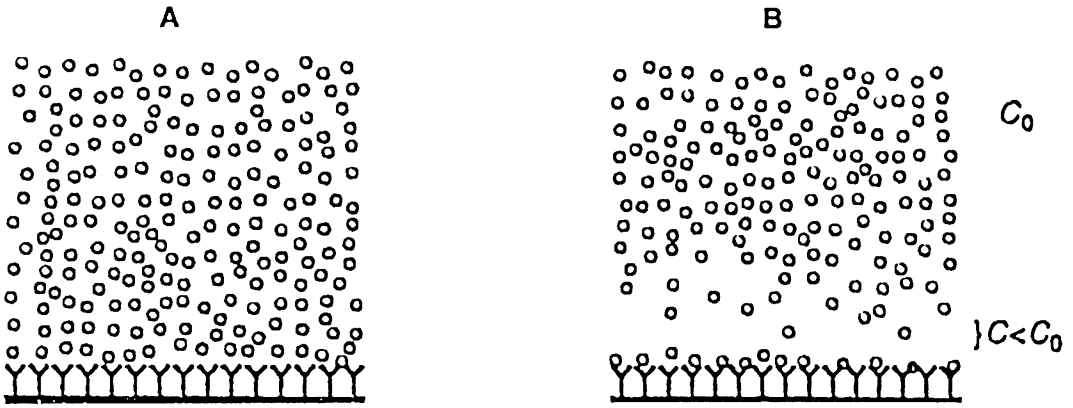


Figure 2.0: Section A refers to the initial reaction stage when there is no antigen concentration disparity. The Y shaped antibody is the primary, immobilized reactant. Section B refers to a later timeframe when the reagent depletion sets in, due to diffusional constraints. Disparity between the bulk antigen concentration $C_0$ and the surface concentration C is clearly seen at this point of time.

A reliable index of the diffusion control for the product formation on surfaces is the Damkoehler number ($D_a$). It is defined as the ratio of maximum reaction at the surface and maximum rate of diffusional mass transfer. For any type of surface, an estimation of this number can help to predict if the progress of the immunoreaction

on a surface of interest will be controlled by diffusion or the inherent forward reaction rate.

### 2.2.3 Implication of the reagent depletion issue

The mass transport limitation effect at the reactor surface makes the classical binding theory-based calculations (26) inapplicable for planar microreactors, like the current PET system being considered. The magnitude of the effect is also dependent on the surface density of the primary, immobilized immunoreactant. The diffusion rate of immunoreactant migration, alternatively, can also vary depending on the geometry of the reactor and this can further make the mass transfer rate limit the progress of immunocomplexation. The pioneering theoretical work of Swedish scientists Nygren and Stenberg (26, 27) in this area of interfacial kinetic theory has focused specifically on these issues. This work has, consequently, suggested some possible assay protocol changes to improve the interfacial kinetics of immunoassays. The general strategies that have been adopted, especially when the assays are carried out in conventional reactors like microwells and microbeads, included continuous reagent mixing (25), increased incubation time (26) and high temperature reaction under minimum reagent evaporation conditions. Out of these possible approaches, the elevation of temperature strategy has received wide attention and has been incorporated into immunoassay protocols.

### 2.2.4 Improvement of interfacial kinetics - Elevated temperature approach

The kinetic association constant $k_f$ is related to temperature by the Arrhenius expression, given by Equation 2.3:

$$k_f = A \exp(-E_a/RT)$$ **Equation 2.3**

Based on the above expression for $k_f$, it can be expected that the elevation of temperature would improve (28) the immunocomplex formation rate. This was also found to be the case from initial data (29) and this observation has led to the inference that the mass transport issues in heterogeneous assays can be partly handled by using the higher temperature conditions during all the reaction steps in the method protocol. The initially observed assay performance improvements at higher incubation temperatures were attributed to the possible elevation of the association rate. The very low value for the reverse rate $k_r$, in general, was not expected to vary significantly as immunoaffinity reactions on surfaces are considered to be practically irreversible, like homogeneous assays (30).

The temperature dependence of the rate-determining step has been found to be in the range of 2-10% / °C (31, 32). Although the rate of reactant diffusion can be improved with temperature, the immunoassay sensitivity did not significantly improve as it depends on the geometry and size of the reactor, apart from the orientation of the immobilized primary reactant. Dutch physicist Beumer and coworkers (33), meanwhile, demonstrated that assay improvements observed at higher assay temperatures were not due to the variation in the association rates, as originally assumed, but were rather due to the thermal activation of mass transfer of the diffusing immunoreagent to the immobilized primary reactant (34). This was based on some novel, non-intrusive temperature distribution experiments in heated assay

reactors like microwells. It was also observed that it was free convection that was responsible for the improvements in mass transfer. It was also proved from this insightful work that the net sensitivity gain obtained from using higher assay temperatures like 37°C was only in the range of 5-10% (35). Forced convection was found to be a much better option for the mass transport enhancement with sensitivity and precision improvements. However the time of the assay steps, even with these assay improvements, was still found to be in the range of 20-30 minutes, only a two-fold improvement in comparison to the one-hour room temperature protocols. Thus, the strategy of using higher temperature incubation offers only very marginal gains. Reduction of diffusion distances for the diffusing immunoreactant was hence considered to be a much better option for achieving rapid assays than temperature elevation.

### 2.2.5 (a) Approaches involving minimization of diffusion distances

The transfer of a diffusing secondary immunoreactant towards the surface immobilized primary reactant is governed by the diffusion distance expression is given by the Einstein-Smoluchowski equation (32):

$$d_{diff} = (2Dt)^{1/2} \qquad \textbf{Equation 2.4}$$

D refers to the diffusion coefficient in $m^2$/sec, t is the time for diffusive migration in seconds and $d_{diff}$ refers to the diffusion distance in meters. As can be seen from the Equation 2.4, the time for diffusive transfer of the immunoreagent is directly dependent on the square of the diffusion distance involved. The rate of reaction of a solution phase immunoreactant with a surface immobilized capture reagent can be

controlled by mass transfer of the diffusing reactant or by the kinetics of the immunochemical reaction itself. If mass transport of the solution phase reagent is the limiting factor, then shortening the diffusion distance should result in driving the heterogeneous immunoreaction to completion more quickly.

Improvements in the microfabrication technologies have led to the possibility that microreactors based on different surfaces like pyrex glass, PDMS, PET and polyethyleneimine can be used to fabricate reaction devices that have dimensions in the range of a few microns. Such microreactors may be suitable to demonstrate the above-mentioned hypothesis that reduced diffusion distances for immunoreactants will help speed up the reaction kinetics. The general strategy in these reactors is to immobilize antibodies using different surface attachment methods and to carry out the immunoassay using different flow modes including the electrokinetic mode, continuous flow mode using syringe pump and forced convection (36).

### 2.2.5 (b) Early examples

The detection methods commonly employed to monitor the antigen-antibody binding event in such microfabricated systems include on-channel refractive index measurement, off-channel fluorescence, electrochemistry or chemiluminescence. Capillary enzyme immunoassays have tried to take advantage of the short diffusion distances inside glass capillaries. This approach was successfully adapted in the case of atrazine detection (37) where covalently immobilized monoclonal atrazine antibody was used to implement a competitive assay for atrazine. Using fluorescently labeled atrazine, a practically useful working range of 0.1 to 10 μg/L was attained.

Continuous reagent flow using a syringe pump was employed in this application. However the detection had to be made electrochemically outside of the capillary and also the capillary dimensions were not very short (550 μm) to afford greatly reduced diffusion distances. This work, however, proved the utility of such microsystems to carry out faster assays, in the range of minutes, when compared to the conventional microtiterplate format for atrazine detection that was performed in a few hours.

Reaction kinetics was found to be quick for the binding reaction between Protein A (pA) and fluorescently labeled rabbit IgG (Rb IgG) in an off-channel detection assay in which a competitive assay format was once again successfully used to detect Rb IgG. The primary immunoreactant pA was immobilized on the microchannel surface using the avidin-biotin chemistry. A pyrex glass wafer was used (38) in the microfabrication step using standard photolithography techniques. The flow channels in this reactor were made by fusing the PDMS slabs with channel imprints onto the glass surface. The washing, incubation and reaction steps were regulated by controlling the flow rates through the channel. The choice of pyrex helped in adapting the electrokinetic mode of liquid flow inside the microchannels. According to the application's hypothesis, the micron range dimensions (50 x 20 μm) of the microchannel meant reaction time could be well reduced. It was found that the kinetics of the assay could be improved such that an incubation of the immunoreactants for 200 seconds only was needed to achieve equilibrium binding conditions. Thus the miniaturized channel proved to be useful in carrying out rapid assays in this application.

The basic issues involved in designing such microchannel-based devices are the fabrication complexity and costs, availability of leak-free flow channels, reproducible antibody immobilization strategy inside the microchannel devices and reasonable bioactivity of the immobilized antibody. The fabrication costs involved in photolithography (39) on modified glass and PDMS are not insignificant. The use of polymeric microsystems in which the fabrication techniques for manufacturing the microchannels are less complicated and less expensive can thus be a useful improvement. Reproducible antibody immobilization is also not a trivial issue as these microfabricated polymeric surfaces, unlike the conventional microtiterplates, have not been well investigated for efficient antibody immobilization. Possibilities for this include adsorption and microsphere-bound antibodies trapped inside the microchannels. Patterned protein deposition strategies have also been attempted to obtain reproducible antibody immobilization in microfabricated devices. For example a hydrogel-based approach for patterned protein deposition was successfully attempted in reactors of 50 – 80 μm dimensions although they are not very practical for routine applications (40). An extensive analysis of different strategies for antibody immobilization on silicon microchannels (25 μm wide x 235 μm deep) for a competitive atrazine assay using chemiluminescence detection clarified certain established facts. The adsorption approach is a useful, simpler alternative in comparison to the covalent immobilization strategies although the latter approach is much better for reagent regeneration and for achieving a higher bioactivity of the immobilized antibody (38).

The objective of achieving rapid kinetics in microfabricated devices has thus been accomplished through different antibody immobilization methods, as discussed above, although assay characteristics may differ in these cases. The improvements in the microfabrication technology, like the availability of the photoablated polymeric materials, to conveniently fabricate microreactors has opened up new possibilities to do rapid immunoassays. The specific focus of this work is the use of photobalated polyethylene terephthlate (PET) microchannels to explore the potential of achieving rapid kinetics for immunoassays.

### 2.2.6 Potential of photoablated polymeric reactors - For rapid immunoassays

It was discovered (41) that the surface characteristics of polymeric films like polycarbonate, polystyrene, cellulose acetate and polyethylene terephthalate (PET) can be modified by high-energy irradiation using pulsed UV sources like ArF excimer lasers. The process, known as photoablation (42), refers to the absorption of short duration laser pulses with concomitant electronic transitions from the ground state to the first excited singlet state that consequently leads to bond-breaking within the long chain polymeric molecules. The pulsed radiation sources can generate energy in excess of 40 $mJ/cm^2$ (41) and this is high enough to cause the ablation of the polymeric surfaces. The process is analogous to the dry etching process in which the local temperature, after excimer laser irradiation, increases significantly resulting in the disruption of the surface morphology. Reaction decomposition products like CO and $CO_2$ are evolved as gases and the extent of surface modifications depend on the irradiation energy beyond a certain threshold level. The ablation process is actually a "self cleaning" process in which the surface is cleared of fragmented debris through

an "ejection by pressure" process in which successive laser pulses function to clean away the surface. This process can be performed under non clean-room conditions (43). The laser photoablation process results in the modification of the chemical nature of the surface and also increases the roughness of the plastic medium. The chemical nature of the ablated surface is altered in such a way that it has an increased hydrophobicity in comparison to the untreated polymer. The increased surface roughness results in an enhanced surface area/volume ratio on the photoablated surfaces, thereby promoting increased protein immobilization on such surfaces. The end result of this photoablative surface modification process has been an effective increase in the adsorption capacities for proteins and other biomolecules on such modified surfaces.

The photoablative treatment, thus, paves the way to utilize such treated polymers as a medium for carrying out antibody immobilization and immunoassays. The ability to mass-produce microreactors based on such polymeric surfaces has further raised the possibilities of extensively using such devices to carry out rapid assays (44, 45). Well-defined flow channels can be laid out by using computer-controlled photoablation. The laser source can be moved across the polymer surface on the XY plane in a regulated way using stepper motors. Computer control is used for this lateral movement of the laser source to generate linear flow paths that have a depth of about 40 microns. The ablated channels can then be sealed using thermal lamination techniques based on sealing materials like polyethylene terephthalate/polyethylene (PET/PE). The ability to seal such devices using just an industrial lamination apparatus is considered to be a huge practical advantage over

photolithography-based approaches. The openings for these flow channels can also be created by using circular masks through which UV radiation can once again be focused to make circular apertures. As seen from this brief discussion, a much-simplified procedure can therefore be used for the fabrication of polymeric microchannels in comparison to photolithography-based methods.

In spite of the increase in the surface hydrophobicity, the surface modifications on these polymeric surfaces has also led to the presence of some charged species that has aided in generating adequate electroosmotic flow (EOF). It is seen that the magnitude of EOF is not as high as in glass or modified silicon that has silanol functionalities but, nevertheless, the possibility of generating EOF has enabled the use of such polymeric devices for the electrokinetic mode of liquid handling during the different assay steps. Although many surfaces like polystyrene, polycarbonate, cellulose actetate and PET have been investigated for manufacturing these photoablated microreactors, we have used PET based microreactors for our immunoassay investigations taking into account some of its superior characteristics including low cost and greatest affinity for protein adsorption. Radiometric detection has been undertaken to establish a very sensitive detection of the proteins immobilized on the microchannel surface. Antibody immobilization was implemented by adsorption. Forced convection was employed to pass the reagents across the channel surface. As mentioned already, the possibility of detecting the toxic protein Staphylococal enterotoxin B (SEB) using a polyclonal antibody is the model assay system for this work.

## 2.3 Materials and Methods

### 2.3.1 Polyethylene Terephthalate (PET) microchannel system - Fabrication

The microfabrication of the channel was performed by using the UV laser photoablation process, which was briefly outlined in the previous section. This was done at Laboratoire d'Electrochimie, Ecole Polytechnique Federale de Lausanne, Switzerland as part of our collaborative effort with the Girault research group. Briefly, the water rinsed PET substrate is laminated on one side with a protective laminate made of PET/PE at 125°C and 2 bar pressure using an industrial lamination apparatus (Morane, UK). For this investigation, a simple line-and-hole mask geometry was employed when fabricating the microchanels. A 10mm x 0.4 mm mask was fabricated in copper foil for the line portion of the microchannel. A circular mask was made by drilling into a steel plate and this was used for the microhole part of the line-and-hole geometry. The PET surface was cleaned by rinsing with distilled water followed by bathing in 0.1 M NaOH for thirty minutes. The samples were then rerinsed with water, dried under pressurized air and mounted on the XY plane for fabricating the flow channels.

The substrate is then mounted in the XY plane (Microcontrol, France) and exposed to a mask patterned 193 nm beam from an excimer laser (ARF, France) generating 23ns pulses (power 10mW) at a frequency of 50 Hz through a 10:1 telescopic objective. The substrate is also moved in the XY plane such that the speed of the displacement and the repetition rate of the laser are optimized to produce a 40 μm deep cavity. The final dimensions attained on the microchannel using this fabrication procedure are shown in Figure 2.1 (a) below. The inlet and outlet aperture serve to

function as the entry and exit points to make the flow through the microchannel. Special care has been given to the fabrication of the inlet and outlet apertures.

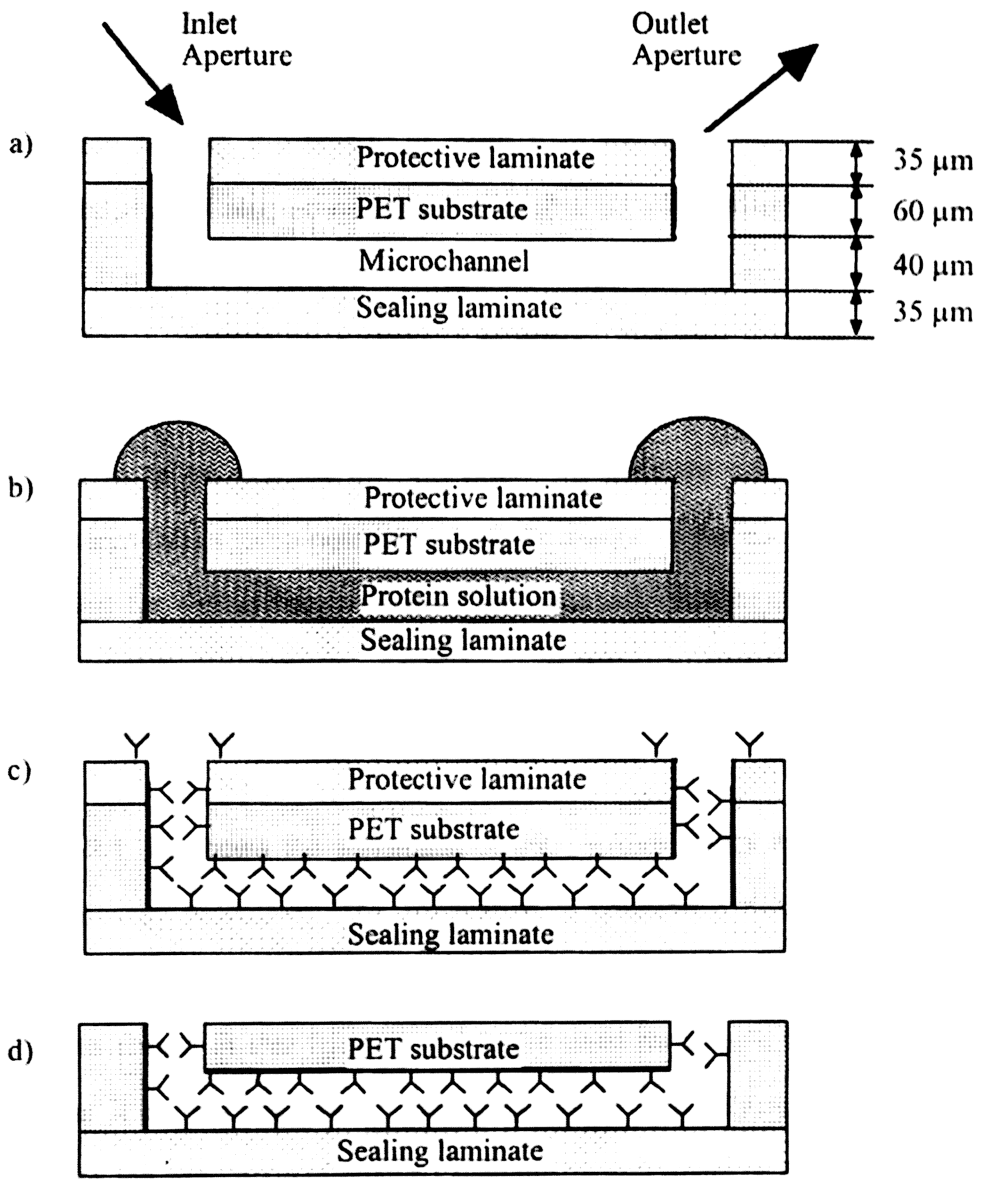


Figure 2.1: The structure of the microchannel shown here consists of a sandwich: protective PET/PE laminate, PET microchannel substrate and the sealing laminate.

The 1x 0.1 $mm^2$ apertures, seen in this figure, are formed by using the circular masks such that the ablation process carefully penetrates both the PET substrate and the protective lamination. The fabricated channel surface is then sealed by using the PE/PET sealing laminate material. The channel architecture thus has a multilayered format with protective lamination layer, PET surface, channel orifice and the sealing lamination forming the layers, as seen from top to bottom. Suitable fabrication modifications can also be performed to enable an electrokinetic mode of liquid flow through the channel although this approach was not utilized for the current study. The channel surfaces were checked to ensure that they are leak free and this is done by passing suitable colored solutions through the microchannel surfaces for an hour. It is to be pointed out the protective laminate can be peeled off when necessary. This is to be noted especially in relation to the way these microchannels are used for the radiometry-based immunoassay investigations in this work. A representative picture for the liquid flow and the procedure by which these assays were carried out, is shown in Figure 2.1 (b-d) above.

Figure 2.1 (b) shows the schematic of microfluidics inside the channel during the immunoassay procedure. The hemispherical projections near the inlet and outlet apertures indicate the drop size of the protein solution used. As the protective laminate shown in this figure is not to be used for quantifying protein inside the channel, it is removed prior to the quantification step. Figure 2.1 (c) schematically indicates the adsorption of protein inside the microchannel prior to the removal of the laminate. This part illustrates the need for the removal of the lamination before the radioactivity counting step. Finally, the effect of removal of the laminate is shown in

Figure 2.1(d). This indicates that antibody that is not present on the microchannel surface is not taken into account during the quantification step.

### 2.3.2 Spectroscopic characterization

The surface state of the PET/PE lamination and the photoablated PET surface were both characterized by scanning electron microscopy (SEM, JEOL 6300F, USA) before and after the laser treatment. The lamination surface, which forms the top of the microreactor was studied by attenuated total internal reflection Fourier transform infrared spectroscopy (ATR-FTIR) using a diamond Golden Gate apparatus (Perkin Elmer, USA).

### 2.3.3 Affinity purification protocol

(a) Preparation of the immobilized SEB column:

Staphylococcal enterotoxin B (SEB), isolated from the strains of gram-positive cocci Staphylococcus aureus, was obtained from Sigma Immunochemicals, MO. Rabbit $\alpha$ SEB antibody (Rb anti-SEB Ab) was also obtained from Sigma. 2 mL of settled Reactigel$^{TM}$, which contains crosslinked agarose with 1, 1 carbonyldiimidazole as the linker for the crosslinked matrix, was used as the affinity purification column material. Purified SEB (2 mg) in 2 mL water is added to 2 mL settled gel of the Reactigel matrix that is preconditioned with the carbonate buffer (0.1 M, pH 8.5) such that the final concentration of the SEB is 0.5 mg/mL. After an overnight incubation of the SEB and the column matrix with stirring, the gel was transferred to a 50 mL centrifuge tube after 15 mL of 1.5 M Tris (pH 9) buffer was added. The unbound sites in the gel matrix are blocked in this step and the gel support was then reconditioned in the carbonate buffer for further use. The efficiency of loading of the protein SEB in this

affinity column matrix was tested by using the standard Bicinchoninic acid (BCA) protein assay. The amount of protein detected after the loading step, from the eluate, in comparison to the total protein (SEB) originally loaded gives an estimate of the protein loading efficiency. The samples for testing this are obtained in the carbonate buffer medium immediately before and after the SEB loading step. The gel, bound with SEB, was later packed into a 0.5 mL column for the antiserum purification.

(b) Using the SEB column for antiserum purification:

The polyclonal antiserum was passed through the 0.5 mL column containing the immobilized SEB at a flow rate of 0.5 mL/min. Multiple washings of the column were done with Tris buffer (0.01 M Tris buffer, pH 7.4) to remove weakly bound antibody. The concentration of the weakly bound fractions was determined using $A_{280}$ on a Cary 50 spectrophotometer. The strongly bound antibody fraction that is held by specific affinity interactions was further eluted using the immunopure gentle Ag/Ab elution buffer (Pierce Chemicals, IL). The use of the immunopure™ gentle elution buffer is equivalent to changing the ionic strength of the buffer drastically to serve as the basis for weakening the biospecific antigen-antibody interactions. The eluted antiserum was later dialyzed in 0.1 M phosphate buffer to be concentrated further, to a final concentration of 1mg/mL.

### 2.3.4 Evaluation of the avidity of the affinity purified antibody - ELISA experiment

The avidity or the cumulative affinity of the affinity-purified Rb α SEB Ab sample can be evaluated using an Enzyme linked immunosorbent assay (ELISA) on the conventional polystyrene microtiterplate. The surface of a 96 well plate was initially

coated with 0.18 μM SEB antigen dissolved in the coating buffer (0.1 M carbonate buffer, pH 8.5). After I hour incubation at 37°C, the unbound surface is blocked using bovine serum albumin (BSA) at a concentration of 2 g/L in washing buffer (0.1 M phosphate buffer, pH 7.4). After the washing steps, the bound antigen is reacted with varying concentrations, in molar excess, of the affinity-purified Rb α SEB Ab. The concentration range used for this step starts from 0.32 mg/mL to 9.78 x $10^{-6}$ mg/mL using serial dilution. The binding curve for this antigen-antibody reaction is then traced using horseradish peroxidase (HRP) labeled Gt α Rb IgG detection antibody. The colorimetric readout for this ELISA is developed by adding the tetramethyl benzidine (TMB) / peroxide substrate. The substrate conversion is read after quenching the reaction with an acid solution and by making the measurement of optical density at 650 nm by using the 96 well microtiterplate reader (Molecular Devices, CA). The avidity is calculated in the form of the $K_d$ value, obtained from the binding curve. The $K_d$ value is normally estimated as the concentration point on the binding curve at which 50% of the antibody binding sites are occupied.

### 2.3.5 Radiolabeling procedure

Amongst the two immunoreactants – SEB and the polyclonal Rb α SEB Ab that were used in the current work, the antibody was radiolabeled for quantitation of the antigen-antibody (Ag-Ab) reaction inside the PET microchannel. $^{125}I$ was used for this purpose. The protocol for the labeling was based on the Markwell method (46). This approach was employed as it was considered to be a more convenient method, in comparison to the conventional Bolton-Hunter method. Radioiodination was performed using the Iodobead™ reagent from Pierce Chemicals, IL. Oxidation of $I^-$ to

$I^+$ is performed using the oxidizing reagent in an immobilized form. N-chloro benzene sulfonamide (sodium salt) is the iodination reactant (oxidant) and it is immobilized on 1/8 inch diameter nonporous polystyrene beads. 5 beads were used for the current procedure. They were initially washed initially in 2.5 mL of 0.1 M phosphate buffer and dried before the iodination reaction.

Five millicuries of $^{125}I$ iodide was added to 2 mL of 0.1 M phosphate buffer and the beads were added to oxidize the $^{125}I^-$ to the $I^+$ form. The oxidation reaction was allowed to proceed for 5 minutes before 3 mg of the affinity purified Rb $\alpha$ SEB Ab in phosphate buffer was added to make a final concentration of 1 mg/mL. The reaction mixture, including the iodobeads, was left for 5 more minutes with frequent mixing before the protein labeling reaction was stopped by separating the reaction mixture from the beads. The reaction mixture was then passed through a Sephadex G25 desalting column that was pre-equilibrated with 0.1 M phosphate buffer (pH 6.5). This is a very important step to remove unreacted, free $I^-$ from the reaction mixture. The protein was eluted from the column using the phosphate buffer in fractions of 0.5 mL each such that free iodine can be removed from the labeled protein fractions. The protein fractions were later pooled and reconcentrated so that the final concentration of the labeled protein can be found by using a BCA protein assay kit. The radioactivity was counted in closed vials using the gamma counter (1282 Compugamma CS, LKB Wallac, 36 MeV).

Safety considerations:

As radioiodination is hazardous, extreme precautions were taken when performing this reaction. A personal lead shield was used during the procedure. Excellent

coordination and help from the KU Radiation Safety Services (RSS) is gratefully acknowledged.

### 2.3.6 Evaluation of the avidity of the radiolabeled Rb α SEB Ab – ELISA

The effect of the radiolabeling on the binding properties of the antibody was estimated using an ELISA. The protocol used for this experiment is identical to the ELISA procedure listed in section 2.3.4 except that the radiolabeled antibody is used in this trial instead of the unlabeled Rb α SEB Ab used previously. The primary antibody that reacts with the immobilized SEB is hence the radiolabeled sample and the detection antibody is the HRP labeled Rb α SEB Ab. Although the assay can be performed by utilizing the radiolabel itself for detection purposes, we chose to use the HRP label on the detection antibody to plot the binding curve for practical convenience, considering the advantages of working less with radiolabeled tracers.

### 2.3.7 Protein adsorption and Immunoassays

(a) Antibody physisorption

The adsorption of the radioiodinated antibody in the microchannel was performed by placing an 8 μL drop of a given antibody concentration, from 1 to 2500 μg/mL in coating buffer (0.1 M carbonate buffer, pH 9.5), on top of the inlet aperture (Figure 2.1 (b)). Most of the solution was then aspirated with a syringe, to effect forced convection, at the outlet aperture. The exact amount of protein in contact with the microchannel was estimated from mass balance calculations. The microchannel was then incubated for 1 hour at room temperature, under wet chamber conditions. The channels were emptied by aspiration in between all the steps in the assays and

washed three times with 10 μL of the washing buffer (Phosphate buffer saline, pH 7.4 with 0.02% Tween 20). The volume of washing buffer employed is about 100 times the volume of the channel.

The protective laminate is peeled off (Figures 2.1(c) and (d)) before the gamma counting was done to ensure that only the protein loaded inside the polymer microchannel, and not around the apertures, is measured. The channels were then individually counted for one minute using the gamma counter. The calibration for specific activity of the labeled protein was made outside the microchannel and this was used further for protein quantitation inside the microchannel. The specific activity refers to the amount of radioactivity in counts per second (cps) / mole of the protein. Radioactive decay corrections were incorporated to ensure the accuracy of the specific activity.

(b) Kinetics studies to determine the rapidity of the immunocomplexation

The kinetic studies of the immunosorption in the microchannel were performed by first adsorbing the Rb α SEB Ab. A fixed amount, using 2 μL of 3.12 nM antibody solution, was adsorbed in different channels for an hour at room temperature. After washing and blocking steps, about 2.1 μL of 35 nM SEB was added to the microchannel and adsorbed during different times, from 1 to 60 minutes. The Ag/Ab reaction was quenched by washing the unreacted SEB, by using the washing buffer, at different times. The biospecifically bound SEB was then quantitated by the adsorption of 1 μL of 0.2 μM radiolabeled Rb α SEB Ab during an incubation time of 1 hour. The radioactivity present in each channel corresponds to the amount of

labeled antibody and is quantitated using the gamma counter, as explained in Section 2.3.7 (a).

(c) Antibody bioactivity determination on the microchannel

The bioactivity of the radiolabeled Rb α SEB Ab was checked with a sandwich assay. It is defined as the ratio of moles of the antigen bound over the moles of the antibody, expressed in percentage. Various amounts of the non-labeled Rb α SEB Ab, from 0.06 to 0.31 pmol, were adsorbed in different channels following the adsorption procedure as mentioned in Section 2.3.7 (a). After this primary incubation step, each channel was rinsed adequately with the washing buffer. A blocking step with 2% BSA solution in the washing buffer is done to prevent subsequent non-specific adsorption. The channels were then incubated with about 5 times the molar excess of SEB antigen when compared to the initial antibody amount. The quantification of the immunosorbed antibody was then performed with a molar excess of radiolabeled Rb α SEB Ab sample. Adequate washing was performed after each of the incubation steps to ensure the removal of weakly adsorbed protein. The bioactivity can be gauged by measuring the amount of bound antibody, assuming parity between the antigen and the antibody. Background counts for the radioactivity were determined and subtracted by using a control microchannel. This sample channel contained only the labeled antibody that was incubated in it for 1 hour and consequently washed using the regular protocol.

## 2.4 Results and Discussion

### 2.4.1 Microchannel architecture

The dimensions of a typical photoablated PET microchannel are the same as shown in Figure 2.1 (a). The depth of the channels, 40 microns in this case, can be changed by altering the laser fluences. The laser power used in the current application (10mW) results in a net fluence that is optimized to create a uniformly ablated microchannel surface. Very high fluences can lead to degradative ablation of the surface that may not lead to a uniform channel surface. Initial investigations in this field established a threshold laser fluence necessary to uniformly ablate the surfaces on polymeric materials like PET. The channels in the current work are 40 x 100 $\mu m^2$ in cross section and 2 cm long. The channel structure along with the microholes at each end is then sealed with the PET/PE lamination. The possibility of sealing at the very reasonable conditions of 125°C and 2 atm pressure highlights the simplicity of manufacturing microfabricated reactors using this approach. The photolithography approach of making μ-TAS devices, in comparison, involves a complicated multi-step process requiring clean room conditions. Although the current approach has involved only a linear flow channel configuration, it is possible to employ other configurations as well. The total initial surface area is calculated to be 0.062 $cm^2$ for the current device and this calculation includes the two channel openings of 1mm x 40 μm dimensions, present at both ends of the microchannel. The mode of liquid flow used in the current application is forced convection and hence the liquid droplets placed near the inlet aperture are removed from the outlet aperture using a syringe. Although this flow mode is not useful for automated flow designs, electrokinetic flow

is also possible in the current reactor configuration by using microelectrodes that can be placed inside flow reservoirs.

### 2.4.2 Microchannel characterization

As outlined in Section 2.2.6, the treatment by a high-energy laser source from ArF pulsed excimer sources results in two main modifications on the surface of PET microchannels; increase of the surface area and an increase in the hydrophobicity of the surface. The initial SEM picture of the unablated PET surface is shown in Figure 2.2 below:

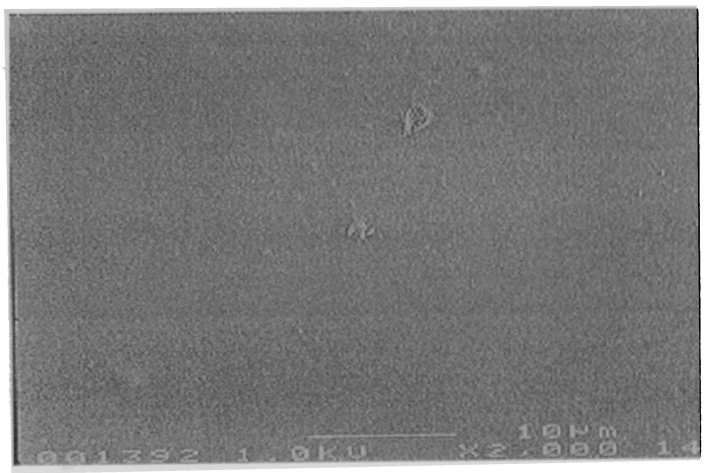


Figure 2.2: A magnified view of a 10-micron section from a SEM picture of the unablated PET polymeric surface. The section taken is picked from a flat PET sheet.

Although a clear structural homogeneity interpretation is not possible with this picture, it is to be pointed out the surface appears to be smooth, devoid of any structural inhomogeneities. A similar cross sectional area of the photoablated surface, obtained using the SEM technique, is shown below in Figure 2.3. This picture qualitatively reflects the difference in the nature of the surface in comparison to its state before the excimer laser treatment.

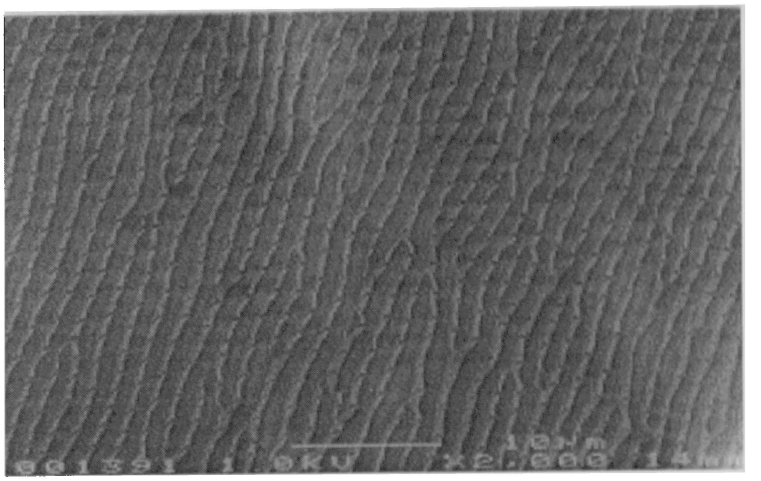

Figure 2.3: A magnified view of a 10-micron section from SEM picture of the photoablated PET surface.

As seen from the Figure 2.3, the increase in the surface corrugation and inhomogeneities are obviously seen in the photoablated polymer. Wagner and coworkers have also confirmed this observation in their work with stretched PET where they have seen more fundamental perturbation of the base structure due to

application of very high laser fluences (47). The microscopic inhomogeneities and the surface corrugations from the laser treatment surface are mainly attributed to the surface roughness arising from the elevated local temperature effect that occurs during the ablation process. In contrast to the effect of a low energy radiation source, the elevated local temperature is not transmitted effectively along the PET surface when excimer laser sources are used for the irradiation. Such corrugations indirectly contribute to the ability of these surfaces to accommodate larger amounts of immobilized proteins or biomolecules on them, due to increases in surface area. ATR-FTIR spectroscopy gives an indication of the surface modifications on such materials. The presence of functional groups arising from the surface oxidation process during the ablation phenomenon can be clearly verified using this technique, as presented in the Figure 2.4:

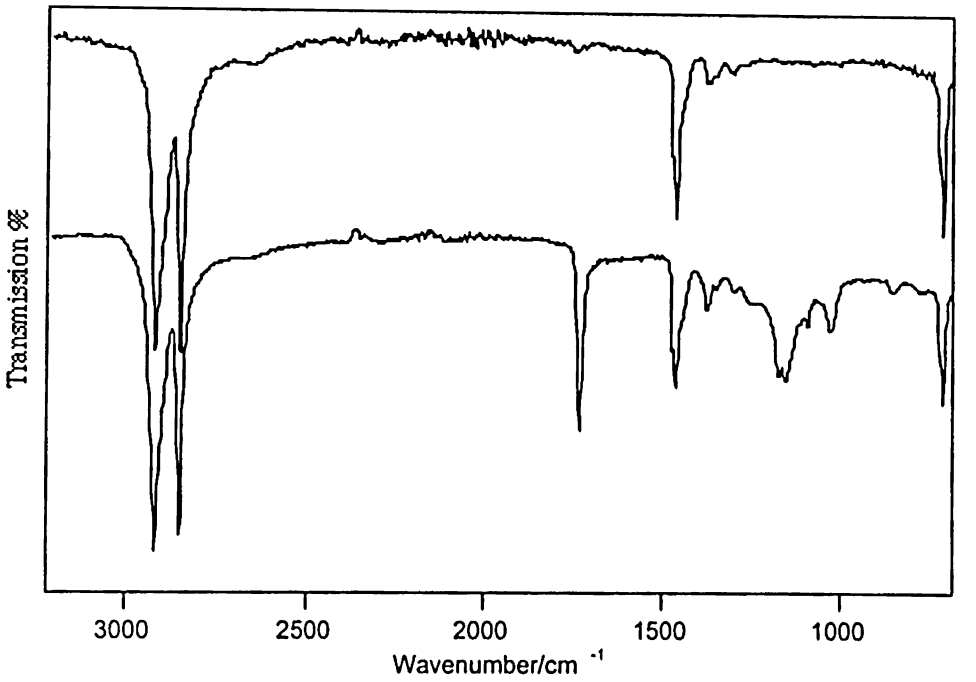


Figure 2.4: Superimposed spectra of the PET/PE laminate of the microchannel, from ATR-FTIR measurements. The top spectrum is from a standard PE polymer whereas the lower spectrum represents the PE that is exposed to the laser treatment as part of the ablation excitation process.

The peaks at 720 and 1462 $cm^{-1}$ refer to the methylene ($-CH_2$) deformation peaks whereas the peaks at 2800-3000 $cm^{-1}$ arise from the CH stretch. As one would expect these peaks are seen in both the sets of PE polymer as it is a common signature peak. The effect of surface oxidation is however clearly seen in the lower spectrum where a peak corresponding to the C=O stretch is seen at 1734 $cm^{-1}$. The

presence of the C-O stretch in the fingerprint region also confirms the presence of the carboxylate functional group due to photoablation. The presence of such functional groups has been well documented in the literature (47). The techniques of SEM and ATR-FTIR are thus extremely useful in characterizing the surfaces of polymeric substrates like PET. The Locasio research group at National Institute of Standards and Technology (NIST) has qualitiatively characterized and imaged the presence of charged carboxylate groups by using a fluorescence probe that will specifically bind to all the carboxylate functionalities on the surface of photoablated microchannels (48).

In spite of the presence of charged functional groups like carboxylate on the ablated PET surfaces as established above, the net C/O ratio of the surface actually increases after the photoablation process, confirming the increase in surface hydrophobicity. This observation has been previously noted (47). The presence of hydrophobic zones has also been confirmed from other works (48). As mentioned earlier, the characteristics of the photoablated PET surface can thus afford increased protein and biomolecule adsorption based on both the accounts – increased surface hydrophobicity and increased surface roughness resulting in enhanced surface area.

### 2.4.3 Antibody purification and avidity determination

The procedure for this section is discussed in Section 2.3.3. The commercial antiserum obtained from Sigma was not an affinity purified sample and so an immunoaffinity column using the purified SEB was prepared to effect the affinity purification. The loading of SEB was accomplished by overnight incubation with Reactigel–6X gel material that is cross-linked agarose in a 50-micron particle size.

Once immobilized with SEB and activated, the gel material was used specifically to isolate the biospecific fraction of the commercial Rb α SEB antiserum.

The loading capacity of the affinity column, defined as the percentage of total SEB loaded that is actually bound to the column, is determined by analyzing the buffer eluate from the gel material at two different stages – a) right before the SEB incubation step and b) after the reaction completion step. A comparison of the total protein content, performed using the BCA protein assay, indicated the SEB loading capacity to be around 95%. This observation is reasonable considering the use of Reactigel – 6X column that is reported to have very high protein retention characteristics. This affinity column was used to purify the antiserum sample such that the enriched fractions are eluted and reconcentrated using dialysis to yield the affinity-purified protein.

The avidity of the purified Rb α SEB Ab was determined using ELISA. The primary antibody was the unlabeled, affinity-purified Rb α SEB Ab whereas the secondary reporter antibody was the HRP labeled Gt α Rb IgG. A reliable binding curve was obtained when performing the assay under the conditions listed in Section 2.3.4. The binding curve of this purified antibody, in comparison to the same antibody after the radiolabeling procedure, is plotted and discussed in Section 2.4.5. The avidity of the antibody for SEB can be estimated from the binding curves. The $K_a$ or the apparent association constant for the unlabeled antibody was determined to be $1 \times 10^9$ $M^{-1}$. This value indicates the high avidity of the purified antibody for SEB and this value

also lies in the typical range of avidity values that can be expected for polyclonal antibodies.

### 2.4.4 Radiolabeling of the Rb α SEB Ab

**Issue of Specific activity**

In radiolabeling biologically active proteins it is necessary to consider the relationship between specific radioactivity and biological activity. Labels like $P^{32}$ and $C^{14}$, that are beta emitters, are typically employed for small molecule applications. Since quantitation of very low amounts of labeled protein inside the microchannels was the current objective, it was decided to use radioiodination (51) as the labeling method of choice. Radioiodination can be performed using two fundamentally different chemistries. $^{125}I$ can be introduced into the primary amines on proteins by using the Bolton-Hunter method (52). This method has the radioactive iodine in the form of 3-(4-hydroxyphenyl) propionic acid N-hydroxy succinimide ester that can be attached to the primary amines of the protein, primarily the ε-amino lysines, with the help of the ester leaving group. This method has the advantage of excluding the free, unreacted iodide that may interfere with the labeled protein's specific activity determination. A second advantage is that the protein is not subjected to oxidizing conditions needed to generate the $I^+$ species. The reaction of $I^+$ is primarily dependent on the presence of tyrosine sidechains in the protein. Strong oxidizing agents like chloramine T are needed for generating the free, radioactive $I^+$ ion to which the protein is exposed. As can be expected, this is a chemically harsher method of labeling the protein as the bioactive protein is exposed to the oxidizing reagent directly.

Considering the obvious differences in the two approaches, the Bolton-Hunter method was our initial method of choice as it has been successfully applied in numerous cases with good labeling efficiency (53) without significant losses in protein biological activity. However, our results from this approach suggested that radiolabeling using the method did not generate sufficient radioactivity to detect the labeled protein samples even at high protein concentrations. To illustrate this problem, the method actually used 250 μCi per 0.25 mL from a 2000 Ci/mmol $^{125}I$ source with the result that, approximately, 1 out of 50000 molecules was labeled. The radioactivity signal measured using high protein concentrations was seen at barely twice the background signal, which is usually about 45 counts per second (cps). The only possible reasoning was that the radiolabeling process was not efficient in incorporating enough specific activity during the reaction, with the protocol used for this trial. The labeling efficiency can be improved by using a higher activity source or by using a different labeling reaction. In the current case, radioiodination was attempted the second time using the new Iodobead™ reagent.

**Iodobead™ regent – Better alternative for higher specific activity**

To counter the issue of insufficient specific activity of the labeled protein, we pursued the iodobead reagent method (54). In this case, the oxidizing agent is a surface immobilized reagent, N-chlorobenzenesulfonamide (sodium salt). A two-phase reaction occurs due to the presence of the immobilized oxidant and thus the reaction is better controlled kinetically than the chloramine T approach. This reaction is better for generating a higher specific activity than the Bolton-Hunter method and it is also milder than the Chloramine T method at the same time. For example, 78.1 pmol of

the labeled Rb α SEB Ab had a radioactivity count of $2 \times 10^6$ cpm, confirming that the specific activity of the labeled protein is high enough for in-channel detection. The calibration for protein quantitation was done outside the channel using the specific radioactivity and this was used to quantitate the protein amounts inside the microchannel. Thus there is no problem in inferring the amount of labeled antibody present inside the channel based on the amount of radioactivity detected using the gamma counter, as explained in our assay methods (Section 2.3.7 (a) through (c)).

### 2.4.5 Effect of the radiolabeling procedure on the avidity of the antibody

The effect of the radiolabeling can lower the binding avidity of the antibody towards the antigen. The harsher labeling procedures that involve the exposure of the antibody to oxidizing agents during radioiodination have a greater impact on the bioactivity of the antibody. Since we have used a surface immobilized oxidant as part of the iodobead labeling procedure, the lowering of avidity for the labeled Rb α SEB Ab was not expected to be severe. The actual effects of the labeling procedure are shown in Figure 2.5:

It can be seen that the binding isotherm is slightly shifted to the right in the case of the labeled antibody, indicating there is a loss of avidity upon the radiolabeling procedure. The avidity of the antibody accordingly changes from $10^9$ $M^{-1}$ to about $10^8$ $M^{-1}$ and this indicates about an order magnitude drop in the binding ability of the antibody.

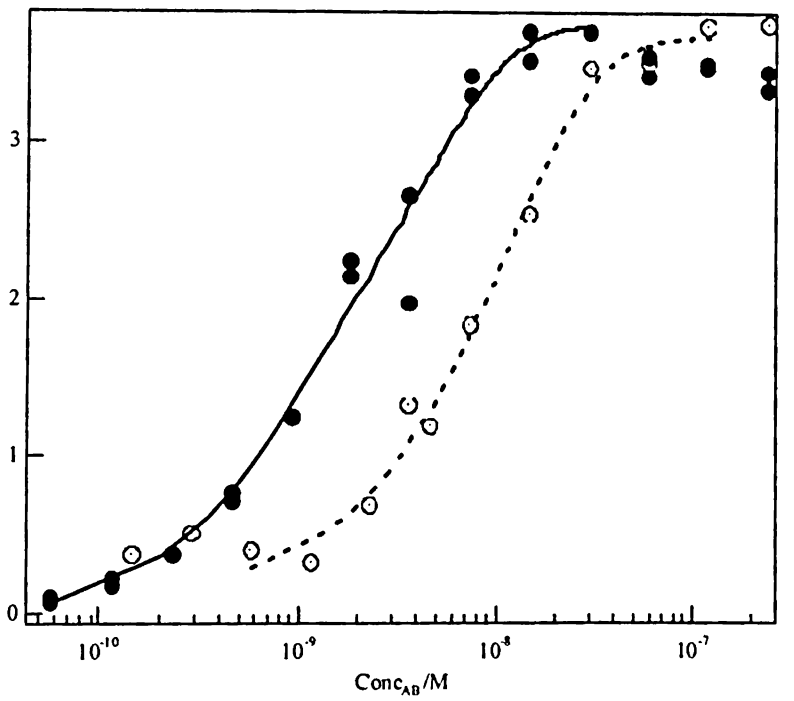


Figure 2.5: The binding curve plots of the Rb α SEB Ab, indicating the avidity measurements before (closed circles) and after (open circles) the radioiodination.

A similar result is also seen in the case of radiolabeling of v-H ras protein (55) that is involved in cell differentiation. Upon labeling by using the iodobead reagent, the drop in the biological activity of this recombinant protein is seen to be minimal as observed by its unhindered ability to induce tissue maturation in the Xenopus laevis oocyte cells. In our case, it was definitely useful to adapt the iodobead method even at the cost of losing a fraction of the antibody's binding affinity as the high specific activity of the labeled sample is the important gain achieved. In fact, we have reinforced the observation, from our studies, that the iodobead reagent is an effective

intermediate option between the Bolton-Hunter method and the chloramine T reaction.

### 2.4.6 (a) Antibody physisorption on PET microchannel

As mentioned in Section 2.2.6, forced convection by aspirating the reagents through the microchannels was the procedure adapted to effect the liquid flow in the current microchannel system. Adsorption was chosen for the immobilization strategy as it was deemed reasonable for testing our current hypothesis. In order to be able to execute immunoassays in this PET microchannel, it is crucial to find the maximum adsorption capacity of the PET for the radiolabeled Rb α SEB Ab sample. Section 2.3.7 (a) discusses the experimental procedure performed to evaluate this. Increasing amounts of the labeled antibody were attempted to be loaded into the microchannel using 1 to 2500 μg/mL antibody concentrations. The result from this experiment is shown in Figure 2.6:

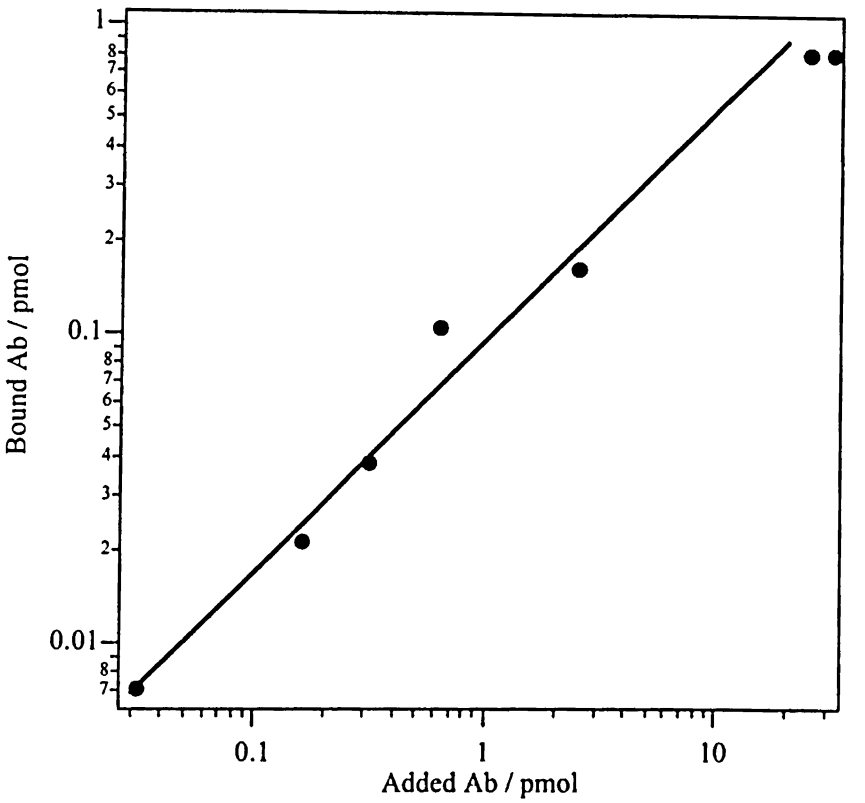


Figure 2.6: Adsorption isotherm of the Rb α SEB IgG protein in the photoablated microchannels. Increasing concentrations (1 to 2500 μg/ mL) of the radiolabeled protein solutions were incubated for 1 hour in a wet chamber at room temperature.

As can be seen from Figure 2.6, the maximum amount of adsorbed protein is about 0.81 pmol per microchannel. A correlation between the increasing amounts of the antibody adsorbed as a function of the amount loaded per microchannel is seen, as expected. This corresponds to 0.062 $cm^2$ of the channel surface, as pointed out in Section 2.4.1. This translates into a surface coverage of about 13.0 $pmol.cm^{-2}$ on the surface of the photoablated PET. The amount of surface coverage is higher than the

conventional value of 0.5 pmol.cm$^{-2}$ observed from conventional reactor surfaces like the polystyrene microtiterplate for similar analytes (55). The reasoning for an improved surface capacity of PET for protein immobilization, as articulated in Section 2.2.6, can be accounted by the presence of the hydrophobic patches and the increased surface area as a consequence of increased roughness, due to the photoablation process.

The microchannel surface, as seen from Section 2.3.1, has a laser treated PET layer and also an outer PET/PE sealing laminate layer. It is interesting to compare the adsorption capacity of these two layers. For this purpose, the sealing laminate that comprises the sealing "roof" of this microreactor was peeled off after 1-hour incubation of the labeled antibody inside the microchannel. It was then determined that the surface capacities of the lamination and the laser treated PET channel material are respectively 5.5 and 19.4 pmol.cm$^{-2}$. The relatively low adsorption capacity is not too surprising considering the fact that the lamination layer is oxidized (Figure 2.4.3) and such oxidized aliphatic polymers are usually very hydrophilic. In fact, this observation is the basis for using polyethylene glycol (PEG) and polyethylene oxide (PEO) as hydrophilic, biocompatible polymer layers in implanted medical devices and biosensors (56,57). The high adsorptive capacity for the photoablated PET surface is also supported by the increased amount of bovine serum albumin (BSA) immobilized on similar photoablated microchannel surfaces (58). By using the adsorption isotherm experiment, we have characterized the adsorptive capacity of the microchannel under consideration. This information will be very useful for designing the immunoassay experiments related to the determination

of actual kinetics and percentage of bioactive antibodies in the microchannel. These two considerations are further discussed in the following sections.

### 2.4.6 (b) Kinetics of Immunocomplex formation – Issue of Mass transport limitation vs Inherent forward rate limitation

The rate of the transport of antigen or antibody follows the principles of diffusion in solution. It is not exactly the same case on surfaces that already have the primary immunoreactant immobilized on it. Both these stages, migration in solution and on the surface, of the reactant transfer, have to be considered when reactions at different surfaces are considered. The simplest expression for the diffusive migration rate $k_0$, in solution, for an immunoreactant is obtained when the diffusion to a reactive disc of radius $r_s$ is considered. It is given by the following expression:

$$k_0=4Dr_s \qquad \textbf{Equation 2.4.1}$$

where D is its diffusion coefficient. The expression gets modified when considering the smaller, reactive region of the immobilized primary reactant for the binding process. The surface migration rate depends on $C_S$, the local concentration of the diffusing reactant, and the packing density of the primary immunoreactant on the surface. To make a comparison of the diffusion rate of the immunoreactant and the inherent forward reaction rate, a dimensionless number called the Damkoehler number, $D_a$, is employed (27). For the simplest case of the immuoreactant diffusing towards a sphere of radius R on which the primary immunoreactant is immobilized with a surface density $\Gamma_0$, $D_a$ is defined by the Equation 2.4.2:

$$D_a = R\, k_f\, \Gamma_0 / D \qquad \textbf{Equation 2.4.2}$$

where R is expressed in cm, $\Gamma_0$ is expressed in moles/cm$^2$ and $k_f$, the maximum inherent forward reaction of the association reaction, is expressed in ml/mol.sec. The Damkoehler number can be interpreted as the ratio of the maximum surface reaction rate and the diffusional rate. Hence, a $D_a$ value of greater than unity indicates that the forward reaction rate does not limit the progress of the immunocomplexaton. It is to be noted that the primary immunoreactant is considered to be immobilized on a sphere of radius R in Equation 2.4.2.

When artificial surfaces and planar reactor surfaces are considered, they can be approximated as macrospheres with radius much higher than a micrometer, in Equation 2.4.2. The Damkoehler coefficient can be estimated, using such an approximation, to determine if the immunocomplexation is likely to be limited by the diffusional rate or the inherent forward reaction rate. Values of $k_f$, $\Gamma_0$ and D are essential to make an estimate for $D_a$. When applying this expression to the current PET microchannel system, it is known from Section 2.2.2 that $k_f$ can be taken as $10^6$ L/mol.sec for antigen-antibody reactions. From Section 2.4.5, the value for surface antibody density $\Gamma_0$ is found to be 13.0 pmol.cm$^{-2}$. The value of the diffusion coefficient D, for protein antigens, can be taken approximately as 4 x $10^{-7}$ cm$^2$/sec. It can, hence, be calculated from the definition of Damkoehler coefficient ($D_a$) that the reaction of SEB-Rb $\alpha$ SEB has $D_a$ values of more than 100 for spheres of radius more than 40 $\mu$M. Considering that a flat, planar PET microchannel can be regarded

as extended macrospheres, it is predicted that the rate of immunocomplex formation will be limited by the diffusion rate of the immunoreactant and not by the inherent forward reaction rate on the surface. This conclusion can also be substantiated by comparing the actual kinetics of the immunochemical reaction and the calculated diffusion rates but the Damkoehler number consideration approach is considered to be more reliable. The real evidence for the reaction being controlled by diffusion rate of immunoreactant arrival can be obtained by comparing the time required for reaction completion, from diffusion theory, and the actual kinetics data.

**Application of Fick's second law for diffusion controlled reactions on surfaces**

An estimate of the diffusion rate of immunoreactant arrival on the microchannel surface is governed by the diffusion theory for molecules using the Fick's second law. In a fixed volume, the Fick's second law is given by the following Equation 2.4.3:

$$\frac{\partial c}{\partial t} + div(-D\,\mathrm{grad}c) = 0 \qquad \textbf{Equation 2.4.3}$$

where c is the concentration of diffusing immunoreactant in the microchannel. This equation represents the concentration of molecules reaching the surface only by diffusion in a given time. In the present channel, the cross sections are 40 x 100 $\mu m^2$ and 2 cm in length. As the third dimension is much larger the calculation can be performed using two dimensions with the boundary conditions being

at $t = 0$, $c = c_0$

at $t > 0$, $c = 0$ at the walls.

The condition c = 0 is imposed at the wall as molecules reach the wall and disappear from the solution. Based on the above Fick's law approach, the rate of diffusive migration can be calculated by assuming the diffusing reactant to be the 160 kDa IgG antibody raised against SEB. In fact, based on the Fick's law for the diffusing reactants, a numerical simulation has been performed using FluxExpert finite element software which predicts the time it takes for proteins of different sizes to reach the surface of dimensions used in the current work. Figure 2.7 depicts such a plot:

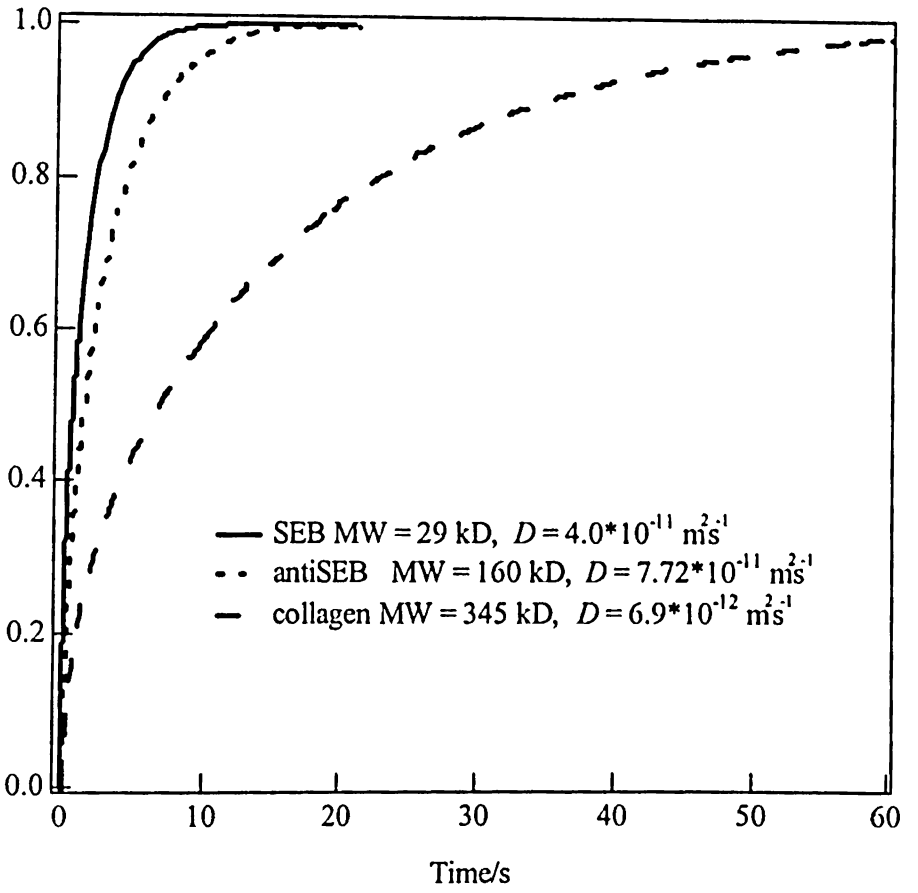


Figure 2.7: Fick's second law based prediction of the diffusion of proteins of different sizes as a function of the reaction incubation time and diffusion coefficient. SEB, Rb α SEB IgG and Collagen are the proteins considered for this simulation.

As seen from Figure 2.8, it is obvious that the incubation time required for different sized proteins to reach the surface is dependent on the molecular weight and diffusion coefficient inversely. Based on this simulation, it is predicted from the

simulation software run that all three proteins having differing diffusion coefficients as seen from Figure 2.7 should be able to reach the surface within a minute, based on the diffusive migration. The immunochemical reaction involving SEB and Rb α SEB Ab is predicted to be complete within a minute. Although this is the theoretical expectation, it is shown to be the case, based on the actual kinetic data shown in Figure 2.8.

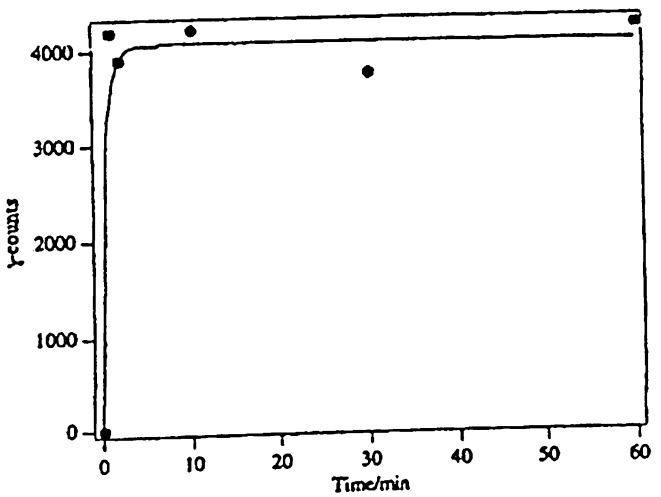


Figure 2.8: Adsorption kinetics of SEB in the photoablated microchannels. The channel was incubated with 3.12 nM of non-labeled Rb α SEB for I hour whereas the solution of SEB was incubated at 36 nM for different times, as indicated in the plot. The final detection of immunocomplexation was done by using radiolabeled Rb α SEB at 200 nM concentration.

The objective of the current work, accomplishing rapid kinetics, can thus be achieved because the immunoassay can be driven to completion within a minute by using the reduced diffusion distances that are possible in microfabricated PET microchannels.

### 2.4.6 (c) Determination of the bioactivity of the immobilized antibody

As the adsorption characteristics of the antibody along with the kinetics of the Ag/Ab reaction had yielded encouraging results, one more important factor of concern is the biological activity of the adsorbed antibody. The issue of losing the biological activity of the immobilized antibody is a significant concern. Irrespective of the immobilization strategy, the loss in the biological activity of the antibody when immobilized on surfaces is not uncommon, as noted in the literature. Covalent immobilization strategies are generally preferred (59) due to the fact that they lend greater stability to the immobilized antibody and are more amenable to surface regeneration. In fact, specific conjugation protocols including linkage through $F_c$ portion (60), through the carbohydrate functionalities (61) or through the sulfhydryl groups (62) of the antibodies have generated biological activity in the range 20% from the immobilized antibodies. Wimalasena (63) investigated the factors that affect the biological activity of immunosorbed antibody in detail. Multi-site attachment, multiple orientations and steric hindrance are found to be important issues in determining the bioactivity of the antibody. In relation to this issue, adsorption strategy is not commonly employed for lack of immunosorbent stability and also for the possibility of generating conformational issues of the antibody that may affect binding efficiency.

The biological activity of the immobilized antibody was obtained in the current microchannel system using the assay where immobilization of different amounts of the unlabeled Rb α SEB Ab was done on the channel surface. The experimental procedure for this sandwich assay is outlined in Section 2.3.7 (c). The range of unlabeled Rb α SEB Ab immobilization was varied from 0.06 to 0.31 pmoles per microchannel and it is to be noted that the maximum amount of the immobilized antibody has been determined to be 0.81 pmoles per microchannel. Molar excess of SEB is then incubated for reaction with the immobilized antibodies. The fraction of the active antibody can be found by using the labeled Rb α SEB antibody as the detection antibody. The percentage of bioactive antibody, determined by calculating the number of moles of antigen bound as a percentage, was calculated to be 30 ± 5.

It must also be pointed out the bioactivity of the immobilized antibody, in any form, on UV treated PET has not been previously reported. Going by the extensive literature available on this issue, the percentage seen in the current case is not unreasonable. It should also be noted, however, that glow discharge treated PET surfaces have had a bioactivity of close to 20% from a previous study (64). The adsorbed antibodies for fluorescein on polystyrene have also demonstrated close to 18% biological activity (65), inspite of not having high stability upon immobilization. This was found to be the case in atrazine antibody immobilization study also (66). While it is possible that the adsorbed antibody is not very stable for a longer period of time in the PET microchannels, this issue has not been studied in this work.

## 2.5 Chapter conclusions and Future work

The need to carry out rapid, specific detection of biowarfare agents and clinical biomarkers are now more important than ever before (67-70), especially in the context of proteomics. The ability to implement rapid, inexpensive point of care and diagnostics assays can be a useful bioanalytical advance. The overall objective of this work was to explore a novel method of carrying out rapid immunosorption assays. It was hypothesized that reduction of the diffusion distances for immunoreactants using miniaturized immunoassay reactors can help achieve rapid reaction kinetics. The technology of microfabricated PET channels, made by excimer laser photoablation techniques, has been tested to carry out this objective successfully. Use of such μ-TAS like systems offers a fundamentally better approach to speed up immunoassays, in comparison to other possible approaches. The specific goal for this current application was to explore the potential of using PET microchannels for rapidly detecting a toxic protein SEB. Fundamental issues that required consideration include the ability to fabricate microchannels without leakage, characterization and chemical nature of the channel surface, utilization of suitable immunoreactants with high binding affinity and estimation of the bioactivity of immobilized antibodies. All of these issues were systematically investigated using appropriate techniques and instrumentation. Radiometry was adapted as the detection method of choice mainly because of the high sensitivity that it can afford and due to the fact it is a mass-sensitive detection method.

An efficient way to fabricate the microchannel reactors, as described in Section 2.3.1, has been found using excimer laser based photoablation of polymeric surfaces

and it has been employed to create suitable photoablated surfaces for the current application of interest. The channel layout used for the application is the simple line-and-ring format whereby linear flow channels are used for the reagent flow. The flow system used here also was devoid of pumps and tubing as the objective was a feasibility study based on forced convection as the flow mode. More detailed investigations employing this approach can include application of different immobilization technologies, use of improved and automated flow systems, employment of a different, non-radioactive detection techniques and optimization of polymeric surface being used.

More work regarding the application of polymeric microfabricated surfaces for effecting rapid immunoassays have surfaced since our work and expectedly, most of them use electrokinetic mode of flow as the preferred approach (71,72). Rossier and coworkers have even used this microchannel system to carry out ELISA based on electrochemical detection and have compared the accuracy of this approach in comparison to the conventional approaches (73). The results from such studies definitely reinforce the excellent potential of these microfabricated systems for carrying out rapid assays. Some of the well-known facts about polymeric, photoablated surfaces including increased surface roughness and hydrophobicity have been confirmed in our work. In the current post-genomics era more applications using similar μ-TAS systems can be expected.

**References:**


1) *Diagnostics in the year 2000*, Singh, P.; Sharma, B. P.; Tyle, P.; Ed. Van Nostrand Reinhold, 1993, p 2-7.

2) *The Immunoassay handbook*, Wild, D.; Ed. Macmillan Press, New York, 1994, p 137-236.

3) Deshpande, S. S. *Enzyme immunoassays*: From concepts to product development, Chapman & Hall, New York, 1998, p 275-353.

4) Yalow, S.; Berson, S. A.; *Nature* **1959**, 184, 1648.

5) Kohler, G.; Milstein, C.; *Nature* **1975**, 256, 495-497.

6) *The Immunoassay handbook*, Wild, D.; Ed., Macmillan Press, New York, 1994, p 389-400.

7) Thomas, C. M. G.; Segers, M. F. G.; Houx, P. C. W. *Ann. Clin. Biochem.* **1985**, 22, 236-246.

8) Papadea, C.; Foster, J.; Grant, S.; Ballard, S. A.; Cate, J. C. I.; Southgate, W. M.; Purohit, D. M. *Ann. Clin. Lab. Sci.* **2002**, 32, 231-243.

9) Tojo, M.; Shibata, N.; Mikami, T.; Suzuki, M; Suzuki, S. *Clin. Chem.* **1987**, 33, 1925-1928.

*10)* Wolf-Rogers, J.; Weare, J. A.; Rice, K.; Robertson, E. F.; Guidinger, P.; Khalil, O. S.; Madsen, G. *J. Immunol. Meth.* **1990**, 191-198.

*11)* Gregorius, K.; Theisen, M. *Anal. Biochem.* **2001**, 299, 84-91.

*12) Quantitative Enzyme Immunoassay*, Engvall, E.; Pesce, A. J.; Ed. Blackwell Publications, Oslo, 1978, p 111-118.

*13)* Beumer, T.; Haarbosch, P.; Carpay, W. *Anal. Chem.* **1996**, 68, 1375-1380.

*14)* Montagne, P. M.; Tregoat, V. S.; Cuilliere, M. L.; Bene, M. C.; Faure, G. C. *Clin. Biochem.* **2000**, 33, 181-186.

*15)* Wang, J.; Pumera, M.; Chatrathi, M. P.; Escarpa, A.; Konrad, R.; Griebel, A.; Dorner, W.; Lowe, H. *Electrophoresis*, **2002**, 23, 596-601.

*16)* Vandaveer, W. R. I. V.; Pasas, S.; Martin, R. S.; Lunte, S. M. *Electrophoresis* **2002**, 23, 3667-3677.

17) Jiang, T.; Halsall, H.B.; Heinemann, W. R. *J. Agric. Food Chem.* **1995**, 43, 1098-1104.

18) Chiem, N.; Harrsion, D.J. *Anal. Chem.* **1997**, 69, 373-378.

19) Roberts, M. A; Rossier, J. S.; Bercier, P.; Girault, H.H. *Anal. Chem.* **1997**, 69, 2035-2042.

20) King, K.D.; Anderson, G.P.; Bullock, K. E.; Regina, M. J.; Saaski, E.W.; Ligler, F. S.; *Biosens. Bioelectron.* **1999**, 14, 163-170.

21) Tempelman, L. A.; King, K. D.; Anderson, G. P.; Ligler, F.S. *Anal. Biochem.* **1996**, 233, 50-57.

22) Rossier, J. S.; Gokulrangan, G.; Girault, H. H.; Svojanovsky, S.; Wilson, G. S. *Langmuir* **2000**, 16, 8489-8494.

23) *Principles and practice of immunoassay,* Price, C. P.; Newman, D. J.; Eds. Stockton Press, NY, 1997, p 17-34.

24) Bell, G. I.; DeLisi, *Cell Immunol.* **1974**, 10, 415-424.

25) Steward, M. W. *Antibodies: Their structure and function* Chapman & Hall, NY,1983.

26) Stenberg, M.; Nygren, H. *J. Theor. Biol.* **1985**, 113, 589-597.

27) Stenberg, M.; Nygren, H. *J. Immunol. Methods* **1988**, 114, 3-15.

28) Pesce, A.; Michael, G.J. *J. Immunol. Methods* **1992**, 150, 111-119.

29) Tyn, M. T.; Gusak, T. W. *Biotechnol. Bioeng.* **1990**, 35, 327-338.

30) Richardson, M.; Turner, A.; Warnock, D.; Llewellyn, P. J. *J. Immunol.* Methods **1983**, 56, 201-207.

31) Hoffman, W. L.; O'Shannessy. *J Immunol. Methods* **1988**, 112, 113-117.

32) *Handbook of Immunology*, Weir, D. M; Ed. Oxford, New York, Vol1 p 38.1-38.17.

33) Beumer, T.; Timmerman, B. *Anal. Chem.* **1997**, 69, 5182-5185.

34) Beumer, T.; Haarbosch, P.; Carpay, W. *Anal. Chem.* **1996**, 68, 1375-1380.

35) Levine, I. N.; *Physical Chemistry* McGraw-Hill, New York, 1983, p 467-470.

36) Dodge, A.; Fluri, K.; Verpoorte, E.; de Rooij, N. F. *Anal. Chem.* **2001**, 73, 14, 3400-3409.

37) Jiang, X.; Ng J. M. K.; Abraham, S. D.; Stephan, D. K. W.; Whitesides, G. M. *J. Am. Chem. Soc.* 2003, 125, 18, 5294-5295.

38) Mao, H.; Yang, T.; Cremer, P. S.; *Anal. Chem.* **2002**, 74, 379-385.

39) Martin, B. D.; Gaber, B. P.; Patterson, C. H.; Turner, D. C. *Langmuir* **1998**,14, 3971-3975.

40) Yakulova, J.; Davidsson, R.; Labanova, A.; Bengtsson, M.; Eremin, S.; Laurell, T.; Emneus, J. *Anal. Chem.* **2002**, 74, 2994-3004.

41) Lazare, S.; Hoh, P.D.; Baker, J. M.; Srinivasan, R. *JACS*, **1985**, 106, 4288-4290.

42) Srinivasan, R.; Braren, B.; *Chem. Rev.* **1989**, 89, 1303-1316.

43) Roberts, M. A.; Rossier, J. S.; Bercier, P.; Girault, H. H. *Anal. Chem.* **1997**, 69, 2035-2042.

44) Rossier, J. S.; Girault, H. H. *Lab Chip* **2001**, 1, 153-157.

45) Rossier, J. S.; Girault, H. H. *Phys. Chem. Chem. Phys.* **1999**, 1, 3647-3652.

46) Markwell, M. A. K.; *Anal. Biochem.* **1992**, 125, 427-432.

47) Wagner, F.; Hoffmann, P. *App. Physics A* **1999**, 69 (Supp), S841-844.

48) Johnson, T. J.; Waddell, E.; Kramer, G. W.; Locascio, L. E.; *App. Surface Sci.* **2001**, 181, 149-159.

49) Rossier, J. S.; Bercier, P.; Schwarz, A.; Loridant, S.; Girault, H. H. *Langmuir* **1999**, 15, 5173-5178.

50) Davison, P. F. *Biochim. Biophys. Acta* **1987**, 926, 195-202.

51) Nakamura, M.; Kuminami, G.; Masa, K. *Radioisotopes* **1991**, 40, 112-117.

52) Bolton, A. E.; Hunter, W. M. *Biochem. J* **1973**, 133, 529-539.

53) Ross, J.; Janero, D. R.; Hrenoik, D.; Weenogle, L. P. J *Biochem. Biophys. Methods* **1993**, 26, 343-350.

54) Harrison, I.; Higgo-Jennfier, J. W. *App. Radiation Isotopes* **1994**, 45, 345-351.

55) Chataway, T. K.; Barritt, G. J. *Mol. Cell. Biochem.* **1994**, 137, 75-83.

56) Nygren, K.; Werthen, M.; Stenberg, M. J. *J Immunol. Methods.* **1987**, 101, 63-67.

57) Sofia, S. J.; Premnath, V.; Merril, E. W. *Langmuir* **1998**, 15, 5059-5070.

58) Mcpherson, T.; Kidane, A.; Szleifer, I.; Park, K. *Langmuir* **1998**, 14, 176-186.

59) Schwarz, A.; Rossier, J. S.; Roberts, M. A.; Girault, H. H.; Roulet, E.; Mermod, H. *Langmuir* 1998, 14, 5526-5531.

60) Peterman, J. H.; Tarcha, P. J.; Chu, V. P.; Butler, J. E. *J Immunol. Methods.* **1998**,111, 271-275.

61) Mifflin, T. E.; Hamilton, M.; Hubbard, E.; Kline, M. J.; Bruns, D. E. *Methods*

*Enzymol.* 1976, 9, 453-476.

62) Cress, M. C.; Ngo, T. T. *Am. Biotech. Lab.* **1989**, 7, 16-19.

63) Wimalasena, R. L.; Wilson, G. S. *J. Chrom. A* **1991**, 572, 85-102.

64) de Alwis, U.; Wilson, G. S. *Anal. Chem.* **1987**, 59, 2786-2789.

65) Safranj, A.; Kiaei, D.; Hoffmann, A. S.; *Biotech. Prog.* **1991**, 7, 173-177.

66) Butler, J. E.; Ni, L.; Nessler, R.; Joshi, K. S.; Suter, M.; Rosenberg, B.; Chang, J.; Brown, W. R.; Cantarero, L. A. *J Immunol. Methods* **1992**, 150, 77-90.

67) Munro, N. J.; Snow, K.; Kant, J. A.; Landers, J. P. *Clin. Chem.* **1999**, 45, 1906-1917.

68) Landers, J. P. *Anal. Chem.* **2003**, 75, 2919-2927.

69) Prieto, M. C.; Koutoun, V. V.; Cotter, R. J. *J Mass Spec.* **2002**, 37, 1158-1162.

70) Sanders, J. C.; Breadmore, M. C.; Mitchell, S. P.; Landers, J. P. *Analyst* 2002, 127, 1558-1562.

71) Linder, V.; Verpoorte, E.; De Roonij.; Sigrist, H.; Thormann, W. *Electrophoresis* **2002**, 23, 740-749.

72) Sato, K.; Tokashi, M.; Kimura, H.; Kitamori, T.; *Anal. Chem.* **2001**, 73, 1213-1218.

73) Rossier, J. S.; Girault, H. H. *Lab on a Chip* **2001**, 1, 153-157.

## Chapter 3

# Optimization of the Fluorescence Polarization Response in the Determination of IgE Employing a DNA Aptamer

## 3.1 Introduction and Current objectives

### 3.1.1 DNA-Protein interactions, SELEX Process and Aptamers

The importance of DNA-protein interactions in the control of growth, differentiation and development of eukaryotic systems (1-3) has been well established. The interactions have key roles to play in the DNA organization, transcription and translation pathways as well in as the DNA replication process (4,5). Specifically, these interactions are involved in the following cellular requirements - packaging and folding of DNA through interactions with histones in the chromatin structure, repressor/enhancer sequence – responsive element interaction to promote transcription, t RNA - aminoacyl t RNA synthetase interactions in the translation process and maintenance of telomeres, besides being an important factor in the DNA replication and recombination processes. The above-mentioned significance of DNA-protein interactions, thus, highlights the need for careful characterization of their association as these complexes can lead to possible therapeutic targets, especially for genetically linked disorders (6). Although the sequence information of the binding DNA for most of the naturally binding proteins is well known, it is possible to isolate new sequences *in-vitro* (7) from new binding experiments for such targets. It is also possible that proteins that are not previously known to bind ss DNA sequences may recognize novel DNA sequences. The process of isolating such novel sequences was facilitated by the Nobel winning discovery of the polymerase chain reaction (PCR) by Mullis and coworkers (8). This technique can be used to amplify such sequences typically upto million fold through simple enzymatic reactions and hence the problem of synthesizing large amounts of the nucleic acid sequences of interest has, since, proven not to be an impediment.

The experimentation related to the *in-vitro* nucleic acid ligand selection has become more practical due to the emergence of novel experimental methods and technologies (9,10) that are focused on using the advantages of PCR in conjunction with combinatorial *in vitro* selection experiments. From an initial combinatorial pool of nucleic acid sequences, specific binding sequences can be isolated using stringent binding conditions. The Selected and Amplified Binding (SAAB) technique was one such method that gained initial prominence. Proteins like bacteriophage R17 coat protein and the basic-helix-loop-helix (b HLH) motif containing c-Myc protein were found to recognize some novel DNA sequences with high affinity using the SAAB technique (11,12). Although the initial progress in this area was made using such DNA binding proteins, these ligand selection experiments were also later extended to non-DNA binding proteins and even small molecules. An improved form of the SAAB technique, termed "SELEX" (**S**ystematic **E**volution of **L**igands using **Ex**ponential Enrichment) became increasingly used. This technique uses the iterative procedure of ligand selection, involving successive rounds of ligand selection, with a progressive rise in the stringency of binding conditions. Each step involved the identical procedural sequence of ligand selection, removal of unwanted or non-binding sequences and finally amplification of the sequences of interest, using appropriate nucleic acid primer sequences. The finally chosen binding DNA sequences, referred to as "Aptamers", provide ligands that serve as molecular recognition elements. The process of SELEX is illustratively shown (13) in Figure 3.1.

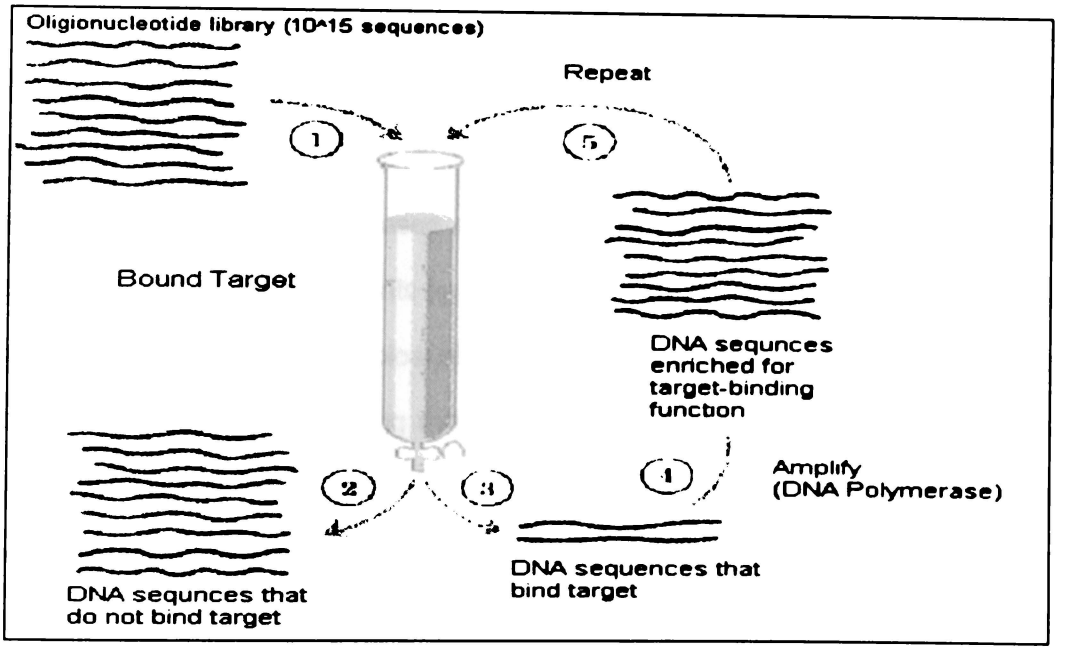


Figure 3.1: Sequential steps involved in the SELEX process: ligand selection, amplification and reselection of nucleic acid ligands. Picture is adapted from Reference 13.

### 3.1.2 Aptamer – Unique biomolecular recognition element

The SELEX procedure has been adapted to identify nucleic acid based ligands for a wide variety of targets including hormones, dyes, peptides, cofactors and proteins (14-18). The fundamental molecular interactions involved in the aptamer-target binding process include hydrogen bonding, electrostatic and intercalative interactions. The predominant force in the binding interaction depends on the specific target involved although adaptive binding has been a recurrent theme (19,20). Aptamers are unique and are, unlike antibodies, much smaller in size. The issues of immunogenicity and extensive animal use that often prohibit the immunochemical

approach are not major concerns when using aptamers. Hence, it was perceived that aptamers could be used as potential substitutes for antibodies in many bioanalytical applications. The high binding affinity for different analytes, especially the protein targets, possible in aptamer-based systems has further encouraged their use. The rapid detection of binding events is critical for advances in drug discovery (21,22), molecular diagnostics and bioanalytical applications that involve biomolecular recognition (23,24). The binding event is often measured by making a separation, typically facilitated by immobilizing the recognition element on a surface, and heterogeneous assays (25) are based on this principle.

The demands of high throughput have, however, put greater emphasis on homogeneous assays that do not require separations. Fluorescence based approaches have often proved to be very sensitive and also rapid to implement. Specifically, fluorescence polarization (FP) (26,27) has been used for a number of years as the basis for clinical diagnostic tests, in particular for immunoassays of therapeutic drug molecules (28,29). The binding of the drug to the antibody restricts motion of the drug, thus altering its FP properties. This approach is, unfortunately, not generally applicable to analysis of proteins because only very small changes in FP can be observed. Use of aptamers (30) opens up the possibility of employing a small fluorescently-labeled biological recognition element to analyze larger molecules. The typical base numbers for the aptamers range from about 12 to 90 and hence they possess molecular weights in the range of 5 to 27 kDa. A further important advantage of using the aptamers for FP applications is the availability of convenient labeling chemistries that can incorporate a wide variety of fluorophores (31). Amongst the nucleic acid ligands, DNA aptamers are generally preferred to

RNA ligands for their better chemical and biological stability. Furthermore, automated aptamer generation platforms (32), innovative SELEX protocols and improved DNA syntheses have opened up more possibilities for using DNA aptamers in analytical method development. In the area of protein detection, both heterogeneous and homogeneous assays using DNA aptamers have been employed (33,34). Very sensitive protein detection has been accomplished using both approaches. The detection of a cancer marker protein, platelet development growth factor (PDGF), has been accomplished using the FP approach in the homogeneous format (34). A few FP applications are also known where the ss DNA sequences used are not aptamers (35-37). These are applications in which labeled DNA ligands have been utilized to carry out sensitive detection of proteins and peptides. Thus the ss DNA aptamers, in comparison to antibodies, are potentially better suited to carry out FP-based peptide and protein detection.

### 3.1.3 Homogeneous IgE detection

Rapid detection of Immunoglobulin E (IgE) is of considerable interest in patients afflicted with allergy-mediated disorders. It is the immunoglobulin component found in the low nM levels in human serum. IgE levels, however, significantly increase in cases of allergic asthma, atopic dermatitis and other immune deficiency related disorders, including the acquired immunodeficiency syndrome (AIDS). A SELEX-based high affinity DNA aptamer D17.4 (38) was isolated by Wiegand and coworkers and is known to bind IgE very specifically. Although other approaches like affinity probe capillary electrophoresis (APCE) have been attempted using the D17.4 aptamer, it is very useful to develop a homogeneous approach for IgE bioanalysis. The hypothesis for the current FP approach hinges on the observable anisotropy

changes during the binding process, as shown using the following schematic (Figure 3.2):

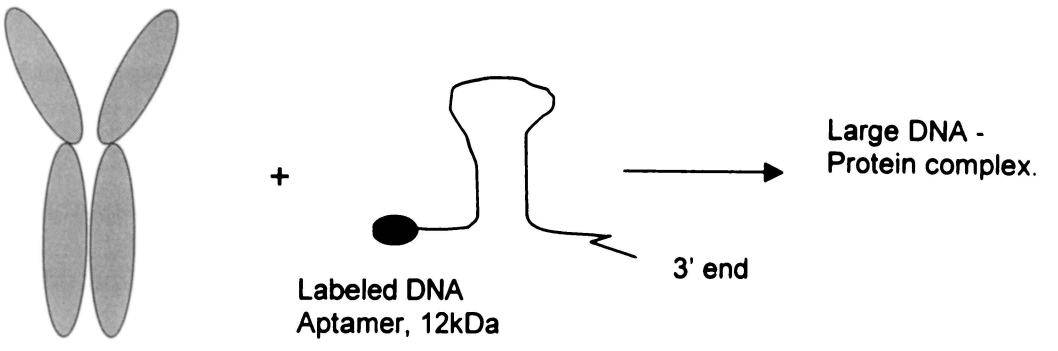


**Figure 3.2:** Hypothesis for IgE bioanalysis using the FP approach: Anisotropy increase upon the DNA aptamer-IgE binding process can be expected due to the difference in size between the labeled DNA ligand and the bound complex.

As shown in Figure 3.2, the steady state anisotropy of the labeled DNA ligand can be expected to increase significantly upon biding to the IgE target. This is due to the fact that the diffusional rotation of smaller, labeled DNA ligand is faster than the larger ligand-target complex. The anisotropy, which is inversely related to the diffusional rate of the labeled molecules, can be measured using a plane-polarized light source (39). Under equilibrium binding conditions, the increase in the anisotropy can then be used to detect IgE. The focus of the current chapter is the detailed analysis of this FP approach in relation to the D17.4 aptamer system.

Although the fluorescence-based techniques are inherently sensitive, it is important to understand the fundamental experimental variables in order to optimize the

sensitivity of FP response that has a direct bearing on the LOD of the analyte. Obtaining the greatest anisotropy change associated with the binding event, however, depends on various factors – the initial anisotropy, $r_0$, or limiting anisotropy of the labeled DNA ligand prior to any depolarization, the steady state anisotropy, r, of the labeled DNA probe and correlation of r to the motion of the DNA to which the fluorophore is conjugated. Comparison of the lifetime, $\tau$, and rotational correlation time, $\varphi$ or $\tau_{rot}$, of the fluorophore when it is conjugated to the DNA and also the size of the analyte to which the labeled DNA ligand is bound must also be considered. Using the 5' end-labeled D 17.4 ligand that has fluorescein or Texas Red (TR) conjugated as fluorophore, we have successfully carried out the homogeneous bioanalysis of IgE based on the measurement of steady state anisotropy changes. It is our aim, in this chapter, to systematically assess and report the relative importance of different experimental factors like the choice of fluorophore, temperature and the labeling strategy in order to optimize the FP response. Suitable DNA-dye conjugates have been designed and used in this current work in order to address the above-mentioned objectives. Although the aptamer used here has a unique conformation, the observations from this work are, nevertheless, expected to be very informative when considering applications for other aptamers using FP.

## 3.2 Prior art and Current Issues

### 3.2.1 Bioanalytical applications of DNA aptamers

Numerous aptamers (14-18) have been isolated for a wide variety of analytes since 1990, when the report of the first SELEX-based ligand was published, and hence the potential to adapt aptamers for analytical applications has always been perceived to be high. The research progress in this area has been, however, surprisingly limited.

The initial analytical applications were based on the well-characterized aptamer systems – the thrombin and ATP binders (40, 41). Fluorescently labeled thrombin aptamer was covalently immobilized to a glass support and free thrombin in solution was detected using the evanescent-wave-induced anisotropy changes of the labeled aptamer. A detection limit of 0.7 attomole of the thrombin target was reported (42) using this approach, although the instrumentation required to use this approach is expansive. An enzyme linked oligonucleotide assay (ELONA) was attempted for the detection of the vascular endothelial growth factor (VEGF) in a microtiterplate, using an approach (43) analogous to the enzyme linked immunosorbent assay (ELISA) format. Unlike the antibody based ELISA, the aptamer based ELONA had severe limitations because the aptamer could only be used in the detection step, but not as the capture reagent, due to the influence of non-specific binding. Although this approach was novel, the accuracy of the method was inadequate. Considering that the aptamers are polyanionic ligands, it is not surprising that non-specific binding was encountered in heterogeneous assays like ELONA. Highly charged recognition elements have a greater propensity for electrostatic interactions and non-specific binding.

Aptamers have been, however, more effectively used as the recognition element in affinity probe capillary electrophoresis (APCE) applications where the bioaffinity interactions of aptamer-target and the separation efficiency of CE are coupled together. The separation of the negatively charged aptamers and the target-bound aptamer complex can be used as the basis for detection of the analyte concentrations. This approach has been successfully used to detect protein targets including thrombin, IgE and the HIV reverse transcriptase (HIV RT) (44,45). Although

the method is not an equilibrium binding experiment, linear dynamic ranges for protein detection have been achieved in all three cases, to varying degrees. The technique has not proven to be user-friendly and reproducibility issues have also been a matter of concern. Affinity chromatography has also involved the use of immobilized aptamers. The ATP binder and L- selectin binder (46) have both been used in this application and the results from these studies have been encouraging. The ATP aptamer has also been successfully conjugated to a porous chromatographic support using the avidin-biotin linkage for frontal chromatography. Immobilized aptamer using this chemistry was found to retain its solution binding characteristics and could discriminate even closely related analogues of adenosine (33). Similar results were obtained for the selectin binder as well, suggesting that aptamer based stationary phases can be used to affinity purify analytes.

Novel work in relation to the use of DNA aptamers as stationary phase materials has also been performed in the McGown labs (47-50) where immobilized aptamers have been used for non- target separation, amino acid mixture separation and protein isomer separations using open tubular capillary electrochromatography (CEC). Although the separation efficiency and the peak resolution for the separations have not been very good, this seems to be a promising new direction in utilizing the DNA aptamers for bioanalytical applications. Another logical application of DNA aptamers, as mentioned in section 3.1.3, is the use of fluorescently labeled aptamers for detecting proteins, peptides and small molecules both in the homogeneous and heterogeneous formats. The ATP aptamer, that was labeled at specific sites with fluorescein or acridine, has been utilized to detect ATP (51) homogeneously based

on the fluorescence intensity changes observed during the binding process. This application was feasible due to the fact that the bases involved in the binding process were identified using molecular modeling experiments and used accordingly for the labeling strategy. Thus the ATP aptamer was indirectly converted into a self-signaling aptamer such that it reports the concentration of the target based on the fluorescence intensity changes observed due to binding interactions with ATP. The FP approach was also taken up in the homogeneous detection of platelet development growth factor (PDGF) (34) and a proof of principle for the approach was accomplished by the Tan group.

The principal advantage of the FP approach in comparison to all the other applications discussed here is that the technique involved is very simple, user-friendly, sensitive and involves the homogeneous format that helps in monitoring of the binding events rapidly. The detailed consideration of the different variables that influence the sensitivity of the FP response is the subject of further discussions in this chapter.

### 3.2.2 Current approach – FP method

End-labeling strategy is the most common FP approach when using labeled DNA systems. The FP approach was applied for the first time in 1990 (52), by Heyduk and Lee, using a 32 base-pair DNA fragment of the lac promoter that contains the primary binding site for the E coli cyclic AMP receptor protein (CRP). The method was used to monitor the receptor-promoter binding. The method was also extended to probe the interactions of labeled DNA with histones and also for monitoring the association of certain transcription factors with specific DNA sequences, which

functioned as promoters or repressors (53-57). The thermodynamic binding constants for the DNA-protein interactions were also obtained in these systems in which the binding stoichiometry was well known. The data obtained from this approach were found to be comparable to filter binding assays and other conventional experimental approaches used for determining the binding constants. Thus the FP approach, theoretically, can be considered as a substitute for radioligand binding assay used to quantify DNA-protein binding interactions. Fluorescein has been the most frequently used dye label in the development of DNA based FP assays. The main reason for this was the absence of reliable alternatives with comparable quantum yield and established high yield conjugation chemistry, from commercial DNA vendors. The availability of newer dyes for FP applications has, however, improved possibilities recently (58).

Two conventional chemistries are followed for incorporating a label on the 5' end of the DNA – appending a fluorescein labeled nucleoside to the last base of the sequence of interest using automated synthetic protocols or by adding a 5'-phosphoramidite that has a variable linker arm with a reactive end group that can be further reacted with a suitable derivative of the dye of interest. The second approach is more versatile because the dye can be appended to the DNA with variable carbon chain lengths on the 5'-end.The second strategy is also more useful because a wide variety of dyes can be appended using different tether lengths on the DNA of interest. The specific concerns associated with the use of fluoresein conjugates are mentioned below.

### 3.2.3 Issues related to the Fluorescein conjugates

The general difficulty encountered in using any fluorescein conjugate is the pH sensitive quantum yield of the fluorophore in its conjugated form. The optimum pH value recommended for its use is around 7.5. The dye at neutral pH is dianionic. This property may lead to electrostatic repulsion by the polyanionic backbone of the DNA and give rise to significant local dye motion, when conjugated to the DNA. The fluorescein conjugates have been consistently used in spite of the fact that the steady state anisotropy of the labeled ligands is far below the values (59) that can be expected, based on the size of the DNA that is labeled. The low initial anisotropy of the fluorescein-labeled ligands can have definite and serious ramifications for the FP approach. The dye can have significant local rotation with respect to the DNA instead of sharing the global motion of the DNA alone. This is, obviously, unfavorable for the FP approach where the principle of the detection method hinges on the fact that the motion of the dye should be coupled to DNA binding. The variation of the linker arm or the tether length may help a bit in that shorter tether lengths usually promote less local dye motion, as noted by the McGown group and others (60). Nevertheless, this is a problem that deserves careful consideration. The availability of newer fluorescent dyes with more favorable photophysical and charge characteristics can be used to overcome this problem. We wanted to confirm if the fluorescein related issues persist with labeled aptamers also and if so, we sought to explore the fundamental factors that dominate the sensitivity of the FP response. It is to be pointed out that the D17.4 IgE aptamer that is used in this work has a stem-loop conformation and, hence, the observations made using this system may not perfectly

apply for other aptamer systems. Nevertheless, it will be very useful to characterize such labeled aptamers to optimize the current system.

### 3.2.4 Conjugates used for the current FP study

Figure 3.3 illustrates the dye-DNA conjugates used in the current work – **1A, 1B** and **1C**.

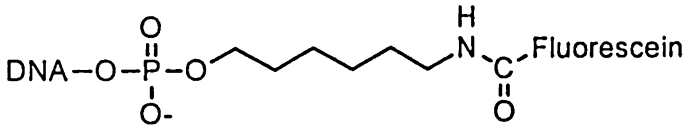


Structure **1A**

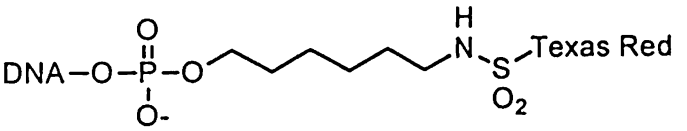


Structure **1B**

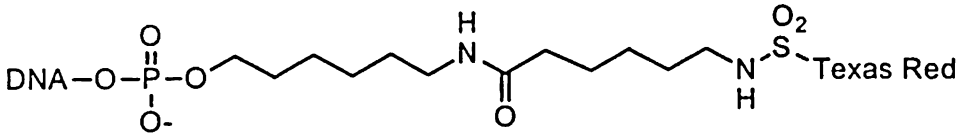


Structure **1C**

**Figure 3.3:** The covalent conjugates of the dye that are coupled to the 5' end of the 37-mer DNA aptamer, the D17.4 stem-loop system.

As seen from the structures of these conjugates, the two variables are the dye itself and the tether length that links the dye to the 5' end of the DNA. It is to be noted that the tether length is chosen to be not too long as such long linker-arms are considered unfavorable to track the global DNA motion efficiently. Titration experiments, involving suitable DNA and protein concentrations, are used to understand the usefulness of these three probes for IgE detection. The analytical figures of merit using this FP approach, in comparison to other reported methods, are also reported in the current work.

### 3.2.5 Experimental factors influencing the FP response

In order to address the main objective of this work, the optimization of the sensitivity of FP response, the following factors are considered to be important from the known FP literature – the labeling strategy that includes the tether linkage and choice of fluorophore, temperature, comparable dye lifetime and DNA rotational correlation time (RCT), size of the analyte and finally the presence or absence of dye-DNA interactions in the conjugates. Alkyl linker arms are typically used to conjugate the active form of the dyes to reactive ends of the phosphoramidite-modified DNA, although such linkers are not very soluble in aqueous solution. In this study, we have also focused on alkyl linker arm based conjugates mainly because it is harder to obtain conjugates that are more hydrophilic, polyethylene glycol (PEG) linkers for example, without compromising on the tether length and the synthetic yield of the DNA. It is to be noted that the length of the dye tether is designed to be not too long in the conjugates used for the current work. This is done to maximize the possibility that the labeled ligand will share the global DNA motion well.

Temperature plays a critical role in the FP approach in two ways – impact on the binding properties of the DNA aptamer and on the shift in the contributions to the total anisotropy from its different components. From steady state anisotropy measurements, it may not be possible to differentiate the two effects, as the measurements are made under averaged signal measurement conditions. The changes in the binding affinity of the aptamer is not considered to be a major issue in the temperature range of 25-37°C as the original SELEX experiment to isolate the D17.4 aptamer is itself carried out at 37°C (38). The lifetimes of both fluorescein and Texas Red (TR) are around 5 ns and this is comparable to the rotational correlation time (RCT) or the tumbling rate of the 37-mer DNA. If the fluorophore lifetime is long in comparison to the tumbling rate of the DNA, then the FP approach will not be useful for tracking the binding process efficiently (39). This is due to the fact that the dye on the DNA can be more easily depolarized during the long lifetime of the fluorophores and hence cannot be relied upon to reflect the global motion of the DNA. Therefore fluorophores with otherwise favorable photophysical features, but with very long lifetimes, may not be useful. The size of the analyte is favorable for the FP approach in the current problem as IgE is 200 kDa in molecular weight when compared to the 12 kDa of the labeled DNA ligand. The anisotropy changes that may be expected from the current system can, hence, be significant. It is hard to predict the probability of favorable dye-DNA interactions in the conjugates that one may work with, but this is a variable that may be used to comprehend some of the consequences when using a specific fluorophore.

Detailed, time-resolved spectroscopic investigations can usually shed more information regarding the microscopic details of the dye-DNA system. The current work is focused on understanding the relative roles of all the above-mentioned experimental factors in the context of optimizing the FP response for the D17.4 aptamer system. There is, of course, more possibility for optimizing the FP reponses using other variables but the focus of this chapter has been to explore the most significant factors.

## 3.3 Materials and Methods

### 3.3.1 D 17.4 Aptamer, DNA conjugates and Sample preparation

D 17.4 aptamer, the 37-mer ss DNA sequence, has the following sequence: 5'-GGGGCACGTTTATCCGTCCCTCCTAGTGGCGTGCCCC-3'. The tertiary structure of the aptamer, as determined by predictive algorithm is given below in Figure 3.4:

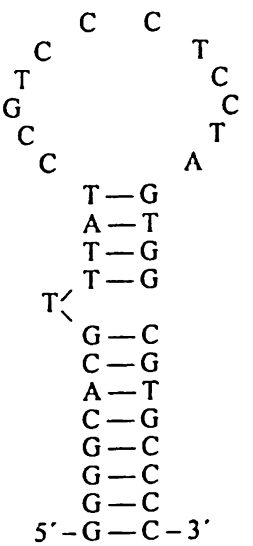


Figure 3.4: Stem-loop motif - The predicted tertiary structure of the D 17.4 IgE binding aptamer.

For the current work, the consensus sequence of the D17.4 ligand was used for designing the FP probes. The structures of the dye-DNA conjugates are shown in Section 3.2.4 with structure **1A** representing the fluorescein conjugate with a 6 carbon linker whereas **1B** and **1C** refer to the Texas Red conjugates with a 6 carbon linker and a 12 carbon linker respectively. Commercially synthesized DNA aptamer with the fluorophore modifications was purchased from Integrated DNA technologies (Coralville, IA) in the case of conjugates **1A** and **1C** whereas the conjugate **1B** was obtained from Midland Certified Reagents Inc (Midland, Texas). The unmodified DNA aptamer, used for various control experiments, was purchased from Integrated DNA Technologies. All the commercial DNA samples were obtained in either HPLC or gel purified form. Polyacrylamide gels (15% non-denaturing) were used to confirm the purity of the commercial DNA samples. High concentration DNA stock solutions were made up in water, for long term storage, and diluted in the appropriate buffer prior to use. Aptamer solutions were melted at 70°C and cooled sufficiently prior to use, in keeping with standard DNA handling practices designed to minimize structural misfolding. The binding buffer composition, based on the reported SELEX conditions (38) was always 8.1 mM $Na_2HPO_4$, 1.1 mM $KH_2PO4$, 1mM $MgCl_2$, 2.7 mM KCl and 138 mM NaCl.

IgE was procured from Athens Research and Technology Inc. (Athens, GA). The protein was obtained in phosphate buffer pH 7.2 and used without further purification. The samples were checked by the vendor's quality control experiments for >95% purity and also verified to give a single blot in immunoblotting experiments. The exact concentration of the stock IgE solutions was also verified by the BCA

protein assay (Pierce Chemicals, Rockford, IL). The protein samples were prepared and left on ice when not used to minimize any denaturation. IgG used for aptamer specificity studies was also obtained from Athens Research and Technology Inc (Athens, GA) whereas BSA, Lysozyme and HSA were all obtained from Sigma Chemicals (St.Louis, MO).

### 3.3.2 Fluorescence Polarization Measurements

An illustrative picture shows the anisotropy measurement below, in Figure 3.5.

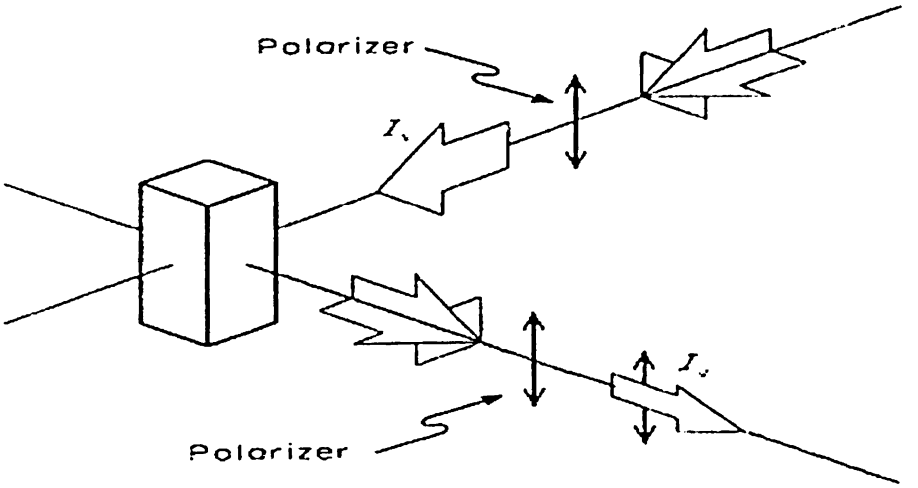


Figure 3.5: Anisotropy measurement: Polarized emission of the fluorophore is measured in the vertical and horizontal planes, using a vertically polarized excitation source. Picture is adapted from Reference 39.

Anisotropy can be determined by making the measurements of the polarized emission in the vertical and horizontal (V and H) planes using a vertical excitation

source is shown in the above figure. The polarizers can be mounted on conventional spectrofluorometer instrumentation, making the FP measurements user-friendly. An appropriate instrument correction factor, termed the G factor, corrects for any intensity bias that may exist either in the vertical or the horizontal plane due to instrument properties. This instrument correction factor has to be checked very often by checking the emission in both planes using excitation in the horizontal plane.

Steady state fluorescence experiments were all performed using a standard Quantamaster Fluorimeter (Photon Technology International Inc., NJ). The spectrofluorimeter is equipped with a thermostat that can yield temperature control precision of ± 0.1°C. A 6 nm slit width was used on both the excitation and emission slits. Both the excitation and the emission polarizers used in this work were non-motorized Glan-Thompson polarizers with medium aperture configuration. (PTI Inc., NJ). Excitation and emission wavelengths for the fluorescein conjugate were 472 and 512 nm respectively whereas they were 592 and 612 nm for Texas Red conjugates, respectively. Four data points, with less than 3% RSD, were collected for all anisotropy measurements and the averaged numbers were used for further data processing. The anisotropy, $\gamma$ or r, of the labeled DNA was calculated based on the following Equation 3.1 (39):

$$\gamma = \frac{\frac{I_{VV}I_{HH}}{I_{HV}I_{VH}} - 1}{\frac{I_{VV}I_{HH}}{I_{HV}I_{VH}} + 2} \qquad \textbf{Equation 3.1}$$

where I represents the intensity of the fluorescence signal and the subscripts designate the orientation of the polarizers at the entrance and exit slits, respectively. Correction data for the background aqueous buffer solutions and for dilution factors were made to ensure that the anisotropy calculations are background subtracted and accurate. Data collection and anisotropy calculations were performed for all the experiments using Felix software for Windows OS from PTI Inc. The sample holder was a sub-micro quartz fluorometer cuvette (Starna Cells, CA) with a sample volume of 100μL. The fluorophore labeled DNA solutions were usually covered with aluminum foil and used the same day. All other chemicals, which are used for experimentation in this work, were obtained from Sigma Chemicals (St.Louis, MO).

### 3.3.3 DNA Melting Experiment

A spectrophotometric procedure was used to determine the melting temperature of the unlabeled D17.4 aptamer. The $A_{260}$ measurements of the DNA can be followed as a function of the temperature to determine this information. A Cary 100 spectrophotometer instrument, fitted with a peltier element based temperature controller, was used to perform the melting experiment. The absorbance was monitored in the temperature range of 10-80°C using a heating rate of 0.5 °C per minute. A 700μL quartz cuvette was used to perform this melting experiment. The data can be transferred to a Microsoft Excel worksheet to be processed for plotting purposes.

## 3.4 Results and Discussion

### 3.4.1 Initial anisotropy – Predictions and Observation

The magnitude of steady state anisotropy changes that can be observed using an FP probe during a binding process, among other factors, depends on the size of the target and good correlation of the measured steady state anisotropy to the global motion of the DNA to which the fluorophore is conjugated. The ability of the dye to track the global motion of the DNA and hence its binding properties, in turn, depends on the labeling strategy used. In order to predict the efficiency of the labeling strategy for the three different probes (Figure 3.3) used in this study, it is necessary to measure the steady state anisotropy of those probes and compare them to a predicted value. The predicted value can be arrived at by using the size of the DNA aptamer along with certain assumptions about the impact of labeling on the DNA, as discussed below. It must be reinforced here that the observed r values are a time-averaged representation of the rotational motions of the fluorophore conjugated DNA. Hence, components of the anisotropy and their amplitudes cannot be resolved using the steady state measurements since only a time-averaged value is always determined.

The predicted anisotropy value for the D17.4 conjugates, calculated below, is based on the assumption that the fluorophore perfectly tracks the global DNA motion without any local motion with respect to the aptamer. For a theoretical estimation of the DNA anisotropy, this is a fair supposition. In fact, this assumption is analogous to a situation where the natural fluorescence of the aptamer, if any, is used to track the

anisotropy values. The relationship between r, $r_o$ (limiting anisotropy of the conjugate), $\tau$ (dye fluorescence lifetime) and $\tau_{rot}$ or $\varphi$ (rotational correlation time or RCT) is given by the Perrin Equation (Equation 3.2), assuming a monoexponential decay for the conjugated fluorophore.

$$\frac{r_0}{r} = 1 + \frac{\tau}{\tau_{rot}} \qquad \textbf{Equation 3.2}$$

The value of $r_o$ is dependent on the angular displacement of the excitation transition dipole from the emission transition dipole, in the labeled DNA. This is the initial anisotropy of the labeled DNA prior to any principal depolarization mechanisms setting in. It is found to be 0.37, based on our concurrent time-resolved spectroscopy studies (62). From the same study, we have also confirmed that the fluorescence decay for the conjugates is indeed monoexponential. The rotational correlation time $\tau_{rot}$ is given by the Stokes-Einstein-Debye Equation:

$$\tau_{rot} = \frac{\eta V}{kT} \qquad \textbf{Equation 3.3}$$

The Stokes-Einstein-Debye equation thus relates $\tau_{rot}$ to measurable solution parameters: viscosity ($\eta$), temperature (T) and solvent included volume (V). The average Connolly solvent excluded volume per DNA base is calculated using Chem3D software from CambridgeSoft to be 231 $Å^3$. The included volume, V, for

the labeled 37-mer IgE aptamer can, in turn, be calculated using the assumption that all bases contribute equally to the hydrated volume of the DNA. This is also not an unreasonable assumption considering the absence of any unusual hydration behavior of specific nucleotides, as checked from the literature. The value of the viscosity of water at room temperature is assumed to be 897 $\mu$Pa·s. The rotational correlation time of the solvated molecule was taken to be twice the value for the anhydrous sphere as described by Yguerabide and coworkers (61) for spherical macromolecules in water. Using a fluorescence lifetime of 4 ns, which is appropriate for both fluorescein and Texas Red, the expected r value of the D 17.4 aptamer in aqueous medium at room temperature is calculated to be 0.19. Though this value is an approximation based on an assumption that the DNA is a hydrated sphere, it is nevertheless useful for comparison to experimental observations. The actually observed r values for the conjugates **1A**, **1B** and **1C**, at different concentrations, are shown in Table 3.1. All the values were found to be within a precision range of ± 0.004.

| [DNA] nM | r (1A) | r (1B) | r (1C) |
|---|---|---|---|
| 20 | 0.040 | 0.180 | 0.160 |
| 40 | 0.044 | 0.182 | 0.161 |
| 100 | 0.042 | 0.184 | 0.162 |

Table 3.1: Steady state anisotropy values of the three DNA-dye conjugates used in this work, measured at varying concentrations.

All experimental r values differ from each other amongst the three conjugates **1A**, **1B** and **1C** and they also different from the theoretically predicted value of 0.19. However, they do not vary with DNA concentration, as expected. The reasoning is that r values will not change with DNA concentrations unless some significant intermolecular interactions occur. These data also suggest that the two important variables in the three dye-DNA conjugates are the linker arm length and the fluorophore itself (Figure 3.3). The Texas Red conjugate with the shorter linker arm, **1B**, has the highest initial anisotropy of about 0.18 in comparison to 0.16 for the conjugate **1C** possessing the same fluorophore on the longest tether. The value of 0.18 for **1B** is closest to the predicted anisotropy value of 0.19 whereas the value for fluorescein conjugate **1A** is the lowest at about 0.04. The low r value of **1A** is comparable to that obtained for the 33-mer system, from the work of the McGown group (47). It is also comparable to those of other aptamer (59) as well as non-aptamer based ss DNA systems that employ fluorescein conjugates (54,55).

It is certainly surprising to note the very low anisotropy of **1A** in which the dye is conjugated close to the DNA, much like the case of **1B**. The initial expectation was that choice of the fluorophore will not influence the initial anisotropy significantly. The low value of **1A** may be due to the fact that anisotropy measured in this case arises from significant segmental motion of the dye, as mentioned in section 3.2.3. The steady state anisotropy corresponding to the dye rotational diffusion is usually very low due to the rapid rotational diffusion of such small molecule fluorophores. Whenever the segmental motion dominates in any conjugate, it tends to decrease the anisotropy value from the theoretically expected values and this is, especially, unfavorable for designing a sensitive FP approach. The steady state anisotropy

measurements, in such a situation, will not be well reflective of the DNA binding properties. On the other hand, the closeness of the anisotropy values in the Texas Red conjugates, **1C** and **1B**, to the predicted anisotropy value emphasizes the importance of the fluorophore itself when designing the FP probes.

In effect, the data from Table 1 data suggest that the Texas Red conjugates reflect the rotational motion of the D17.4 system better and hence can be expected to be a more sensitive label system. The choice of the tether length influences the labeling strategy to a lesser extent for this dye. This observation is supported by the comparison of the two Texas Red conjugates that have different tether lengths but not differ significantly in their initial anisotropies.

### 3.4.2 Anisotropy changes - Initial Study

The relevant working range for IgE bioanalysis in human serum samples is 1-60 nM, according to World Health Organization (WHO) recommendations. The binding affinity of the original, unmodified D 17.4 IgE aptamer was found to be 9 nM ($K_d$) from filter binding studies (38). To test the feasibility of using the three conjugate systems designed in this study, binding studies of the labeled DNA in titration experiments were attempted. Figure 3.6 shows the result from the initial binding curve for the fluorescein conjugate **1A**.

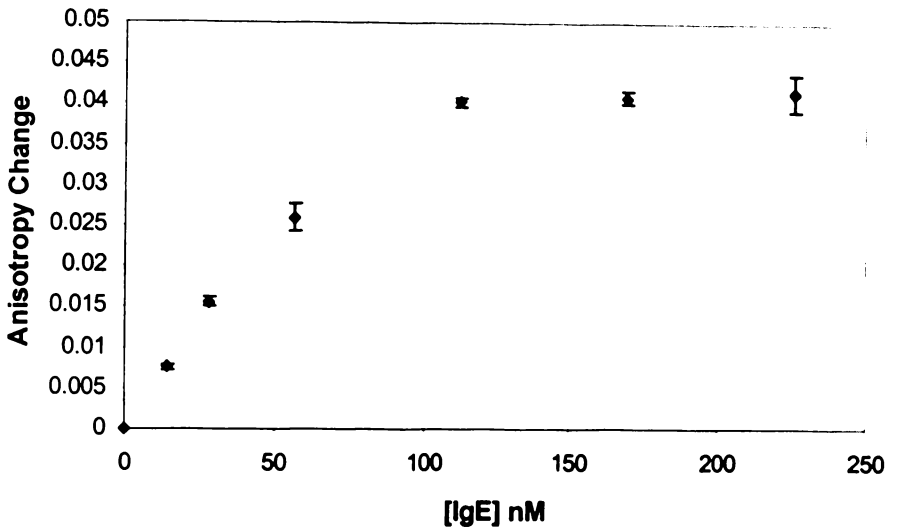


Figure 3.6: Titration curve of conjugate **1A** (20 nM) in the binding buffer at pH 7.4. Anisotropy change refers to the difference (in the steady state anisotropy from the initial DNA anisotropy) at 25° C.

Conjugate **1A** (20 nM) was used in the binding buffer for this experiment. As can be seen from the anisotropy plot, the FP approach reflects the aptamer-IgE binding phenomenon through measurable, monophasic anisotropy changes. The basal anisotropy of the labeled DNA aptamer is about 0.04, as seen from Table 3.1. The data plotted here shows the changes in the anisotropy from the basal values of 0.04 upon the addition of different IgE concentrations. The approach is seen to respond to IgE levels in the range of 1-100 nM beyond which there is no further increase in anisotropy of the labeled ligand when using the 20 nM labeled DNA. The response is

linear in the relevant range of interest of 1-60 nM. The working range may be expanded using a higher concentration of aptamer although our focus was mainly in the low nM working range for sensitive IgE detection. It must be pointed out that the anisotropy change in this DNA-protein binding reaction occurs rapidly, in a few seconds. This opens up the possibility of examining the kinetics of the reaction, but the current FP instrumental setup is such that rapid changes of the FP signal changes may not be followed accurately with adequate time resolution. Addition of automatically controlled polarizers to the instrumentation may help in accomplishing this objective. The positive control experiment, using the conjugate **1A**, confirmed the absence of anisotropy changes in the absence of any added IgE. Such an observation was observed to be independent of the specific conjugate used, as expected.

The sensitivity of **1A** based on anisotropy changes, however, is not high as the final anisotropy is only about twice that of the initial value of the labeled DNA measured in the absence of any added protein. This may also be due to a significant segmental dye motion, which is already reflected in the low r value (Table 3.1) for this conjugate. As segmental motion and the contribution of such a rotational component cannot be resolved and verified in the steady state anisotropy measurements, we have approached this issue using time-resolved spectroscopy by adapting the technique of Time Correlated Single Photon Counting Spectroscopy (TCSPC) (62). TCSPC can be helpful to characterize the finer spectroscopic details of this binding phenomenon with very high time resolution. The details of this work are reported in

the next chapter. In any case, as the FP method held promise, the responses of the other conjugates for similar binding studies were also evaluated.

### 3.4.3 Comparison of the FP Responses

To make a direct comparison of the efficiency of all the three conjugates as sensitive FP probes, a titration experiment using fixed concentration of the aptamer was performed for all the conjugates. The result from such an experiment, using a 10 nM aptamer concentration, is shown in the following plot, Figure 3.7:

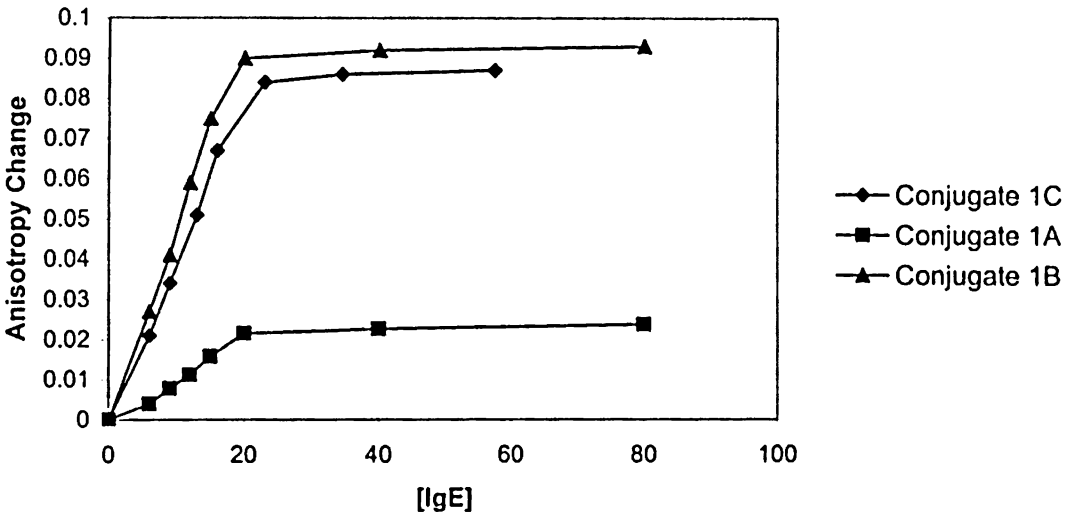


Figure 3.7: A comparative FP response of conjugates **1A, 1B** and **1C** for IgE bioanalysis in titration experiments when 10 nM ss DNA aptamer was used at 25° C. The experiments were performed in binding buffer, pH 7.4.

As can be seen, the FP responses are dependent on the conjugate used. The working ranges, as expected, are different from Figure 3.6 as 10 nM aptamer is

being used in the current experiment. The Texas Red conjugate **1B** has much greater sensitivity for the FP approach when compared to the fluorescein conjugate **1A** that has a similar 8-atom linker arm. The Texas Red conjugate **1C**, that has a much longer tether, has sensitivity comparable to **1B**. These observations are in line with our expectation, based on the initial r values of the conjugates (Table 3.1) and our previous discussion (section 3.4.1). The surprisingly higher sensitivity of Texas Red probes over the fluorescein probe **1A** confirms the effect of the fluorophore in FP probe design. The fact that **1B** and **1C** also have similar sensitivities, independent of the tether length, suggests the possibility of favorable Texas Red-DNA interactions in these two probes. Such an interaction is absent in **1A**. Further analysis from a concurrent TCSPC study has validated this possibility, although characterizing the exact nature of the interaction is beyond the scope of our current work.

The local dye rotation in the conjugate **1A**, thus, affects the suitability of its use as a sensitive FP probe. The magnitude of this effect was evident from the TCSPC spectroscopy data (62) from which it was observed that the amplitude of the local dye motion predominates the global DNA motion at room temperature. Previous studies from the McGown group (47) have documented similar observations. The Texas Red conjugates **1B** and **1C** that are seen to have comparable, higher sensitivity in detecting IgE than **1A** (Figure 3.7) and both can be, conversely, expected to have lower dye segmental motion. This has also been seen to be the case from our analysis (62) where it is seen that the amplitudes of the local dye motion is considerably lower in both these conjugates when compared to conjugate

**1A**. In fact, the amplitudes of the rotational components for **1B** and **1C** are nearly identical. This can also explain the nearly identical binding behavior of these 2 probes, as seen in Figure 3.7. Our initial expectations about the FP performance of all the 3 probes, based on predicted anisotropy calculations, have thus been justified by the time-resolved spectroscopy studies as well. Based on the above observations for the IgE aptamer system, we can infer that the sensitivity of the current FP approach is guided more by the fluorophore characteristics and less by the dye tether length. The working ranges of the IgE detection were, unlike sensitivity, unchanged when using these different labeled probes, as seen for example from Figure 3.7. Under room temperature conditions, Texas Red conjugates are thus found to be better FP probes for the current application.

### 3.4.4 Effect of Temperature on the FP Responses

The effect of increasing temperatures on anisotropy changes can be estimated from the Perrin equation (Equation 3.2) and Equation 3.3. As the rotational correlation time, $\tau_{rot}$, is inversely related to the temperature, increasing temperatures may reduce the FP responses from the probes. This is a reasonable expectation even when considering the fact that viscosity itself is temperature dependent. The sensitivity of each of the three conjugates under consideration may thus be lowered with increasing temperature. In relation to this expectation, the effect of changing the assay temperature to 37°C from 27°C was studied. It is possible that the binding affinity of the aptamer may also be changed at different temperatures especially given that DNA is conformationally labile. However, considering the fact that the SELEX experiment was itself performed at 37 degrees, this was considered not to be

a major issue. The results of anisotropy changes are shown in Figure 3.8 for conjugate **1A**.

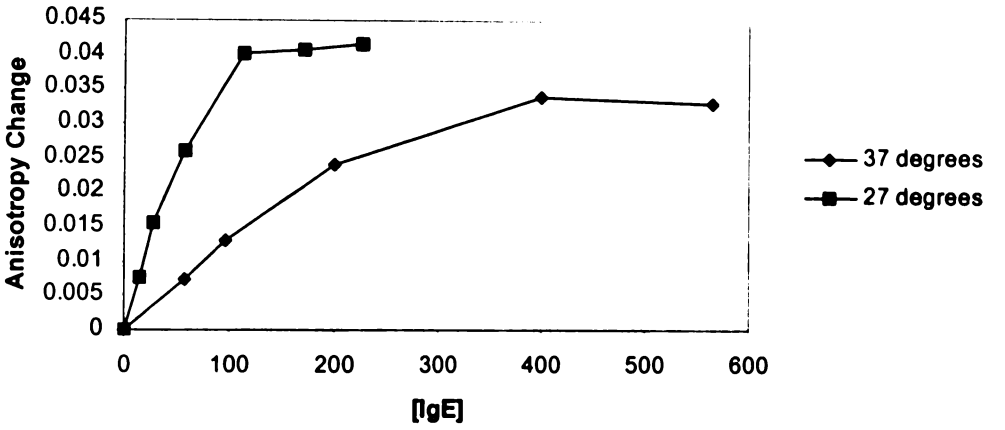


Figure 3.8: FP responses from conjugate **1A** as a function of IgE concentration and temperature. 20 nM DNA aptamer was used for this experiment in binding buffer, pH 7.4.

The effect of temperature is quite drastic even when the temperatures considered here were only 27°C and 37°C. The anisotropy changes are significantly lower in response to added IgE at 37°C. The ability of the probe **1A** to track the binding event is seemingly reduced at 37°C. Once again, the predominant role of fluorophore local motion is noted while the role of temperature related conformational changes appears to be minimal. The fact that this same probe had a low initial anisotropy (Table 3.1) and showed low sensitivity in comparison to the Texas Red conjugates at

room temperature (Figure 3.7) suggests that dye local motion is possibly more significant at higher temperatures. Our TCSPC study once again corroborates this possibility (62). Thus the temperature dependence of anisotropy changes cannot be explained by the Perrin equation alone (Equation 3.2), which relates viscosity changes with temperature, but requires consideration of the rotational dynamics of the specific probes.

Considering the better success with the Texas Red probes at room temperature (Figure 3.7), we expected them to be superior probes at higher temperatures also. Specifically, the FP response of **1C** was comparable to **1B** and better than **1A** at room temperature. The sensitivity of this probe would thus be expected to be better than **1A** at higher temperatures also. This was confirmed to be the case (Figure 3.9) when **1C** provides sensitivity twice that of **1A** had, using 8 nM labeled DNA aptamer at 37 degrees.

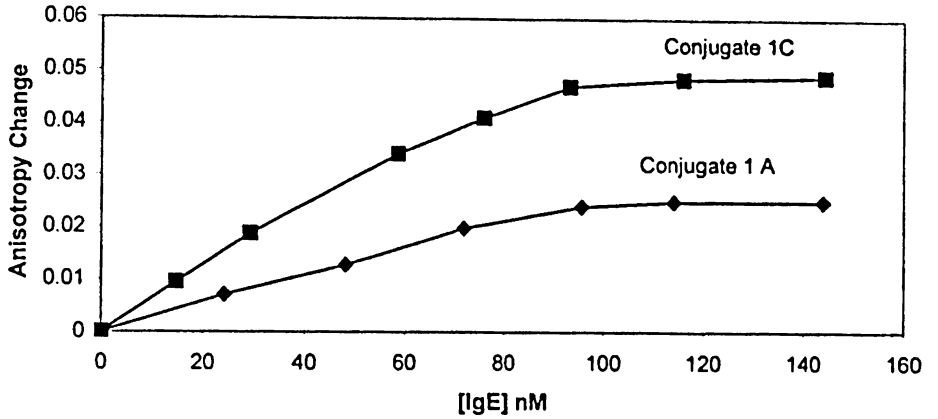


Figure 3.9: Comparison of FP responses of **1A** and **1C** to increasing IgE concentrations at 37°C. FP responses were recorded under identical solution conditions of binding buffer at pH 7.4. 8 nM aptamer concentration was used.

This magnitude of the sensitivity gain using **1C** instead of **1A**, as seen in Figure 3.9, is also consistent with its 3-fold sensitivity gain observed at room temperature, as seen from Figure 3.7. Once again, the assay sensitivity seems to be dependent on the probe used. The working range, expectedly, depends on the aptamer concentration but not on the dye itself. The strong temperature dependent responses when monitoring the FP changes have led us to characterize the temperature dependent DNA rotational dynamics for all the three systems using TCSPC spectroscopy.

All the three probes were found to have two rotational correlation times with the global DNA motion along with the local dye motions accounting for the correlation times. At a temperature of 37 degrees, the amplitude of the dye motion completely

dominates the global DNA motion in **1A** and hence the total anisotropy arises almost entirely from this local motion. It was contrary to the observations made for the Texas Red probes. In fact, the temperature studies performed for the Texas Red probes, **1B** and **1C**, using TCSPC spectroscopy confirmed the melting temperature of the aptamer at 60-65°C that was obtained from spectrophotometric measurements. This observation points to the fact that global DNA motion is reliably tracked when the Texas Red probes are used. The TCSPC spectroscopic studies that we have undertaken have thus helped to relate the solution dynamics of the aptamer to its anisotropy characteristics and also to validate all of the temperature dependent steady state anisotropy observations. Choosing **1B** or **1C**, especially, under room temperature conditions, can thus optimize the assay conditions for IgE bioanalysis.

### 3.4.5 Specificity Studies

The usefulness of molecular recognition based bioanalysis for real samples will depend on the specificity of the binding process or, in effect, the impact of interfering proteins and closely related analytes. Aptamers have had moderate success in terms of binding specificity and the D17.4 aptamer has shown good properties in this regard. This was confirmed by a previous study using quartz crystal microbalance (QCM) as the biosensing technique. Liss and coworkers (63) used different protein mixtures for specificity studies in this work and obtained encouraging responses. In our case, the measured signal is the relative FPA responses of the DNA aptamer for proteins found in biological samples. The result of this test is reported in Figure 3.10.

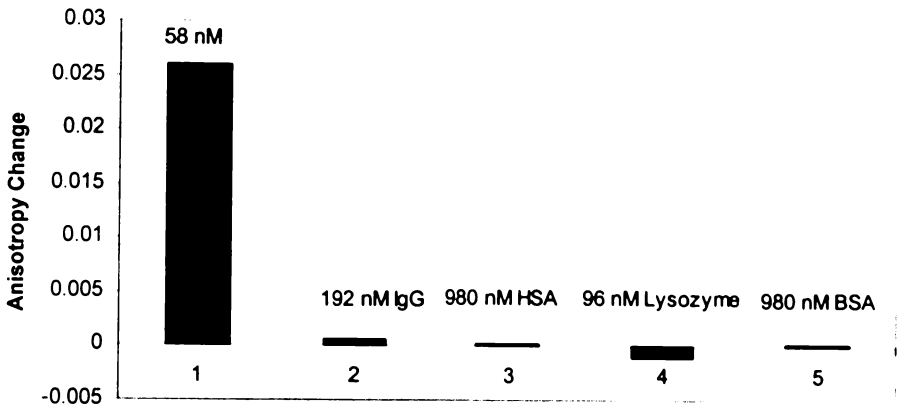


Figure 3.10: Specificity of 20 nM **1A** towards potential protein interferences. All the responses are anisotropy changes upon protein addition. Measurements were made under identical solution conditions, in binding buffer at pH 7.4.

The interfering proteins that were tested include BSA, HSA, Lysozyme and IgG. It should be noted that the IgG is similar to IgE structurally and thus can serve as a good test protein for the aptamer binding specificity. The concentrations of the albumin proteins are chosen to be very high, as they would be in serum samples. The relative responses of the interferences, as seen in Figure 3.10, are insignificant in comparison to the specific binding response with IgE, in agreement with the previously reported work. The relatively low interferences from HSA and BSA are very encouraging considering the high percentage of these serum proteins in biological samples. Although the reported data here has been obtained using the fluorescein labeled aptamer, the binding trend is seen to be similar with conjugates **1B** and **1C**. Hence the specificity is not found to be dependent on the dye conjugation strategies, as expected.

### Effect of Cations on Aptamer Binding

The binding properties of the aptamers in solutions are influenced by the presence of certain cations. The binding buffer (BB) composition in the case of D17.4 aptamer is made of 2.7 mM $K^+$ and 1 mM $Mg^{+2}$ and the flexibility of the ss DNA motif is primarily governed by the counterion interactions. Hence the effect of varying the binding buffer is monitored by varying the concentration of potassium and magnesium ions. The buffer composition can have a direct effect on the binding ability of the aptamer. Divalent cations like Magnesium ions thus typically play more than just a backbone charge compensation role and are important in determining the extended stem-loop configuration predicted in the case of the D17.4 ligand.

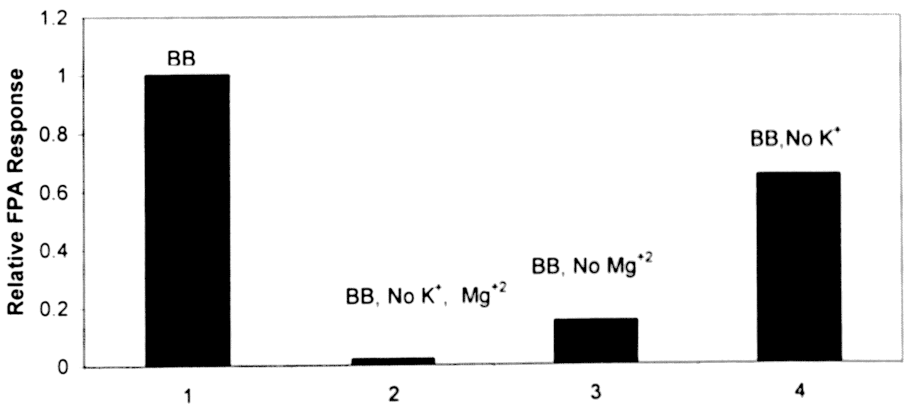


**Figure 3.11:** Effect of varying the ionic composition in the binding buffer (BB). All responses are plotted in relation to a value of 1 for the specific detection of IgE, using 20 nM **1C**.

As seen from Figure 3.11, the magnesium ion concentration is quite important for efficient binding. As seen in trial 4, changing the magnesium ion concentration to the binding buffer composition levels, even in the absence of potassium ions, restores the binding ability of the DNA Aptamer to 65% of the original activity. The importance of the magnesium cation is in contrast to the importance of $K^+$ species in stabilizing G quartets, as seen in the case of the thrombin aptamer. As expected, the absence of both the $K^+$ and $Mg^{+2}$ ions totally inactivates aptamer binding activity. The effect of the ions seen here is an indication of the importance of the binding buffer that was employed in all the steps of SELEX and presents a situation seen typically for aptamers in the different analytical applications in which they are used.

**Comparison to other current methodologies**

The FP method reported here presents a simple, rapid, homogeneous and practical method for IgE detection. It can be performed at low nM levels but the working range is dependent on the solution conditions, especially on the concentration of the aptamer. The working range attained in this work is quite relevant when considering the need for real samples. It has been reinforced, using negative control experiments, that anisotropy changes are observed only when labeled aptamer is present and not when merely the free dyes are reacted with IgE. The analytical figures of merit considered here include sensitivity, specificity and LOD. The sensitivity of the FP method depends more on the fluorophore characteristics and on the dye linker length to a lesser extent. An unoptimized LOD of 350 pM has been observed, using **1C**, from our trials and this is comparable to the 500 pM LOD achieved using the QCM technique (63). The specificity of aptamer binding, as seen

from this study has been found to be adequate. The anisotropy changes are robust and the LOD attained may be improved by making some improvements to the instrument optics. The QCM and APCE approaches, that have also used the D17.4 DNA ligand, are useful methods for performing IgE detection but the FP approach stands out for its simplicity and user-friendly nature. Careful considerations of the factors influencing the labeled DNA aptamers, discussed in this work, can aid in designing very sensitive bioassays that can be extended to real samples as well.

**Chapter conclusions and Future Work:**

In the current post-genomics and proteomics era, improvements in performing rapid, sensitive protein and peptide detection can be a useful bioanalytical advance. It has been shown that rapid, sensitive detection of a clinically relevant protein, IgE, can be performed based on a FP approach, using a DNA aptamer. The effects of labeling strategy, choice of fluorophore, temperature and binding buffer conditions are found to influence the FP responses significantly. The importance of minimizing the segmental motion of the dye is clearly seen in this work. The role of specific cations, specifically the role of divalent magnesium ion, in determining the binding ability of the ss DNA aptamers is also reinforced in this study. Careful consideration of these issues can help when using other aptamer systems. The current work has extended the applicability of DNA aptamers in specifically detecting large proteins, using the FP approach.

The spectroscopic details of the DNA system like the lifetime distribution, anisotropy components, their dependence on temperature and other solution conditions have to be investigated in detail to understand their effects on the steady state anisotropy

changes. The necessity of the time-resolved spectroscopy in answering certain steady state phenomena has been clearly seen, based on the data presented in the current chapter. The next chapter in this report deals with the details of time-resolved spectroscopic studies for the D 17.4 aptamer that helps in understanding the steady state observations better.

**References:**


1) Carvin, C. D.; Dhasarathy, A.; Freisenhahn, L. B.; Jessen, W. J.; Kladde, M. P. *Proc. Natl. Acad. Sci.* **2003**, 100(13), 7743-7748.

2) Martin, D.W.; Munoz, R. M.; Oliver, D.; Subler, M. A.; Deb, S. *Virology* **1994**, 198(1), 71-80.

3) Yoshida, T.; Ishikawa, I.; Uno, Y.; Imai, T.; Suzuki, R.; Osamu, Y. *J. Immunol.* **1999**, 163(6), 3295-3303.

4) Ingmer, H.; Cohen, S. N.; *J. Bacteriol.* **1993**, 175(18), 6046-6048.

5) Stillman, B.; Diffley, J. F.; Prelich, G.; Guggenheimer, R. A.; *J. Clin. Oncol.* **1986**, 4, 453-463.

6) Umov, F. P.; Fyodov, D.; Rebar, E. J. *Biochem. Pharmacol.* **2002**, 64, 919-923.

7) Denison, M. S.; Fisher, J. M.; Whitlock, J. P. *Proc. Natl. Acad. Sci.* **1988**, 85(8), 2528-2532.

8) Saiki, R.; Scharf, S.; Falona, F.; Mullis, K. B.; Hurn, G. T.; Erlich, H. A.; Arnheim, N. *Science* **1985**, 230, 1350-1354.

9) Tuerk, C.; Gold, L. *Science* **1990**, 249, 505-510.

10) Veldhoen, N.; You, Q.; Setzer, D. R.; Romaniuk, P. J. *Biochemistry* **1994**, 33(24), 7568-7575.

11) Blackwell, T. K.; Weintraub, H. *Science* **1990**, 250, 1104-1110.

12) Blackwell, T. K.; Kretzner, L.; Blackwood, E. M.; Eisenman, R. N.; Weintraub, H. *Science* **1990**, 250, 1149-1151.

13) Noxxon AG pharmaceutical company homepage – www.noxxon.net (Accessed on 07/30/03).

14) Famulok, M. *Curr. Opin. Struct. Biol.* **1999**, 9, 324-329.

15) Jayasena, S. D. Clin. Chem. **1999**, 45, 1628-1650.

16) Romig, T. S.; Bell, C.; Drolet, D. W. *J. Chrom. B* **1999**, 731, 275-284.

17) Knight, R. D.; Landweber, L. F. *RNA* **2000**, 6(4), 499-510.

18) Bock, L. C.; Griffin, L. C.; Latham, J. A.; Vermaan, E. H.; Toole, J. J. *Nature*, **1992**, 355, 564-566.

19) Patel, D. *J. Curr. Opin. Chem. Biol.* **1997**, 1, 32-46.

20) Patel, D. J.; Suri, A. K. *J. Biotechnol.* **2000**, 74, 39-60.

21) Valenzano, K. J.; Miller, W.; Kravitz, J. N.; Samama, P.; Fitzpatrick, D.; Seeley, K. *J. Bimol. Screen.* **2000**, 5, 455-461.

22) Bacher, J. M.; Ellington, A. D.; *Drug Discov. Today* **1998**, 3, 265-273.

23) Singh, P.; Sharma, B. P.; In Diagnostics in the year 2000; Tyle, P.; Ed.; Van Nostrand Reinhold, 1993, pp 477-527.

24) O' Sullivan, C. K. *Anal. Bioanal. Chem.* **2002**,372, 44-48.

25) Pietras, K.; Ostman, A.; Sjoquist, M.; Buchdunger, E.; Reed, R. K.; Heldin, C. H.; Rubin, K. *Cancer Res.* **2001**, 61, 2929-2934.

26) Turek, T. C.; Small, E. C.; Bryant, R. W.; Hill, W. A. *Anal. Biochem.* **2001**, 299, 45-53.

27) Huang, W.; Zhang, Y.; Sportsman, J. R. *J. Biomol. Screen.* **2002**, 7(3), 215-222.

28) Haver, V. M.; Avdino, N.; Burriss, S.; Nelson, M. *Clin. Chem.* **1989**, 35, 138-140.

29) Armbruster, D. A.; Schwarzhoff, R. H.; Hubster, E. C.; Liserio, M. K. *Clin. Chem.* **1993**, 39, 2137-2146.

30) McGown, L. B.; Joseph, M. J.; Pitner, J. B.; Vonk, G. P.; Linn, C. P. *Anal. Chem.* **1995**, 67, 663 A-638A.

31) Stojanovic, M. N.; De Prada, P.; Landry, D. W.; *J. Am. Chem. Soc.* **2001**, 123, 4928-4931.

32) Cox, J. C.; Ellington, A. D. *Bioorg. Med. Chem.* **2001**, 9, 2525-2531.

33) Deng, Qing.; Watson, C.; Kennedy, R. T.; *J. Chrom. A* 2003, 1005, 123-130.

34) Fang, X.; Cao, Z.; Beck, T.; Tan, W. *Anal. Chem.* **2001**, 73, 5752-5757.

35) Royer, C. A.; Ropp, T.; Scarlata, S. F. *Biophys. Chem.* **1992**, 43,197-200.

36) Cheng, X.; Kovac, L.; Lee, J. C. *Biochemistry*, 1995, 34, 10816-10821.

37) LeTilly, V.; Royer, C. A. *Biochemistry* **1993**, 32, 7753-7757.

38) Wiegand, T. W.; Williams, P. B.; Dreskin, S. C.; Jouvin, M.; Kinet, J.; Tasset, D. *J. Immunol.* **1996**, 157, 221-230.

39) Lakowicz, J. R. Principles of Fluorescence Spectroscopy, 2nd Ed.; Kluwer Academic/Plenum: NY, 1999, PP 212-248.

40) Griffin, L. C.; Toole, J. J Leung, L. K. *Gene* **1993**, 137, 25-31.

41) Huizenga, D. E.; Szostak, J. W. *Biochemistry* **1995**, 34, 656-665.

42) Potyraislo, R. A.; Conrad, R. C.; Ellington, A. D.; Hieftje, G. M. *Anal. Chem.* **1998**, 70, 16, 3419-3425.

43) Drolet, D.; Moon-McDermott, L.; Romig, T. S. *Nat. Biotech.* **1996**, 14, 1021-1025.

44) German, I.; Buchanan, D.; Kennedy, R. T. *Anal. Chem.* **1998**, 70, 4540-4545.

45) Pavski, V.; Le, X. C.; *Anal. Chem.* **2001**, 73, 6070-6076.

46) Romig, T. S.; Bell, C.; Drolet, D. W. *J. Chrom. B* **1999**, 731, 275-284.

47) Rehder-Silinski, M. A.; McGown, L. B. *J. Chrom. A* **2003**, 1008 (2), 233-235.

48) Charles, J. A. M.; McGown, L.B. *Electrophoresis* **2002**, 23(11), 1599-1604.

49) Rehder, M. A.; McGown, L. B. *Electrophoresis* **2001**, 22(17), 3759-3764.

50) Kotia, R. B.; Li, L.; McGown, L. B. *Anal. Chem.* **2000**, 72, 197-209.

51) Jhaveri, S. D.; Kirby, R.; Conrad, R.; Maglott, E.; Bowser, M.; Kennedy, R. T.; Glick, G.; Ellington, A. D. *J. Am. Chem. Soc.* **2000**, 122, 2469-2473.

52) Heyduk, T.; Lee, J. C. *Proc. Natl. Acad. Sci.* **1990**, 87, 1744-1748.

53) Carver, T. E.; Hochstrasser, R. A.; Millar, D. P. *Proc. Natl. Acad. Sci.* **1994**, 91, 10670-10677.

54) Kwok, R. P.; Lundblad, J. R.; Chrivia, J. P.; Richards, H. P.; Bachinger, R. G.; Roberts, S. G.; Green, M. R.; Goodman, R. H. *Nature*, **1994**, 370, 223-225.

55) Perz-Howard, P. A.; Weil, P. A.; Beechem, J. M., **1995**, *Biochemistry*, 34, 8005-8010.

56) Bailey, P.; Hagmar, D.; Millar, D. P.; Davidson, B. E.; Tong, G.; Haralambidis, J; Sawer, W. H. *Biochemistry*, **1995**, 34, 15802-15807.

57) Tuschl, T.; Gohlke, C.; Jovin, E.; Westhof, E.; Eckstein, F. *Science* **1994**, 266, 785-790.

58) Mei, S. H. J.; Liu, Z.; Brenna, J. D.; Li, Y. *J. Am. Chem. Soc.* **2003**, 125, 412-420.

59) Hill, J. J.; Royer, C. *Methods Enzymol.* **1997**, 278, 390-416.

60) Kumke, M. U.; Shu, L.; McGown, L. B.; Walker, G. T.; Pitner, J. B.; Linn, C. P. *Anal. Chem.* **1997**, 69, 3, 500-506.

61) Yguerabide, J.; Epstein, H. F.; Stryer, L. *J. Mol. Biol.* **1970**, 51, 573-590.

62) Unruh, J.; Gokulrangan, G.; Johnson, C. K.; Wilson, G. S. *Manuscript submitted to Biophysical Journal.*

63) Liss, M.; Petersen, B.; Wolf, H.; Prohaska, E. *Anal. Chem.* **2002**, 74, 4488-4495.

64) Isom, L. M.; Sines, C. C.; Williams, L. D. *Curr. Opin. Struct. Biol.* **1999**, 9, 298-304.

65) Hamaguchi, N.; Ellington, A. D.; Stanton, M. *Anal. Biochem.* ***2001***, 294, 126-131.

## Chapter 4

## Characterization of Fluorescence Properties and Rotational Dynamics of a Dye Labeled DNA Aptamer – D17.4 System

## 4.1 Introduction and Current Objectives

### 4.1.1 Monitoring DNA-Protein Interactions – Biochemical approaches

The central importance of DNA-Protein interactions (1) has underlined the need for reliable, sensitive and informative experimental tools to characterize them. Such complexation processes have been conventionally investigated using techniques like gel-shift assays, footprinting and filter binding assays. Gel-shift assays are based on the electrophoretic isolation of the complex and are usually coupled with radiometric detection (2,3). Footprinting refers to the analysis of DNA fragments obtained using restriction enzymes on the bound and free DNA ligand of interest, to map out the bases involved in binding. It may be based on an enzymatic or a chemical approach and is considered to be informative for knowing about the structural as well as thermodynamic details of the complexation (4,5). Filter binding assays (6,7) are routinely applied for determining the binding affinity of receptor proteins towards small molecule ligands using radiometric detection. Although these conventional approaches are still used, the inadequacies that are mentioned below about these methods support the urgent need for adapting new analytical techniques.

Gel-shift assays can be applied to a wide variety of protein targets when considering the binding of small or large nucleotide sequences. The main problem with this method is that it is a non-equilibrium approach and hence there is possibility for complex dissociation, leading to inaccurate quantitation of the bound species. Also DNA can bind to protein targets in a variety of modes and some of them may not be amenable to electrophoretic analysis (3). Finally the gel-shift assay is not found to be convenient for rapidly testing the effects of variables like temperature, salt

concentration and pH on the binding process. The footprinting approach has the problem that the effects of temperature and other variables can be convoluted with the effects of enzymatic digestion or chemical modification. Quantitation of the complexation has also proved to be tedious with this method (5). The filter binding approach has the limitation that the binding conditions are very specific and not ideal for moderate affinity binders to yield reliable binding parameters. Occasionally, two other approaches – site-specific mutational analysis (8) and X-ray crystallographic analysis (9, 10) have been adapted to understand the complexation characteristics. Both these methods are very informative but have restricted applicability.

The disadvantages that exist in all the above-mentioned biochemical approaches point to the need for solution-based analysis methods that can afford high sensitivity but which avoid radiometric detection and electrophoretic separation. Fluorescence - based approaches have recently proven to be a feasible alternative (11) for monitoring the DNA-Protein binding interactions. Fluorescence resonance energy transfer (FRET) (12,13) and fluorescence polarization (FP) methods (14-16) have been commonly employed while some studies have also relied on correlation of fluorescence intensity changes resulting from the binding reaction (17,18). Among all the fluorescence approaches, the FP method is the most advantageous to use as it is simple and not affected by the dye quenching issues that may possibly arise with the use of fluorescently labeled DNA ligands.

### 4.1.2 Fluorescence Polarization approach

Fluorescence Polarization (FP) approach has been used for quantitating the ligand-receptor interactions (14). It has also been shown to yield reliable binding data that are comparable to the conventional biochemical approaches (19,20). As mentioned in Section 3.4.7 of the previous chapter, it stands out for its simplicity and user-friendly characteristics. The technique involves the measurement of steady state anisotropy changes to track the DNA-Protein binding process by using a conventional spectrofluorometer, fitted with suitable polarizers. The advantage of performing the binding studies in solution makes it more likely that true equilibrium binding conditions will be met. Medium effects on the binding process can also be readily determined. The DNA ligand can be labeled with suitable dyes having high quantum yield for the procedure and standard conjugation strategies are also available to obtain labeled DNA with acceptable synthetic yield.

The main cause for the steady state anisotropy (r) changes of the labeled DNA in the FP method is assumed to arise from complexation with a larger protein target. However, changes in the anisotropy can also arise without any changes in the dynamic or time-resolved anisotropy of the labeled ligand. This may be due to changes in the contribution of the segmental dye motion, arising from conformational reorientation, during the process of binding (21). The perturbations in the photophysical characteristics, including fluorescence lifetimes, of the labeled ligand can also give rise to changes in steady state anisotropy during the binding process without any changes in the dynamic anisotropy (22). In order to identify the source of steady state anisotropy changes during binding, it is thus imperative to characterize

the lifetime information and rotational dynamics of the labeled DNA probe using time-resolved spectroscopic experiments. It is also advantageous, as mentioned in the previous chapter, to perform this characterization in order to determine the solution conditions that will maximize the sensitivity of the FP approach. Dynamic anisotropy characterization can shed light on anisotropy components, dye-DNA interactions, DNA-DNA interactions and the rigidity of the dye-DNA linkage. Such microscopic details cannot be resolved from the steady state anisotropy measurements, which only indicate a time-averaged anisotropy value. Time-resolved spectroscopic studies can be performed either in the time domain (TD) or in the frequency domain (FD). Advances in the instrumentation and availability of suitable data analysis software have continued to simplify the process of data collection and interpretation. Time Correlated Single Photon Counting (TCSPC) spectroscopy (23-25) is a standard technique for performing time-resolved spectroscopy.

The D17.4 DNA ligand (8) has been successfully used to monitor the specific binding to Immunoglobulin E (IgE) using different analytical techniques, as mentioned in the previous chapter. This ligand has been isolated by *in vitro* selection. The discussions in the previous chapter also highlight the usefulness of the D17.4 aptamer, labeled with fluorescein and Texas Red, in monitoring the binding to IgE homogeneously using FP. End-labeling chemistry was useful for observing the anisotropy changes with high sensitivity, especially in the case of Texas Red probes. However, various steady state anisotropy data gathered in that study could not be interpreted clearly without obtaining the time-resolved spectroscopy results for the labeled D17.4 ligand. The objective of this chapter is to discuss the fluorescence and rotational dynamics

data obtained by using TCSPC spectroscopy and correlate the results with those obtained from various steady state anisotropy experiments. All the experimental work in relation to this chapter has been performed in the time domain.

### 4.1.3 Specific advantages of using TCSPC spectroscopy

The process of conjugating the fluorophore to the DNA can modify the photophysical properties of the dye such that the fluorescence decay profile may become more complex. The number of fluorescence lifetime components may increase due to possibilities of more than one conformation or due to intramolecular dye-DNA interactions. Additional short lifetime components have been detected in some dye systems due to the conjugation process. The presence of a gaussian distribution of lifetimes for fluorescein conjugated DNA ligands, for example, is also not unusual. The presence of such changes in the lifetime characteristics of the dye, that may be indirectly unfavorable for the FP approach, can be found using TCSPC spectroscopy. Extensive intramolecular quenching interactions of the dye with the DNA of interest may also make a specific dye not ideal for FP applications, although this approach is based only on relative intensity measurements. This can also be checked using time-resolved spectroscopy. The suitability of a specific dye conjugate for the FP approach may thus be gauged by performing some preliminary TCSPC experiments. The technique can also generate the time-resolved anisotropy profiles of the conjugate. The deconvolution of this data will provide the amplitudes of the different components that contribute to the total anisotropy. This can clarify if the segmental dye motion or the global DNA motion dominates the net value of steady state anisotropy, which is measured in the binding experiments. Such

characterization data can be crucial to understanding of the effect of variables like temperature, ionic composition and pH on the binding data, based on the steady state anisotropy changes.

## 4.2 Principles, Prior art and Current approach

### 4.2.1 Lifetime and dynamic anisotropy/rotational dynamics data - Overview

In time-resolved spectroscopy measurements using time-domain (TD) measurements, also termed pulse fluorometry, the fluorophore is excited by a pulsed source whose width is very short and usually much lower than the lifetime of the fluorophore of choice. The time-dependent fluorescence intensity following the excitation pulse is measured and the lifetime can be calculated from the slope of a plot of I(t) vs time (t). For lifetime measurements, the decays are measured at a magic angle of 54.7° from the vertical z-axis, such that the interfering effects of rotational diffusion or anisotropy are minimized. Suitable data analysis software can be used to interpret the deconvoluted data. The calculated lifetime is indicative of both radiative and non-radiative rates that depopulate the excited electronic state of the fluorophore. Presence of multiple lifetimes indicates the differing environments in which the fluorophore is present due to conformational or solvation reasons. As the variation of dye lifetime upon conjugation to DNA has direct consequences in the values of steady state anisotropy, it is imperative to have the magic angle data processed accurately and interpreted appropriately for such samples.

In contrast to the steady state anisotropy measurements, dynamic anisotropy or time-resolved anisotropy is measured by tracking the time dependent decay information for both the vertically (parallel) and horizontally (perpendicular) polarized

emissions. Prior to any depolarization, the time-zero anisotropy or $r_0$ would be close to the theoretical maximum of 0.4, assuming that the absorption and emission transition dipoles are collinear and that the initial intensity of the parallel component would be three times that of the perpendicular component.

The fundamental reason for the parallel component to be greater can be traced to the fact that the parallel excitation transition dipole biases the initial emission transition dipole in that direction, leading to anisotropy values greater than zero. Except for small fluorophores, the $r_0$ values routinely deviate from 0.4 due to the existence of different sources of depolarization, including solvent interaction. Figure 4.1 represents the typical situation for observed anisotropy decay profiles.

The decay profiles in the parallel ($I_{||}$) and perpendicular directions ($I_{||}$) and perpendicular directions ($I_{\perp}$), are shown in comparison to the total intensity decay of the fluorophore ($I_t$). The decay profiles for the vertical and horizontal directions are different mainly because the vertical direction signal decays via two processes – intensity decay with lifetime $\tau$ and rotation out of the vertical direction with a correlation time $\theta$ (RCT) whereas the horizontal direction is slower as it is continuously repopulated by rotation from the vertical direction.

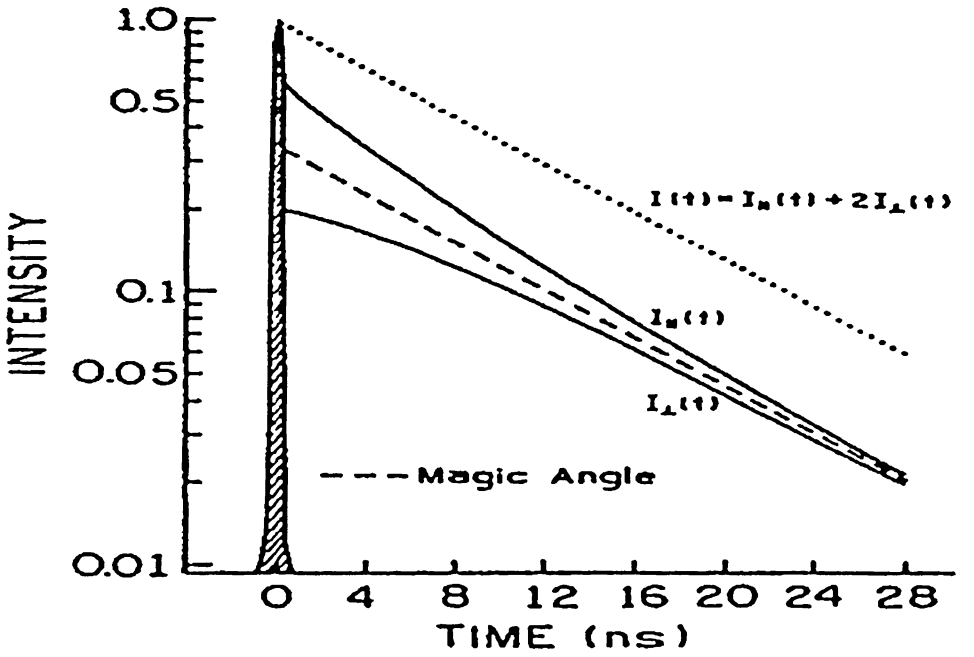


Figure 4.1: The representative diagram of the anisotropy decay profiles, in both parallel and perpendicular directions, for any fluorophore. I(t) refers to the total intensity decay. The diagram is adapted from Reference 22.

### 4.2.2 Description of the TCSPC spectroscopic technique

The principle of this technique can be better discussed based on the instrumental schematic that is shown in Figure 4.2.

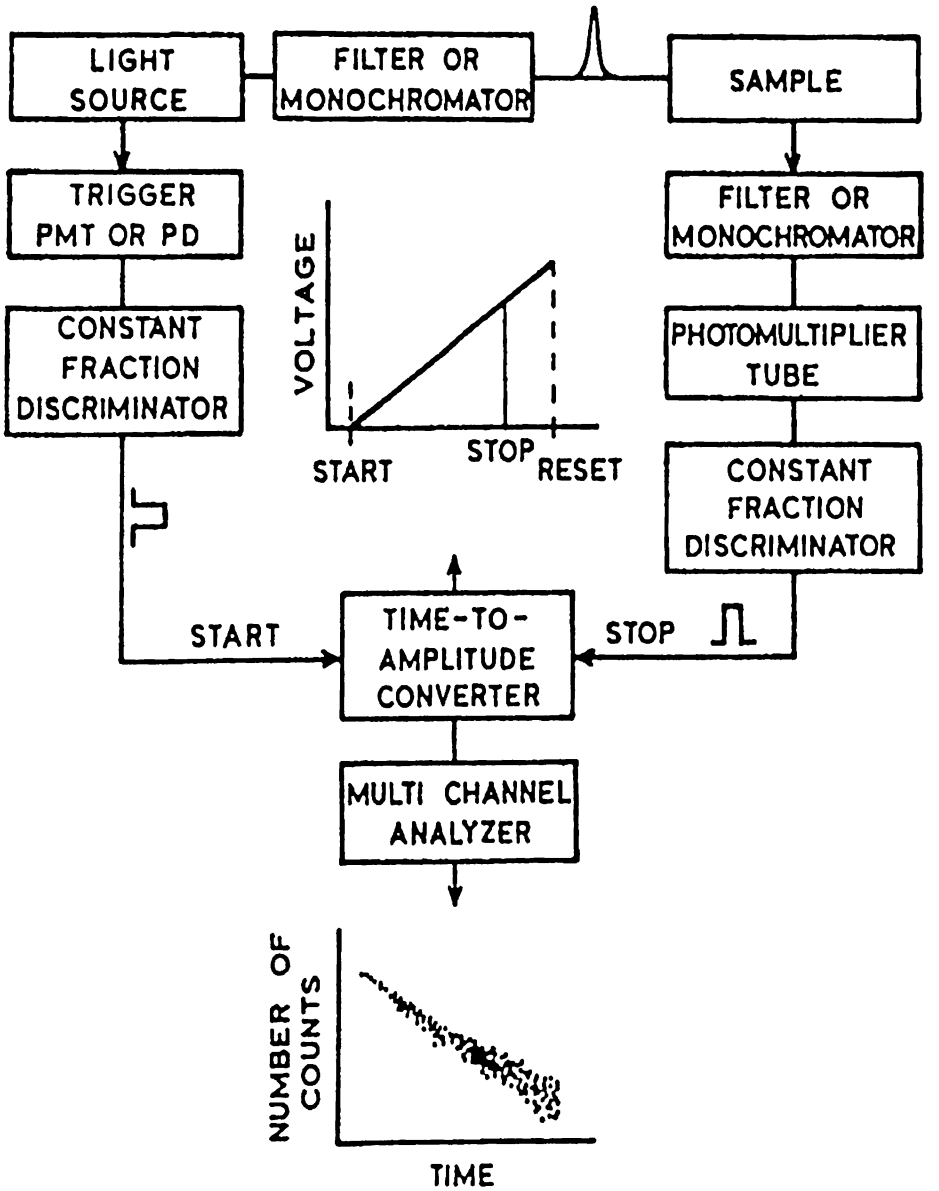


Figure 4.2: Schematic of the general TCSPC instrumentation, as adapted from Reference 22.

The experiment is initiated with the excitation pulse that excites the sample and starts the time-measurement clock. The technique itself is a digital technique with the fluorescent photons counted using ultra fast digital electronics, in relation to the excitation pulse. The excitation pulse activates a voltage ramp of a time-to-amplitude (TAC) converter, as seen in figure 4.2. The voltage ramp is stopped when the first fluorescent photon is detected. The TAC provides an output pulse whose voltage is proportional to the time between the start and stop signals. A multichannel analyzer (MCA) converts this voltage to a time channel using an analog-to-digital converter (ADC). Using the signal from different pulses continuously, the MCA builds up a probability histogram of counts versus time channels. The experiment is performed until a total photon count of about 10,000 is achieved. The detection rate of fluorescence photons is roughly 1 in about 100 pulses, owing to the response of the detection electronics. The instrument response function has to be checked frequently by using a zero-lifetime sample such that a correction factor can be used for deconvoluting the data for lifetime and anisotropy determination. The fluorescence and anisotropy decay profiles are deconvoluted from the histogram profiles. Multiple data sets are taken to ensure statistical validity.

### 4.2.3 Characterization of labeled oligonucleotides – Prior art

TCSPC has been increasingly used (26-29) in characterizing the fluorescently labeled oligonucleotides. Chang and coworkers used it (26), in one of the early works, to characterize the lifetimes of the common dyes when they are conjugated to DNA. Fluorescein isothiocyanate (FITC), tetramethyl rhodamine isothiocyanate (TMR), Texas Red and 4-chloro-7-nitrobenzo-2-oxa-1,3-diazole (NBD) were all

characterized in solution and gel medium to ensure that their conjugation to ss DNA did not alter lifetime properties significantly. It was indeed found to be the case in this study. This was done in the context of finding suitable dyes for the 3-dye and 4-dye strategies, towards optimizing DNA sequencing protocols using capillary electrophoresis. Recent works have focused on the impact of labeling strategies and the DNA conformation changes on the photophysical properties of the labeled oligonucleotides (27). Nazarenko and coworkers noted the specific quenching interaction of guanosine with dyes like fluorescein in this work and such an interaction has been observed in different secondary structures of the nucleic acids. The extent of the interaction and the end-result of this dye-DNA interaction is observed to depend on the exact sequence.

An important objective in such reports was to determine if the fluorescence intensity of such labeled DNA could be predicted to increase or decrease when they bind to their complementary DNA probe during hybridization experiments. More work by Nord and Siedel (28,29) has also confirmed the existence of prominent base specific quenching, especially in relation to the Guanosine residue. This effect was, again, more pronounced in certain ss DNA sequences. The quenching phenomenon was also characterized as a static quenching process (28) and the reason for the interaction was determined to be a photoinduced electron transfer reaction. It is to be noted that a majority of the anisotropy studies have been performed using fluorescein as the dye of choice, mostly due to convenient conjugation strategies that are available without compromising on the DNA yield.

The McGown research group, using frequency domain studies, has also made time-resolved anisotropy measurements (30) of labeled oligonucleotides. The effort was mainly to determine if hybridization experiments show concomitant steady state anisotropy changes of the labeled ss DNA probes, especially for those of about 30 bases in length. The effect of tether arm length and temperature on the anisotropy changes has been reported in this work. The group went on to investigate the effects of temperature and collisional quenching (31) on the hybridization properties of similar probes. An interesting finding reported from this work was the possible presence of two conformations for fluorescein labeled oligonucleotide probes that may collapse into a single conformation at higher temperature. It is however concluded that the choice of dye, tether length, temperature and ionic composition of the solution have key roles to play in determining the fluorescence properties and rotational dynamics of labeled oligonucleotides.

Rusinova and coworkers have reported the favorable characteristics of Alexa 488, Oregon Green 488 and Oregon Green 514 labeled DNA probes when used for FP applications. The photophysical properties of such probes are not altered significantly even at higher temperatures proving their suitability as FP probes. More groups have recently adapted single molecule fluorescence studies in an effort to understand the details of the solution behavior of all such probes at a molecular level (33,34). All the above-mentioned works have can be informative when interpreting the time-resolved spectroscopic data obtained for the labeled D17.4 aptamer.

### 4.2.4 Current approach for the TCSPC study

The present time-resolved study is undertaken with twelve and six-carbon tether linker for the dyes, fluorescein and Texas red, as shown below in Figure 4.3.

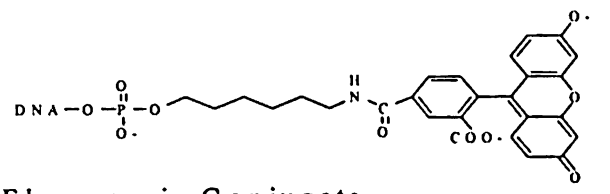

Fluorescein Conjugate

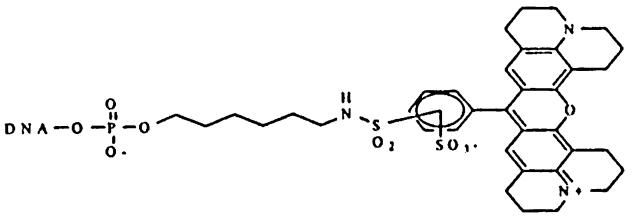

Texas Red Conjugate: 6 carbon linker

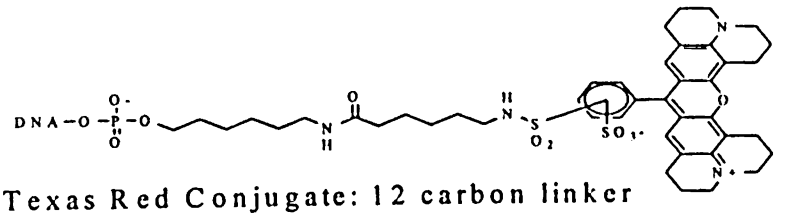

Texas Red Conjugate: 12 carbon linker

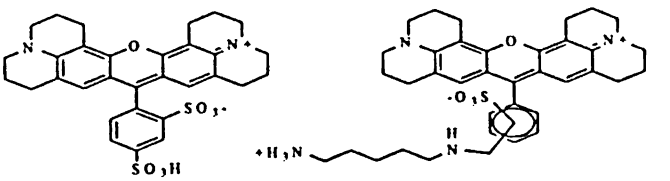

Sulforhodamine 101 Texas Red Cadaverine

Figure 4.3: Structures of the dye-DNA conjugates and fluorophores that are characterized in the current study.

DNA in figure 4.3 refers to the D17.4 aptamer. Sulforhodamine 101 (S 101) and Texas Red Cadaverine are model compounds for Texas Red without and with a linker attached, respectively. The dyes are conjugated to the DNA on the 5' end and the tether arm length is designed to be not too long. This has been done with the view that a very long tether length promotes local dye motion, as found from previous reports (31).

## 4.3 Material and Methods

### 4.3.1 Flurophores and DNA conjugates

The consensus sequence for the D17.4 aptamer is 5'-GGGGCACGTTTATCCGTCCCTCCTAGTGGCGTGCCCC-3'. Texas Red conjugate with a 6-carbon linker, TR 6-aptamer, was obtained from Midland Certified Reagents Inc. (Midland, Texas) whereas all other DNA reagents, including the unlabeled aptamer, were obtained from Integrated DNA technologies (Coralville, IA). TR cadaverine was purchased from Molecular Probes (Eugene, OR). Sulforhodamine 101 (S 101) was purchased from Sigma Chemicals (St. Louis, MO). DNA samples were purchased in the HPLC or gel purified form. Aptamer solutions were treated as described in Section 3.3.1. The binding buffer for all the experimentation was also the same as described for the steady state experiments in Section 3.3.1. The concentration of the Texas Red labeled conjugates, unless specified otherwise, was 20 nM whereas the fluorescein conjugate was used at 200 nM. IgE was obtained from Athens Research and Technology Inc. (Athens, GA) and used without further purification. The product is verified to be greater than 95% in purity from immunoblotting experiments and the absolute concentration is also verified using the

BCA protein assay. The procedure for the BCA assay is followed according to manufacturer's instructions, adapted for the microwell format. The time-resolved fluorescence experiments were performed using a quartz cuvette (Starna Cells, CA) that uses a sample volume of 700 μL.

### 4.3.2 Time-resolved fluorescence

The TCSPC instrumentation setup (35) for the current experiments is similar to the general instrumentation template shown in Figure 4.2. This work was performed in collaboration with the Johnson research group at the University of Kansas. A mode-locked Nd:YAG (Antares from Coherent, Santa Clara, CA) laser pulse, frequency-doubled by a BBO crystal, was used to synchronously pump a home-built Rhodamine 6G dye laser operated at 590 nm. The pulse width was approximately 5 ps. This laser was cavity-dumped at either 7.6 MHz or 3.8 MHz. The cavity dumper is an acousto-optic device placed within the dye laser cavity. The resulting beam was attenuated using neutral density filters to the appropriate signal level for these experiments. The excitation beam was focused on to the sample using a 10-cm lens. The focal point was set near the sample cell to minimize reabsorption.

For excitation of fluorescein, a 440 nm picosecond pulsed diode laser (LDH 440 from Picoquant GmbH, Germany) was operated at 20 MHz under maximum power conditions. Fluorescence was collected at held in a temperature controlled sample cell. The detection monochromator was a DB-10 American Holographic (Fitchburg, MA) subtractive dispersion double monochromator with a bandpass of 10 nm for the TR experiment and 20 nm for the fluorescein experiment. The emission wavelength

was 612 nm for TR experiments and 512 nm for the fluorescein. Fluorescence signals and reference signals from a fiber optic delay were processed by a constant fraction discriminator (Ortec and Tennelec, respectively, Oak Ridge, TN) and a time-to-amplitude converter (TAC) (Tennelec). The constant fraction discriminator is used to minimize the effect of pulse amplitude variations. The TAC uses a capacitor for charging and to build a voltage ramp in it. The amplitudes of the resulting signals were binned using the PCA-II multichannel analyzer (MCA) (Canberra, Oak Ridge, TN). The data were collected in reverse mode and the signal level for all experiments was kept at much less than 1% of the repetition rate in order to eliminate pulse pileup. The reverse mode operation of the TAC is more convenient as the TAC capacitor is charged only when an emission photon is detected. MCA performs the analog-to-digital data conversion to yield the photon count as a function of time. Polarization of the fluorescence was selected using a HN32 polarizer (3M, Norwood, MA).

All intensity decays were collected at the magic angle of 54.7 degrees from vertical. The normalization of collection intensity of parallel and perpendicular anisotropy decays was accomplished by collecting all decays to the same integrated intensity in a tail-matching region at long time delays such that no anisotropy effects are seen within the tail-matching region. The tail-matching method was not employed when the data for IgE binding is handled because anisotropy is still present at long time delays. For these studies, a correction factor was obtained from the steady state anisotropy values, reported in the previous chapter.

### 4.3.3 Data Fitting

Time-resolved data were analyzed with the Globals Unlimited decay analysis software (Laboratory for Fluorescence Dynamics, University of Illinois at Urbana-Champaign, Urbana, IL). The instrument response function was collected using a dilute colloidal solution of non-dairy creamer. The fit to the decays was corrected using the instrument response for every set of vertical, horizontal, and magic angle files. The magic angle intensity decays were globally fit to a sum of exponentials in the form $I(t) = \Sigma a_i \exp(-t / \tau_i)$, where $a_i$ is the amplitude of component i and $\tau_i$ is the fluorescence lifetime of component i. For some samples, describing the fluorescence lifetime by a discrete set of exponentials is not adequate. This may indicate that significant conformational heterogeneity is present in the sample. In this case, the data may be fit to a gaussian distribution of exponentials (36).

The vertically and horizontally polarized decays were, respectively, globally fit to equations of the form shown below:

$$I_{VV}(t) = 1/3\, I(t)\,[1 + 2\, r(t)] \qquad \textbf{Equation 4.1}$$

$$I_{VH}(t) = 1/3\, I(t)\,[1 - r(t)] \qquad \textbf{Equation 4.2}$$

The anisotropy, *r(t)*, is described by

$$r(t) = r_0 \Sigma \beta_i \exp(-t / \varphi) \qquad \textbf{Equation 4.3}$$

where $r_0$ is the anisotropy at time zero for the fluorophore, $\beta_i$ is the amplitude of component i and $\phi_i$ is the rotational correlation time of component i.

The $r_0$ value was fit in each analysis with the fluorescence lifetimes fixed at a value determined from the magic angle decays. The $r_0$ value for all TR samples was 0.37 ± 0.03. The $r_0$ value for the fl samples was 0.25 ± 0.05 except at 75 °C where it is 0.14. The low values of the initial anisotropy for fluorescein are most likely due to the fact that the excitation source (440 nm) is to the blue of the absorbance maximum for fluorescein (495 nm). Time resolved fluorescence cannot be used to measure rotational correlation times much longer than the fluorescence lifetime. The rotational correlation time expected for overall rotation of the IgE molecule is more than an order of magnitude greater than the fluorescence lifetime of any of the probes used in this study. Therefore a rotational correlation time was added to the analysis with a fixed value of 50 ns to account for the long anisotropy decay component, similar to other works from the McGown group (31). For purposes of visualizing the trends in the time-resolved anisotropy, raw anisotropy decays were calculated from the equation (36).

$$r(t) = [I_{VV}(t) - I_{VH}(t)] / [I_{VV}(t) + 2I_{VH}(t)] \qquad \textbf{Equation 4.4}$$

Since $I_{VV}(t)$ and $I_{VH}(t)$ are convoluted with the instrument response function, this is only a visual tool and values of the anisotropy calculated in Equation 4.5 are incorrect at short time scales. Therefore, all plots of raw anisotropy decays omit the

initial data points. All rotational correlation times were determined from Equations 4.2 and 4.3 by iterative reconvolution with the instrument response function. Estimates of error limits for global non-linear least squares fits were obtained using the support plane method (37,38). All errors reported in this study are at one standard deviation.

### 4.3.4 Data Analysis: Conformational dynamics

The rotational correlation time for a fluorophore gives an indication of the tumbling rate of the molecule in solution. It can be described by the Stokes-Einstein-Debye equation:

$$\phi = \frac{\eta V}{kT} F \qquad \textbf{Equation 4.5}$$

where $\phi$ is the rotational correlation time, $\eta$ is the viscosity, V is the molecular volume, k is the Boltzman constant, T is absolute temperature, and F is a coupling factor that depends on the shape of the molecule and the hydrodynamic coupling. The temperature dependence of viscosity for a solvent can be described (39).

$$\ln \eta = -b\,(T - T_0) + \ln \eta_0 \qquad \textbf{Equation 4.6}$$

where $b$ is the thermal friction coefficient and $\eta_0$ is the viscosity at a reference temperature $T_0$. This relationship, in combination with the Stokes-Einstein-Debye

equation, predicts a temperature dependence of the rotational correlation time given by the following expression (39-41).

$$\ln (\eta \cdot T) = -b (T - T_0) + \ln (\eta_0 VF/k) \qquad \textbf{Equation 4.7}$$

The coefficient *b* can be found by determining the Arrhenius plot of ln ($\varphi$. *T*) vs. *T* for a substance strongly coupled to solvent viscosity or by simply measuring the viscosity of the solvent as a function of temperature. As can be predicted, the value of b is an indication of the effect of solvent interactions involved for conjugated fluorophores.

## 4.4 Results and Discussion

### 4.4.1 Fluorescence Lifetimes

As mentioned in Section 4.1.3, the fluorescence lifetimes of Sulforhodamine 101(S101), which consists of Texas Red (TR) without any linker, and TR cadaverine that has the alkyl linker attached (Figure 4.3) are also determined. DNA samples used for this experiment included TR6-aptamer, TR12-aptamer, TR12-aptamer bound to IgE, and fl-aptamer (fluorescein conjugate). The results from this experiment are reported below in Table 4.1:

| Sample | $\tau_0$ (ns) | $\sigma$ (ns) | $\chi^2$ |
|---|---|---|---|
| S 101 (20 nM) | 4.11 ± 0.02 | - | 1.46 |
| TR-cadaverine (20 nM) | 3.96 ± 0.02 | - | 1.33 |
| TR6-aptamer (20 nM) | 4.67 ± 0.02 | - | 1.58 |
| TR12-aptamer (20 nM) | 4.72 ± 0.02 | - | 1.70 |
| TR-12 aptamer (20 nM + 26 nM IgE) | 4.60 ± 0.02 | - | 1.43 |
| fl-aptamer (200 nM) | 3.57 ± 0.07 | 1.3 ± 0.1 | 2.23 |

Table 4.1: Fluorescence lifetime data of the fluorophores and the DNA conjugates.

All compounds and conjugates are seen to exhibit monoexponential decay kinetics except the fl-aptamer which required a Gaussian distribution of lifetimes for adequate fitting. The fluorescence decay of fluorescein can be fit just as well with two exponentials but this requires four fitting parameters while the Gaussian fit only requires three. Therefore the Gaussian distribution is considered the better model for the data. These data are in line with previous reports for both fluorescein and Texas Red (26,31). DNA conjugates of Texas Red have not been extensively investigated for their photophysical characteristics and the lifetime data reported here for the D17.4 ligand is useful new information.

The values of the fluorescence lifetimes of the Texas Red labeled aptamers are encouraging, considering the lack of heterogeneity in the decay. The absence of

changes in the fluorescence lifetime with different labeling strategies means that the steady state anisotropy changes are not due to any lifetime perturbations. In fact, the information that the lifetime of the TR-12 probe does not change during the binding process itself, as shown in Table 4.1 when 26 nM IgE is used in the data determination, confirms this observation. The choice of 26 nM for the concentration of IgE is based on the steady state FP data, as discussed in the previous chapter, which has shown measurable anisotropy changes at that protein concentration (Figure 3.6). It is also important to note that the variation of the dye tether arm in Texas Red case has not altered the lifetime properties of the probes. The gaussian distribution requirement to fit the lifetime data in the case of the fluorescein conjugate has also been encountered in other DNA-fluorescein conjugates, as reported from the work of Kumke and coworkers (31). The concentration of the aptamer used in the DNA samples is not an issue of concern as this variable has been studied, at nM levels, to ensure that the data from Table 4.1 do not vary significantly with concentration. Such an expectation is reasonable, considering that inter-molecular DNA interactions have not been observed to be a concern at such low concentrations.

It is also of interest to evaluate the temperature dependence of the lifetimes of these conjugates using the Arrhenius plots, as mentioned in Section 4.3.4. It has been found in our concurrent work (42) that the TR conjugates do not have any new quenching pathways although the fluorescein conjugate is seen to have a second quenching pathway, especially at higher temperatures. The slope of the Arrhenius plot gives an idea of the activation energies for each system. It has been observed

that the initial activation energies, at 20-50 °C, of both the types of conjugates are, however, found to be similar. The emergence of a second quenching pathway for the fluorescein conjugate at higher temperatures may be due to a greater accessibility of some of the guanosine residues in the D17.4 aptamer motif, during DNA melting. This result reinforces the strong possibility of a fluorescein-guanosine quenching interaction, as seen in other examples from the literature. In contrast, the free dye S101 has no temperature dependence, as seen from the Arrhenius plot (42). This is not unexpected as the free dye S 101 is not known to have shown temperature - dependent conformational changes. Lifetime analysis has proven to be a useful tool to characterize that the TR probes are a better choice than the fl-conjugate for this application. Although knowing about the exact mechanism in relation to the second quenching pathway for fluorescein conjugate is of considerable interest, it is beyond the scope and objectives of the current work.

### 4.4.2 Time-Resolved Anisotropy Data

Similar to the lifetime data analysis, the anisotropy of S101 and TR cadaverine were analyzed before any attempt was made to interpret the anisotropy information of the conjugated fluorophores. S101 shows a monoexponential anisotropy decay with a rotational correlation time ($\varphi$ or RCT) of 180 ± 10 ps. TR cadaverine has a rotational correlation time of 230 ± 20 ps. Table 4.2 shows the differences in the rotational characteristics of the fluorophore after it is conjugated to the aptamer.

| Aptamer | $\phi_1$ (ns) | β1 | $\phi_2$ (ns) | $\beta_2$ | $\chi^2$ |
|---|---|---|---|---|---|
| 10 nM TR-12$ | 0.7 ± 0.2 | 0.27 ± 0.05 | 5.1 ± 0.4 | 0.73 ± 0.05 | 1.68 |
| 20 nM TR-12$ | 0.5 ± 0.2 | 0.28 ± 0.04 | 5.0 ± 0.4 | 0.72 ± 0.05 | 1.91 |
| 50 nM TR-12 $ | 0.6 ± 0.2 | 0.27 ± 0.04 | 4.9 ± 0.4 | 0.73 ± 0.05 | 1.13 |
| 20 nM TR-6$ | 0.5 ± 0.2 | 0.26 ± 0.04 | 5.1 ± 0.4 | 0.74 ±0.04 | 1.56 |
| 200 nM fl-6* | 0.65 ± 0.05 | 1.0 | - | - | 2.63 |

* Anisotropy fitting function: $r(t) = r_0 \exp(-t/\phi)$

$ Anisotropy fitting function: $r(t) = r_0 \sum_i \beta_i \exp(-t/\phi_i)$

Table 4.2: The anisotropy components, their amplitudes (β) and the rotational correlation times (ϕ) of the DNA conjugated are tabulated.

The anisotropy decay of the TR12-aptamer is seen to be biexponential. Two components including one fast and a slow component are seen in this distribution. At room temperature, the rotational correlation time of the fast component is 500 ± 200 ps while the rotational correlation time of the slow component is 5.0 ± 0.4 ns. The value of φ for the fast component is nearly the same as expected for the local motion of the fluorophore, based on our calculations and previous reports (31,43). It is longer than the reorientational time seen for TR cadaverine, but this is reasonable considering the dye is conjugated to the DNA though a tether arm that can impose reorientational constraints. The slow rotational correlation time is on the same order of magnitude as predicted for a hydrated DNA molecule of 37 bases (44). Therefore,

it can be inferred that we are probing the motions of both the tethered dye molecule and the aptamer as a whole. The β value of each rotational motion refers to the amplitude or the percentage of the total anisotropy, for all the labeled DNA molecules, arising from that specific anisotropy component. For example, the amplitude ratio of the TR-12 conjugate is approximately 7:3 (Table 4.2) with the overall DNA motion dominating the segmental motion of the dye. It can thus be expected that the net anisotropy value of this probe will be derived mainly from the DNA rotational properties although the dye segmental motion is not insignificant. In other words, this probe shares the anisotropy property of the aptamer closely. It is also to be pointed out that the TR-6 conjugate also reflects the aptamer rotational characteristics in a manner very similar to the TR-12 conjugate. Hence there is a strong possibility of favorable dye-DNA interactions in TR probes, which is independent of the dye tether length. The nature of the interaction is not clear from our observations but it is useful to note here that the TR is zwitterionic whereas fluorescein is dianionic in charge, under the current solution conditions.

As the amplitudes of the global DNA motion dominate the overall anisotropy in the Texas Red conjugates (Table 4.2), it may be expected that the probes will be sensitive for monitoring the binding process to IgE. It may also be seen from Table 4.2 that the fluorescein conjugate exhibits only a fast rotational component, similar to that of the free dye rotation. The long component of the rotation is hardly detected and this suggests the dominance of the local dye motion relative to the global DNA motion. This information does indicate that the fluorescein probe cannot be expected to be a sensitive probe in reflecting the anisotropy changes. This has also been our

experience, as seen from the data and discussions in the earlier chapter. This observation is not altogether surprising when compared with work from the McGown group (31) where different fluorescein conjugates of similar lengths show very low amplitude DNA motion. It is to be pointed out that none of the DNA probes used in that study has aptamer-like binding properties. The favorable characteristics of the TR probes thus suggest the need for careful consideration of the choice of fluorophore when deciding the DNA labeling strategy.

The steady-state anisotropy of the fl-aptamer is rather low and undergoes small changes upon binding to the target (44), as seen from section 3.4.2 of the previous chapter. The present time-resolved spectroscopy results show that this is due to a large amplitude of free reorientation of the dye relative to the aptamer molecule. Concurrent data also indicate that at all temperatures for the fl-aptamer the dye rotates almost independently of the aptamer as is evidenced by the lack of a long rotational correlation time corresponding to the global rotation of the system (42). Kumke and coworkers have shown that this can be remedied somewhat by decreasing the dye linker length (30). This factor, in any case, is a severe impediment to the development of a sensitive and reproducible binding assay. The importance of understanding the rotational dynamics for the FP probes seems to be critical in order to rationalize their steady state anisotropy changes. This has especially proven to be the case, from the perspective of the D17.4 system. The TCSPC studies that we have undertaken has provided significant clarity in understanding the binding data obtained in the steady state experiments. It has, thus, served as an ideal biophysical characterization tool for the current problem.

### 4.4.3 Dependence of Anisotropy on Temperature

In order to comprehend the temperature dependent sensitivity data that was obtained from the steady state work, it was sought to determine the variation of rotational dynamics of these probes with temperature:

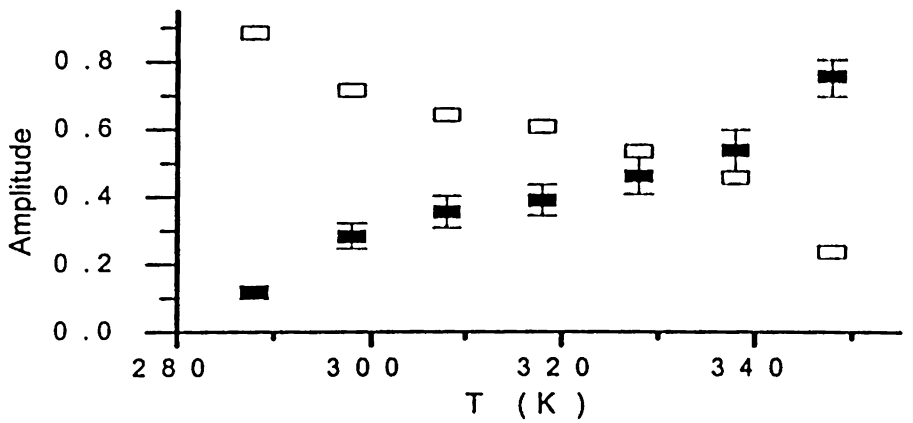


Figure 4.4. Relative amplitudes of the rotational components of the TR12-aptamer as a function of temperature. Open squares: amplitude of the slow rotational component; closed squares: amplitude of the fast component.

The anisotropy is dominated by the slow rotational motion at low temperatures. As temperature increases, the fast rotational motion becomes more prominent and dominates the anisotropy at 65°C. This coincides with the melting temperature of the aptamer tertiary structure, shown by spectrophotometric studies to occur at around 60 °C (44). The dye-DNA interaction is probably dependent on the presence of the

stem loop structure of the aptamer. A recent NMR study by Gaiko and co-workers (45) shows an interaction in 5' Rhodamine 6G (R6G) labeled DNA between R6G and the double stranded DNA helix. The dye is determined to be in a stacking arrangement on the terminal base pair of the helix. The major difference between R6G, TR, and fluorescein is the charge distribution. TR and R6G are both zwitterionic at neutral pH whereas fluorescein is a dianion at neutral pH. The nucleic acid backbone is highly electronegative. Similar to the R6G case, TR can have favorable interactions with the DNA, which may or may not be dependent on the sequence. Preliminary investigations into the interactions of the free Texas Red in binding buffer with the unlabeled DNA aptamer did not reveal a spectroscopic handle to characterize these interactions better.

The data from Table 4.2 and Figure 4.4 indicate that fluorescein is repelled from the DNA surface and therefore does not participate in any favorable interaction. The time-resolved anisotropy of the fl-aptamer was also analyzed for its distribution. No evidence for a biexponential anisotropy decay at any temperature between 15 and 75 °C was observed. The value of the rotational correlation time at room temperature is 650 ± 50 ps. The lack of a long rotational component indicates that the dye motion is to a large extent uncoupled from the global aptamer rotation in this system. The differences between the anisotropy of the TR-aptamer and fl-aptamer are visualized by observing the actual anisotropy decay in Figure 4.7 below.

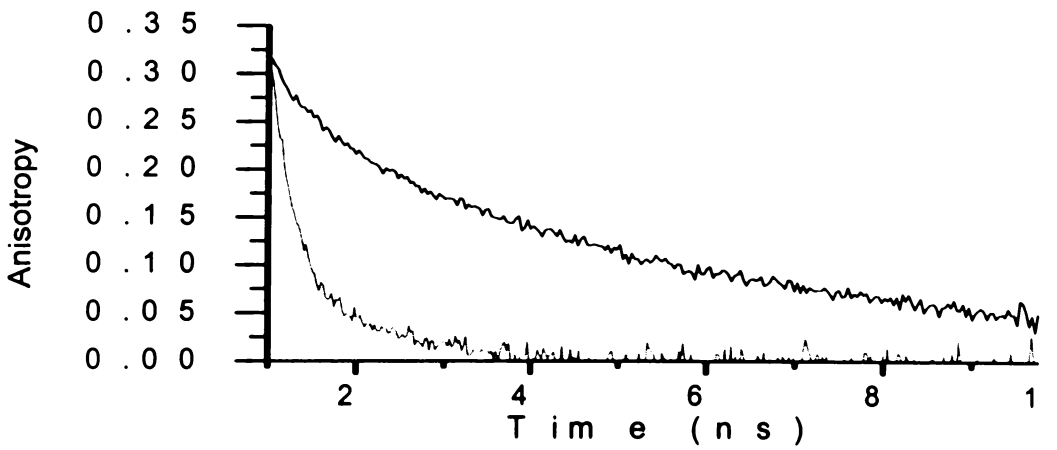


Figure 4.5: Comparison of the raw anisotropy decays of fl-aptamer (grey line) and TR6-aptamer (black line). The anisotropy decays were calculated from parallel and perpendicular polarized fluorescence decays. Data at early times are omitted due to irregularities caused by the instrument response function.

The significant point of interest in the decay profile is the differences in the two systems, in relation to their rapidity. This translates into single component decay for the fluorescein conjugate and two-component decay for the TR conjugates.

### 4.4.4 TR-6 and TR-12 probes – Comparison of Rotational dynamics

In order to understand the similarities in the anisotropy properties of the TR-6 and TR-12 probes and also to compare their rotational dynamics, the TR-6 aptamer was

analyzed for its anisotropic components. The result from this experiment is shown in Figure 4.6 below.

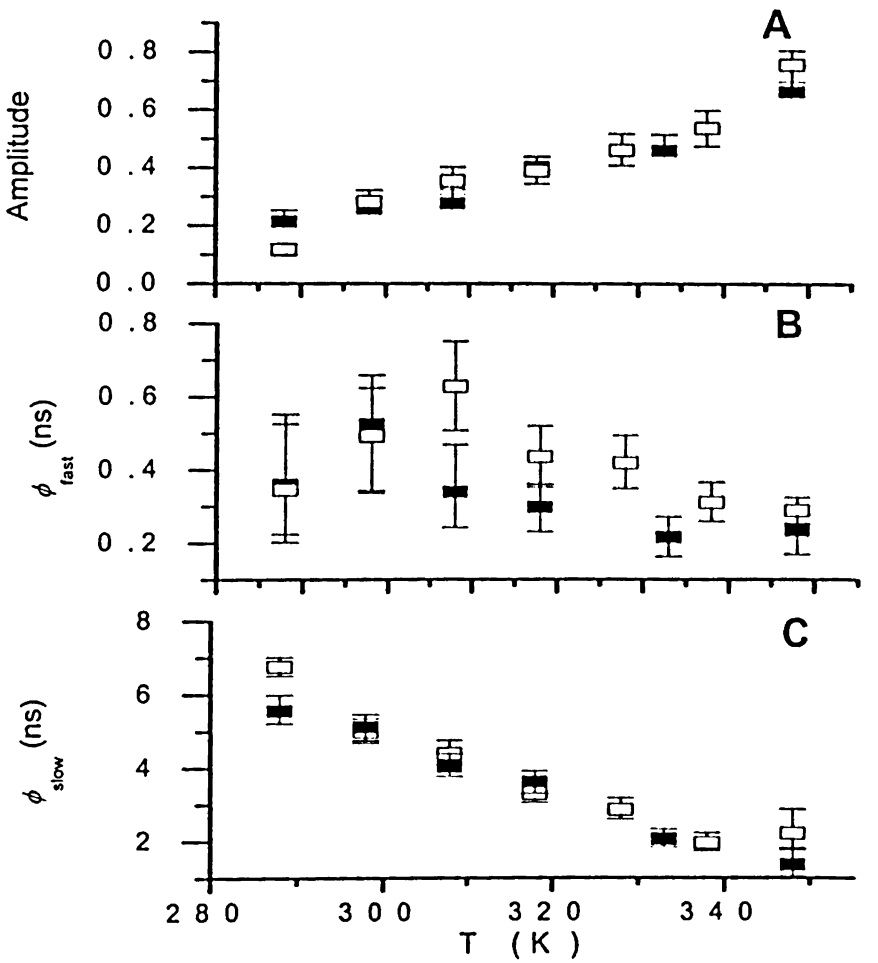


Figure 4.6: Comparison of the A) rotational amplitudes, B) fast rotational correlation times, and C) slow rotational correlation times of the TR12-aptamer (open squares) and TR6-aptamer (closed squares) as a function of temperature.

As seen from Figure 4.6, this aptamer conjugate showed almost identical anisotropy and fluorescence characteristics to the twelve-carbon linker. It appears that the length of the linker arm has minimal effect on the anisotropic properties of the dye-labeled aptamer for TR. In contrast, a dependence on the length of the linker has been shown for fluorescein, where the value of the fast rotational correlation time decreases with increasing linker length (31). This observation, once again, illustrates favorable dye-DNA interactions, independent of tether arm length, in the TR probes that help them in being more sensitive probes. This observation also justifies the comparable behavior of the two TR conjugates in terms of FP sensitivity, which was seen from the steady state anisotropy data (Figure 3.7) in the previous chapter. It is also to be noted that the similarity in working ranges obtained in our studies possibly point to the binding affinity not being severely altered amongst the three FP probes considered here.

### 4.4.5 Effect of Aptamer Concentration

It is important to ensure that the various time-resolved measurements reported in this work are not skewed by effects of intermolecular DNA interactions. It is especially important to analyze the labeled aptamers for such interactions in the concentration range useful for IgE bioanalysis. The date for TR12-aptamer in Table 4.2 shows the effect of concentration on the rotational correlation times and rotational amplitudes at 10, 20, and 50 nM. It can be inferred from these data that self-association is not an issue at the concentrations used in this study. Steady-state data have shown a similar trend up to 100 nM with both fl-aptamer and TR12-aptamer (Table 3.1). At concentrations up to 200 nM, the rotational correlation time of the fl-aptamer also

does not show any evidence of self-association. This is an important observation for the current studies as variation of anisotropy properties with concentration will complicate the interpretation of the steady state behavior of the FP probes under current consideration.

### 4.4.6 Monitoring the binding process

Binding of Aptamer to IgE

It is informative to confirm the presence of the complex in solution using time-resolved measurements, based on the rotational population data. It is also important to understand the microscopic details behind the changes in reorientational mobility of the labeled DNA upon binding. Changes in protein or aptamer structure can lead to anomalous changes in steady state anisotropy due to reorientational freedom of the dye label and segmental motions of the aptamer. Another point of interest is the impact of dye segmental motion on the binding ability of the aptamer itself. To evaluate and answer these queries, time-resolved characterization of the equilibrium mixtures of the aptamer and IgE were performed. Table 4.3 shows the fluorescence anisotropy parameters of TR12-aptamer with varying concentrations of IgE.

**Aptamer- IgE binding at 25 °C**

| [IgE] | $\varphi_1$ (ns) | $\beta_1$ | $\varphi_2$ (ns) | $\beta_2$ | $\varphi_3$(ns) | $\beta_3$ |
|---|---|---|---|---|---|---|
| 0 nM | 0.5 ± 0.2 | 0.28 ± 0.04 | 5.0 ± 0.4 | 0.72 ± 0.04 | - | - |
| 5 nM | 0.5 ± 0.2 | 0.26 ± 0.06 | $4.9^{+1.4}_{-0.8}$ | 0.61 ± 0.05 | 50 | 0.14 ± 0.07 |
| 10 nM | 0.7 ± 0.3 | 0.26 ± 0.11 | $4.7^{+2.9}_{-1.2}$ | 0.50 ± 0.08 | 50 | 0.24 ± 0.13 |
| 15 nM | 1.0 ± 0.5 | 0.25 ± 0.16 | $4.6^{+6.8}_{-1.6}$ | 0.39 ± 0.13 | 50 | 0.36 ± 0.19 |
| 26 nM | 0.5 ± 0.3 | 0.17 ± 0.12 | $2.8^{+1.5}_{-0.8}$ | 0.28 ± 0.07 | 50 | 0.54 ± 0.14 |
| 150 nM | 0.7 ± 0.3 | 0.23 ± 0.07 | $4.3_{+4.8}$ | 0.28 ± 0.05 | 50 | 0.49 ± 0.09 |

Table 4.3: Anisotropy parameters for the DNA-Protein mixtures, evaluated under equilibrium binding conditions, as seen in binding buffer at pH 7.4. $\varphi$ refers to the rotational correlation times and $\beta$ refers to the amplitude of rotational populations.

As seen in the table, it is found that there are two rotational contributions in addition to the long rotational contribution that corresponds to the overall rotation of the aptamer-IgE complex. This is true even in the limit where all of the aptamer is apparently bound to 150 nM IgE, as determined from steady state data (Figure 3.7).

This indicates the presence of a segmental motion other than the local motion of the dye in the bound state.

The fraction of long rotational population ($\beta_3$) increases linearly with increasing IgE concentration as expected (Figure 4.10, inset) to a value of approximately 50%. This is the population of the DNA-aptamer complex itself in solution. In addition, the fraction of the intermediate rotational correlation time ($\beta_2$) decreases linearly in the same fashion to a final value of approximately 30%. This behavior mirrors the expected change in populations of bound and free aptamer, respectively. Theoretically, it would have been expected that $\beta_2$ will drop all the way to zero and $\beta_3$ will increase up to about 70% since that was the initial available population of unbound, free DNA aptamer. However the data observed here are seen to indicate the presence of an added dye rotational component even for the fully bound aptamer. The fraction of segmental motion due to local dye motion ($\beta_1$) is similar to that observed in the free aptamer at all points in the titration. This situation possibly indicates a two state bound-unbound equilibrium system. It is necessary to point out that the accuracy in determining the amplitudes of the rotational components is reduced at high protein concentrations due to data analysis constraints that arise from the extremely slow rotational rate of the DNA-Protein complex.

Additionally, no changes are seen in the fraction of the fast local dye motion. This indicates that the dye-DNA interaction is insensitive to IgE binding. Nevertheless, there is some segmental mobility, other than the local dye motion, even at saturating concentrations of IgE. This segmental motion occurs on the same time scale as the

overall rotation of the aptamer. It should also be pointed out that the additional dye rotational component could be due to fractional reorientational freedom for the aptamer that might be due to complex dissociation issues. This possibility is unlikely but is not impossible. Though this mobility does not affect the linearity of the bioanalysis, it does indicate that the aptamer is not rigidly bound to IgE and that some reorientational freedom of the aptamer remains upon binding. Further work is due in this aspect to be able to specify the exact reasoning for this unexpected observation.

**Chapter Conclusions and Future work**

Time-resolved measurements of the dynamics of fluorescently labeled biomolecules provide valuable information about intermolecular and intramolecular interactions. This information can be particularly valuable for understanding and optimizing fluorescence-based analyses of biomolecular interactions. In recent years, steady-state fluorescence anisotropy has become a valuable tool for measuring binding equilibria (11). However, the dynamic basis of the observed changes in steady-state anisotropy may not be apparent without time-resolved measurements. In this chapter, time-resolved fluorescence measurements are used to characterize the physical basis of fluorescence detection of molecular recognition by DNA aptamers. It has been demonstrated that the dye-DNA interactions are important for determining the anisotropy changes.

The TR-aptamer fluorescence lifetimes are homogeneous with a weak temperature dependence that is insensitive to the state of the aptamer stem. In contrast, the fl-

aptamer fluorescence lifetimes are heterogeneous and are sensitive to changes in DNA structure, showing quenching upon melting of the aptamer stem structure. Importantly, the TR-aptamer anisotropy reflects the global rotation of the aptamer better due to a favorable dye-aptamer interaction. In contrast, the fl-aptamer anisotropy is dominated by local dye motion and therefore provides poor sensitivity to global rotational dynamics. It is also important to observe that rotational dynamics of the labeled IgE aptamer changes significantly with changes in temperature. This phenomenon indicates the reasoning for sensitivity variations with temperature. Thus, factors such as choice of dye and the nature of dye-DNA interactions at the temperature of interest are crucial to using labeled aptamers in the FP approach. More detailed investigations can be done to specify the origin of an additional segmental motion during the binding process. Similarly, it can be determined if other dyes similar to Texas Red can also be favorable for the DNA based FP approach.

**References:**


1) Liu, P. Q.; Yang, M.; Chan, C.L. *J. Biol. Chem.* **2001**, 276, 11323-11334.

2) Lutz, M. P.; Pinon, D. I.; Miller, L. J. *Anal. Biochem.* **1994**, 220(2), 268-274.

3) Czernik, P. J.; Shin, D. S.; Hubert, B. K. *J. Biol. Chem.* **1994**, 269, 27869-27877.

4) Wei, S.; Mizuchi, K.; Craigie, R. 1 *Proc. Natl. Acad. Sci* **1995**, 18, 10535-10540.

5) Storek, M. J.; Ernst, A.; Verdine, G. L. *Nat. Biotechnol.* **2002**, 20, 183-186.

6) Carpenter, M. L.; Kneale, G. G. *J. Mol. Biol.* **1998**, 281(2), 271-284.

7) Scaria, P. V.; Will, S.; Ghosh, S. S.; Millar, D. P. *Nat. Biotechnol.* **2002**, 20(2), 183-186.

8) Crowe, M.; Fried, M. G. *Eur. J. Biochem.* **1993**, 212, 539-546.

9) Eis, P. S.; Millar, D. P. *Biochemistry* **1993**, 32, 13852-13859.

10) Overman, L. B.; Bujalowski, W.; Lohman, T. M. *J. Biol. Chem.* **1988**, 263, 4629-4638.

11) Hill, J. J.; Royer, C.A. *Methods. Enzymol.* **1997**, 278, 390-414.

12) Clegg, R. M.; Murchie, A. I.; Lilley, D. M. *Biophys. J.* **1994**, 66, 99-105.

13) Maliwal, B. P.; Kusba, J.; Lakowicz, J. R. *Biopolymers*, **1995**, 35,245-255.

14) Kim, C.; Paulus, B. F.; Wold, M. S. *Biochemistry* **1994**, 33, 14197-14205.

15) Giedroc, D. P.; Khan, R.; Barnhart, K. *Biochemistry*, **1991**, 30, 8230-8239.

16) Wittung, P.; Norden, B.; Takahashi, M. *Eur. J. Biochem.* **1994**, 266, 5395-5403.

17) Clendenning, J. B.; Schurr, J. M. *Biophys. Chem.* **1994**, 52, 227-233.

18) Casas-Finet, J. R.; Karpel, R. L.; *Biochemistry*, **1993**, 32, 9735-9743.

19) Erskine, S. G.; Halford, S. E. *Gene*, **1995**, 157, 153-163.

20) Carey, J. *Proc. Natl. Acad. Sci* **1988**, 85, 975-979.

21) Harms, G. S.; Freund, W. L.; Johnson, C. K. *J. Phys. Chem.* B **1998**, 102, 5004-5010.

22) Lakowicz, J. R. 1999, *Principles of Fluorescence Spectroscopy*, Kluwer Academic/Plenum, New York.

23) Demas, J. N., 1983, *Excited State Lifetime Measurements*, Academic Press, New York.

24) O' Connor, D. V.; Phillips, D., 1984, *Time Correlated Single Photon Counting*, Academic Press, New York.

25) Ware, W. R., 1971, Transient luminescence measurements, in *Creation and detection of excited state*, Vol. 1A, Lamola, A. A. Ed., Marcel Dekker, NY, P213-302.

26) Cheng, X.; Kovac, L.; Lee, J. C. *Biochemistry* **1995**, 34, 10816-10824.

27) Nazarenko, I. R.; Pires, B.; Lowe, M.; Obaidy, A.; Rashtchian, R. *Nucleic Acids Res.* **2002**, 20, 2089-2095.

28) Nord, S. L.; Parry, H. H.; Liu, B. A.; Connolly, B. A. *Biochemistry*, **2001**, 40, 2484-2494.

29) Siedel, C. A. M.; Schulz, M.; Sauer, M. *J. Phys. Chem.* **1996**, 100, 5541-5553.

30) Kumke, M. U.; Li, G.; McGown, L. B.; Walker, G. T.; Linn, C. P. *Anal. Chem.* **1995**, 67, 3945-3951.

31) Kumke, M. U.; Shu, L.; McGown, L. B.; Walker, G. T.; Pitner, J. B.; Linn, C. P. *Anal. Chem.* **1997**, 69, 500-506.

32) Rusinova, E.; Ladokhina, V.; Vele, O.; Senear, D. F.; Ross, A. *Anal. Biochem.* **2002**, 308, 18-25.

33) Edman, L.; Mets, U.; Rigler, R. *Proc. Natl. Acad. Sci.* **1996**, 93, 6710-6715.

34) Eggeling, C.; Fries, J. R.; Brand, L.; Gunther, R.; Siedel, C. A. M. *Proc. Natl. Acad. Sci.* **1998**, 95, 1556-1561.

35) Harms, G. S.; Pauls, S. W.; Hedstrom, J. F.; Johnson, C. K.; *J. Fluoresc.* **1997**, 7, 273-282.

36) Fleming, G. R. 1986. Chemical Applications of Ultrafast Spectroscopy. New York: Oxford University Press. p 82-85.

37) Johnson, M. L.; Faunt, L. M. *Methods Enzymol.* 1992, 210, 1-37.

38) Ha, T.; Glass, T.; Enderle, D. S.; Chemla, D. S.; Weiss, S. *Phys. Rev. Lett.* **1998**, 90, 2093-2096.

39) Weber, G. S.; Scarlata, M.; Rholam, M. *Biochemistry*, **1984**, 23, 6785-6788.

40) Bothwell, T. G.; Unruh, J.; Johnson, C. K. *Biopolymers*, **2003**, 69, 351-362.

41) Harms, G. S.; Pauls, S. W.; Hedstrom, J. F.; Johnson, C. K. *J. Fluoresc.* **1997**, 7, 273-281.

*42)* Unruh, J. R.; Gokulrangan, G.; Johnson, C. K.; Wilson, G. S. *Manuscript submitted to Biophysical Journal.*

43) Birks, J. B. 1970. Photophysics of Aromatic Molecules. Wiley and Sons, New York.

44) Gokulrangan, G.; Unruh, J.; Ingram, B.; Johnson, C. K.; Wilson, G. S. *Manuscript under preparation for Analytical Chemistry.*

45) Gaiko, N.; Volkmer, A.; Berger, S.; Schaffer, J.; Eggeling, C.; Siedel, C. A. M.; Griesinger, C. **2003**, *Biophys. J* 84, 313 A.

## Chapter 5: Overall Conclusions, Critical review and Future directions

### Microchannel system for SEB detection

The strategy of reducing the diffusion distances has been proven to be a very promising one, based on the experimental data reported in the current dissertation. The diffusion distances can be reduced in two ways – by using microfabricated devices like the one that is used in the current work or by employing microparticles and nanoparticles. The essential requirements of either approach will include reproducible protocols for antibody immobilization, convenient reagent flow techniques, high affinity immunoreagents and sensitive detection methods that do not involve radiometry.

The two inherent ways of performing rapid heterogeneous assays further leads to the need to compare these two analogous methods themselves. The microparticle approach can benefit from automatable techniques to carry out particle modification, reagent flow and rapid analysis of the immunoreaction. For example, the pioneering efforts of the Ruzicka research group in the development of flow injection surface regenerable immunoasssay (FIRSI) has established feasibility of the use of antibody-immobilized microparticles for immunoassays in a flow mode. This method also has the advantage that the immunosorbent is effectively renewable. Varying detection methods including electrochemical and fluorescence approaches can be adapted to this technique. The recent advances in nanotechnology has also highlighted the possibility of such smaller particles for immunochemical applications. However the important factor for the particle approach is the combination of suitable flow techniques and particle handling technologies.

On the other hand, the use of microfabricated immunoreactors is promising as the surfaces of such reactors can be suitably modified to accommodate covalent immobilization strategies. When such a possibility is coupled to the previously optimized micro total analysis system (μ-TAS) instrumentation, this can be a powerful approach to carry out rapid heterogeneous immunoassays. The bottleneck at this point of time is the availability of suitable surface modification technologies that will allow different antibody immobilization schemes. Such an approach will also address the need of better antibody stability when immobilized on the microreactor surface. The excimer photoablation is also promising in generating novel surfaces with different functional groups and geometries. Ultimately, the coupling of microparticles inside the microchannels can be most efficient in carrying out rapid assays as the diffusion distances can be further reduced.

**Fluorescence Polarization approach using aptamers**

The use of labeled aptamers in the homogeneous detection of protein targets has been shown in the current work. The problem of local dye mobility in fluorescein conjugates can be addressed by using other fluorophores like Texas Red. The dye-DNA interaction needs to be carefully considered as this can be used to improve the sensitivity of FP probes. The nature of such an interaction is not clear even in successful applications, although involvement of the guanosine residue in all such interactions is speculated. This is due to its ability to donate electrons easily for photoinduced charge transfer reactions when interacting with the common fluorophores.

The use of homogeneous assays seems to be most appropriate when employing DNA aptamers for analytical applications. Issues relating to their conformational stability seem to affect their binding ability when immobilized on surfaces. The FP approach has very good sensitivity attributes and this is, hence, a productive approach for analyzing proteins. The need to minimize dye segmental motion has been clearly seen in this work and so alternate strategies that can accomplish this objective can also be employed. This will ultimately help in extracting the maximum sensitivity when using a specific dye. The specificity of the aptamers is very high and this raised the possibility of their being used for analyzing clinical samples of interest. The heavy dependence of the sensitivity is surprising and this underscores the need to choose the most favorable dye when designing such applications. More work in relation to obtaining the binding data can shed light on the impact of labeling on the binding characteristics of the aptamer.

TCSPC spectroscopy has proved to be an ideal biophysical tool for understanding most of the steady state observations. Exciting the fluorescein more to the red may have improved the accuracy of the data related to the fluorescein conjugate. This is due to the fact that data handling procedures can always be better when operating with anisotropy profiles of larger magnitude in signal than otherwise. This limitation may be overcome by using tunable lasers with wide ranging operating wavelengths. In any case, understanding the rotational mobility of the labeled DNA is key to comprehend most steady state observations.

**Future Directions**

As we have had reasonable success with the homogeneous approach using the FP method in monitoring the DNA-Protein binding interactions, it is also desirable to test the efficiency of immobilized aptamers for a similar objective. We have currently employed Surface Plasmon Resonance (SPR) spectroscopy for this purpose. This technique is dependent on the changes of refractive index at a gold-solution interface. The aptamer can be immobilized on the gold surface using suitable surface conjugation strategies such that its binding interactions with protein samples can be monitored by measuring the refractive index. Although data for such experimentation are not discussed here, we have already observed reliable binding data using the self-assembled monolayer (SAM) strategy for the thiol-labeled D 17.4 system. It will be interesting to pursue this preliminary work further to evaluate the analytical utility of immobilized IgE aptamer, on the biosensor surface.

Our experience in characterizing the labeled aptamers using TCSPC spectroscopy has further prompted investigation of complex DNA probes with multiple labeling sites. These are probes that are used for improving signal levels when used for applications like fluorescence in-situ hybridization (FISH). However, extensive labeling can lead to unfavorable dye-dye interactions. The effect of such interactions is another aspect of future research that has emerged from the current work.